AWARD NUMBER: **W81XWH-10-1-0434**

TITLE: **Targeted Nanoparticles for Kidney Cancer Therapy**

PRINCIPAL INVESTIGATOR: **Suzy V. Torti, Ph.D.**

CONTRACTING ORGANIZATION: **University of Connecticut Health Center**
Farmington CT 06030-2806

REPORT DATE: December 2014

TYPE OF REPORT: Final

PREPARED FOR: U.S. Army Medical Research and Materiel Command
Fort Detrick, Maryland 21702-5012

DISTRIBUTION STATEMENT: Approved for Public Release;
Distribution Unlimited

REPORT DOCUMENTATION PAGE

Form Approved
OMB No. 0704-0188

1. REPORT DATE	2. REPORT TYPE	3. DATES COVERED
December 2014	Final	15 Sep 2010 - 14 Sep 2014

4. TITLE AND SUBTITLE
Targeted Nanoparticles for Kidney Cancer Therapy

5a. CONTRACT NUMBER

5b. GRANT NUMBER
W81XWH-10-1-0434

5c. PROGRAM ELEMENT NUMBER

6. AUTHOR(S)
Suzy V. Torti

E-Mail: storti@uchc.edu

5d. PROJECT NUMBER

5e. TASK NUMBER

5f. WORK UNIT NUMBER

7. PERFORMING ORGANIZATION NAME(S) AND ADDRESS(ES)

University of Connecticut
Health Center
263 Farmington Ave
Farmington CT 06030-2806

8. PERFORMING ORGANIZATION REPORT NUMBER

9. SPONSORING / MONITORING AGENCY NAME(S) AND ADDRESS(ES)

U.S. Army Medical Research and Materiel Command
Fort Detrick, Maryland 21702-5012

10. SPONSOR/MONITOR'S ACRONYM(S)

11. SPONSOR/MONITOR'S REPORT NUMBER(S)

12. DISTRIBUTION / AVAILABILITY STATEMENT

Approved for Public Release; Distribution Unlimited

13. SUPPLEMENTARY NOTES

14. ABSTRACT The long-term objective of this proposal was to design nanotubes that would preferentially target cancer cells and surrounding endothelial cells, and then to use these materials as transducers of near-infrared radiation for laser-induced thermal therapy of kidney cancer. In the work supported by this grant, we developed carbon nanotubes designed to bind to uPAR, a surface receptor overexpressed in kidney cancers and supporting endothelium that is involved in growth, migration, proliferation, metastasis and angiogenesis. We used D5, a peptide designed in the laboratory, as the targeting ligand. We demonstrated that the D5 peptide is cytotoxic to kidney cancer cells and proliferating endothelial cells. We expressed and purified a D5-GST fusion protein, and showed that this binds to the uPAR receptor. We showed that the combination of nanotubes and near-infrared radiation is effective in inhibiting the clonegenic survival of cultured kidney cancer cells. We conjugated the D5 peptide to nanotubes, showed that this new material disperses well in aqueous media, produces heat following exposure to near-infrared radiation, and profoundly reduces the viability of kidney cancer cells. We also developed fluorinated graphene oxide as a new, more flexible carbon nanoparticle, and showed that this material is also highly effective in producing heat in response to near-infrared radiation and effectively induces cell death of kidney cancer cells. This award also supported the training of pre-doctoral students in experimental approaches to the use of nanomaterials in kidney cancer ablation. These students gained extensive hands-on experience, made presentations, and attended conferences to advance their training. Overall, the research we conducted demonstrates that D5-conjugated nanotubes are highly effective kidney tumor cell cytotoxic agents, and that fluorinated graphene oxide has promise as a more flexible material nanomaterial that can effectively substitute for nanotubes as a backbone for D5 conjugation.

15. SUBJECT TERMS NOTHING LISTED

16. SECURITY CLASSIFICATION OF:			17. LIMITATION OF ABSTRACT	18. NUMBER OF PAGES	19a. NAME OF RESPONSIBLE PERSON
a. REPORT	b. ABSTRACT	c. THIS PAGE			USAMRMC
Unclassified	Unclassified	Unclassified	Unclassified	85	19b. TELEPHONE NUMBER *(include area code)*

Table of Contents

Page

1. INTRODUCTION

The goal of this proposal was to combine two individually effective and mechanistically dissimilar anti-tumor strategies in a single nanoparticle: (1) a tumor selective peptide that has anti-angiogenic and anti-tumor properties; and (2) a laser activated carbon nanoparticle for photothermal ablation. We hypothesized that this combination will produce an effective therapy for renal carcinoma. The Specific Aims were to fabricate these particles and then test them in cultured cells and in a mouse tumor model. The Tasks associated with accomplishing each Specific Aim are delineated below. This is a mentor/predoctoral award, and an additional objective was to train the next generation of graduate students in nanomaterials and kidney cancer.

In July of 2012 we moved the laboratory from Wake Forest School of Medicine in North Carolina to the University of Connecticut Health Center. This move caused a substantial disruption in research activities. This was partly due to the time it took to transfer the grant from one institution to the other: the award was not fully transferred until May 2013. We received a no-cost extension to enable us to continue these experiments. Because of the short time remaining at the time the grant was re-activated and the change in personnel that ensued following the move, a modified SOW was approved that included the following modifications (1) testing of a new nanomaterial, fluoridated graphene, as a substrate for conjugation of D5. (2) Use of a kidney tumor xenograft model to test the anti-tumor efficacy of these materials.

2. KEYWORDS: Nanotubes/Urokinase Plasminogen Activator Receptor (UPAR)/kininogen/kidney/kidney cancer/photothermal therapy/graphene/graphene oxide/fluorinated graphene oxide

3. OVERALL PROJECT SUMMARY

Specific Aim 1. Synthesize nanotube-based particles ligated to D5s

Task 1: Objective: Obtain linear, Y-branched and dendritic nanoparticles
Results, Progress and Accomplishments: Our co-investigators at Rice (Dr. Ajayan) and WFU Physics Department (Dr. Carroll) fabricated each of these nanomaterials. Dr. Ajayan successfully prepared Y-branched and dendritic nanoparticles, but was not able to sufficiently scale-up synthesis to enable us to systematically test these materials. We therefore focused on linear nanotubes, provided initially by Dr. Carroll and subsequently obtained commercially. As described in the modified Statement of Work, Dr. Ajayan also provided us with fluorinated graphene oxide, a newer material that his laboratory developed and which his laboratory was able to provide in sufficient quantity to use in our experiments.

Task 2: Objective: conjugate linear, Y-branched and dendritic nanotubes to the synthetic peptide, D5s.
Results, Progress and Accomplishments: We obtained the synthetic peptide D5s commercially from Anaspec. Our co-investigator at the WFU Department of Chemistry (Dr. King) was able to successfully conjugate this peptide to linear nanotubes using EDC (1-ethyl-3-(3-dimethylaminopropyl) carbodiimide). We did not use Y-branched or dendritic nanotubes due to the scale-up problems described in Task 1.

Specific Aim 2. Test binding, cytotoxic and thermoablative properties of D5s-nanoparticles in vitro.

Task 2.1: Objective: Test specificity of binding of D5a-nanoparticles.
Results, Progress and Accomplishments. We first confirmed that uPAR, the receptor targeted by D5, is expressed in renal cancer and endothelial cells, since these are the cells we plan to target with our D5-nanotube conjugate.

Protein expression of uPAR was assessed in the following cell lines by immunoblotting: HUVEC (human umbilical vein endothelial cells), Human Primary Renal Epithelial Cells, CRL 1932 (human renal clear cell adenocarcinoma), and RENCA (mouse renal adenocarcinoma).

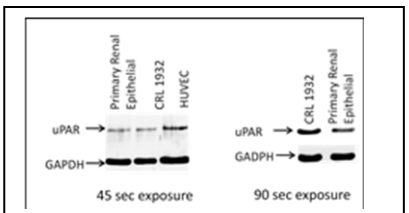

Figure 1. uPAR is expressed in kidney cancer cells and proliferating endothelial cells. Western blots are shown.

Figure 1 shows that as expected, there is increased expression of uPAR in HUVECs compared to normal and cancer cells and increased uPAR expression in cancer cells compared to normal cells.

Task 2.2 Objective: Confirm that binding occurs via binding to UPAR.

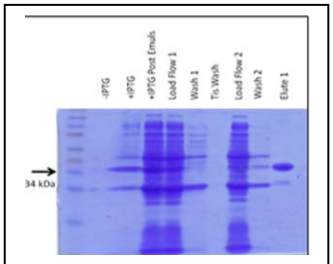

Figure 2. Purification of D5-GST

Results, Progress and Accomplishments: To test binding of D5 to uPAR, we first produced and purified a recombinant D5-GST fusion protein (**Figure 2**). GST pulldown experiments were then performed using cell lysates and GST-tagged D5. 20 ug of each cell lysate were incubated with GST-D5 or GST and rotated overnight at 4^{o} C. The lysates were then incubated with GST-binding agarose beads, washed, eluted, and run on SDS PAGE. Binding was detected by immunoblotting (**Figure 3**). These experiments demonstrate binding of D5 to UPAR in kidney cancer cells and endothelial cells.

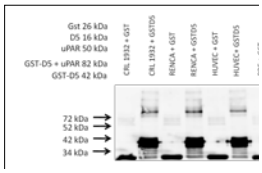

Figure 3. Immunoblot of D5-GST pulldown of uPAR

Task 2.3. Objective: Test ability of D5s-nanoparticles to bind proliferating endothelial cells.

Results, Progress and Accomplishments: We demonstrated that D5 binds to endothelial cells via the UPAR receptor (above). We did not repeat these experiments with D5-nanoparticles since these particles were only successfully synthesized later in the project.

Task 2.4. Objective: Assess anti-proliferative effects of D5a-nanoparticles.

Results, Progress and Accomplishments: To determine the anti-proliferative effects of D5 conjugated to MWCNTs, we first assessed the anti-proliferative effect of D5 alone. HUVEC, CRL1932 and RENCA cells were plated and incubated with recombinant D5, HKa (cleaved high-molecular-weight kininogen), or staurosporine (control). Dose-dependent decreases in viability (determined by MTT assay) were seen in HUVEC and CRL1932 cell incubated with D5. (**Figures 4 and 5**) as well as RENCA cells (not shown). This indicates that D5 has the expected cytotoxic effect on endothelial cells and kidney cancer cells.

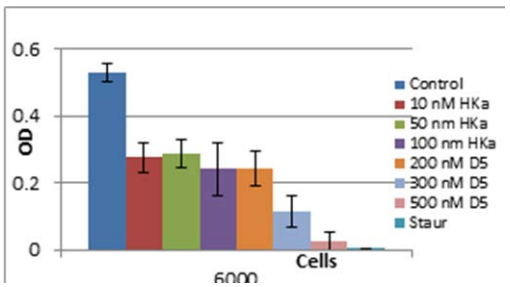

Figure 4. MTT assay of HUVECs incubated with HKa or D5 for 24 hrs.

Task 2.5. Objective: Assess thermal ablative properties of D5a-nanoparticles.

Results, Progress and Accomplishments: D5-conjugated MWCNTs and fluorinated graphene oxide (FGO) and were dispersed at different concentrations in aqueous solvents (PBS or water) to confirm their compatibility with aqueous media. As shown in **Figure 6**, all materials were well dispersed. We then tested the ability of these materials to increase temperature in response to illumination with NIR. Materials were dispersed and illuminated for 0-35 sec with a 975 nm fiber optic laser, and the change in temperature measured. As shown in **Figure 7**, a dose-dependent increase in temperature was observed with both materials.

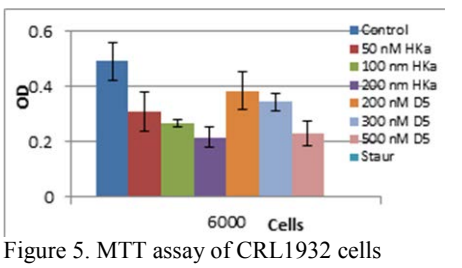

Figure 5. MTT assay of CRL1932 cells incubated with HKa or D5 for 24 hrs.

To assess the effect of CNT heating on cell survival, RENCA cells were treated with FGO or D5-MWCNT, exposed to NIR, and viability measured using an MTS assay. As shown in **Figure 8**, both materials induced a profound decrease in cell viability. These results demonstrate that these materials are suitable for further testing in an in vivo model.

Specific Aim 3. Perform in vivo testing of tumor ablative properties of unconjugated and conjugated nanomaterials using a subcutaneous xenograft model (The tasks in this Aim were modified during the no-cost extension as described above).

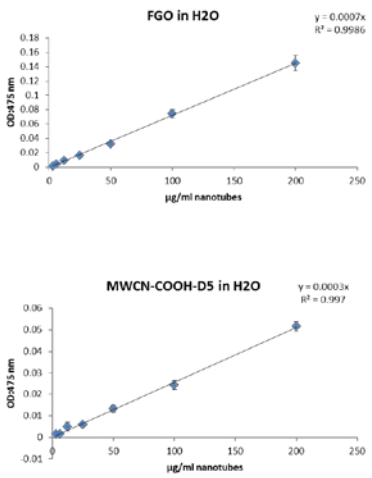

Figure 6. D5-MWCNT and FGO are well dispersed in aqueous media.

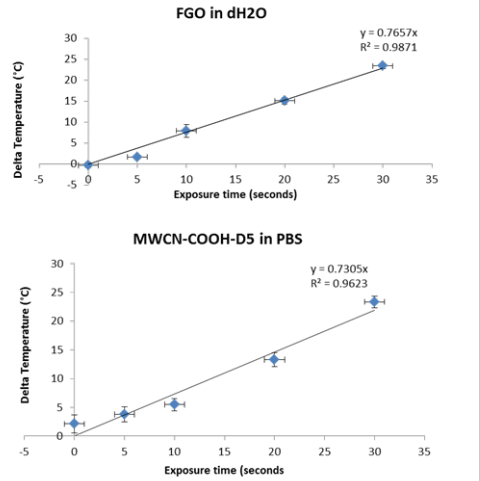

Figure 7. D5-MWCNT and FGO cause an increase in temperature following illumination with NIR.

Task 3.1. Objective: Determine number of cells necessary to achieve efficient tumor take.
Results, Progress and Accomplishments: We determined that we could reproducibly obtain tumors of the appropriate dimension to be encompassed by the laser beam (~6 mm) by implanting RENCA tumor fragments of 2 mm^3 into the flanks of athymic mice. Tumors reached maximal size (1000mm^3) in approximately 4 weeks.

Task 3.2 Objective: Assess the anti-tumor efficacy of unconjugated and D5 conjugated nanomaterials following direct injection into tumors.
Results, Progress and Accomplishments: We injected mice with tumor fragments to initiate these studies, but the tumors have not yet grown to sufficient size to enable injection of nanoparticles. Although we did not have time to complete these studies within the timeframe of this award, we plan to complete these studies with support from the PI's start-up funds. In particular, we will inject tumors with either saline (vehicle control), unconjugated MWCNT, FGO, or D5 conjugated MWCNT. Tumors will be illuminated with near-infrared laser light, and tumor growth monitored.

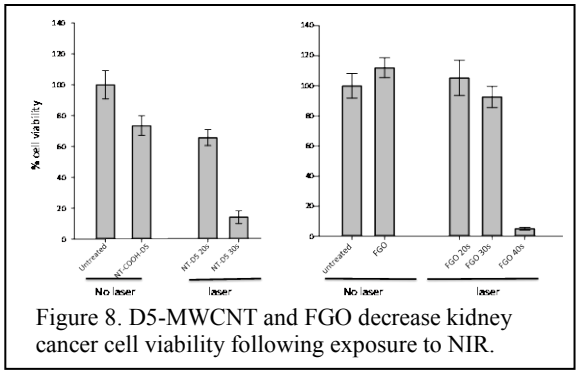

Figure 8. D5-MWCNT and FGO decrease kidney cancer cell viability following exposure to NIR.

Task 3.3. Objective: Assess the anti-tumor efficacy of unconjugated and D5 conjugated nanomaterials following intravenous injection.
Results: None to report. (However, see "other achievements" for experiments relevant to intravenous delivery of nanomaterials).

4. KEY RESEARCH ACCOMPLISHMENTS

- Determined that D5, a peptide derived from kininogen, can target UPAR and exert cytotoxic effects on kidney cancer cells and proliferating endothelial cells
- Successfully conjugated D5 to nanotubes
- Determined that D5-conjugated nanotubes are markedly effective in inhibiting the growth of kidney cancer cells
- Determined that fluorinated graphene oxide (FGO) is also effective in ablating kidney cancer cells and may be a suitable platform for further development

5. CONCLUSION

The research we conducted demonstrates that D5-conjugated nanotubes are highly effective anti-tumor agents in vitro. Since this grant was first awarded, concerns have surfaced about off-target toxicities of nanotubes. Our work has also demonstrated that fluorinated graphene oxide has promise as a nanomaterial that can effectively substitute for nanotubes, since it is characterized by many of the same beneficial attributes without

the potentially concerning "asbestos-like" attributes of nanotubes. Our goal is to follow-up on these findings in future work.

6. PUBLICATIONS, ABSTRACTS, PRESENTATIONS

1. Narayanan TN, Gupta BK, Vithayathil SA, Taha-Tijerina J, Xie B, Torti SV, Kaipparettu BA and Ajayan PM. Hybrid 2D Nanomaterials as Dual-mode Contrast Agents in Cellular Imaging. Advanced Materials 24:2992-8, 2012. PMID:22573478.
2. Ravi N. Singh*, Peter Alexander*, Andrew R. Burke, Frank M. Torti, Suzy V. TortiCarbon Nanotubes for Thermal Therapy. *In* Cancer Nanotechnology: Principles and Applications in Radiation Oncology. Edited by Sang Hyun Cho, Ph.D., Georgia Institute of Technology and Sunil Krishnan, M.D., The University of Texas M. D. Anderson Cancer Center CRC Press, Taylor & Francis Group, Boca Raton, FL, 2013.
3. Carboni, E, Torti SV, Ma A. A microfluidic study of nanoparticles in simulated blood flows: understanding the effect of margination The Society of Rheology 84th Annual Meeting, Pasadena, CA, Feb. 2013.
4. Singh R, Torti SV. Carbon Nanotubes in hyperthermia therapy. Adv Drug Deliv Rev 2013 Aug 8. doi:pii: S0169-409X(13)00184-1. 10.1016/j.addr.2013.08.001. [Epub ahead of print] PMID: 23933617
5. Romero-Aburto R, Narayanan TN, Nagaoka Y, Hasumura T, Mitcham TM, Fukuda T, Cox PJ, Bouchard RR, Maekawa T, Kumar DS, Torti SV, Mani Sa, Ajayan PM. Fluorinated graphene oxide: a new multimodal material for biological applications. Adv Mater 2013; 25(39):5632-7.
6. Torti SV. Nanomaterials in Photothermal Therapy. Invited seminar, Dept. Material Science and Engineering, Rensselaer Polytechnic, NY, Oct 29 2014.

Personnel receiving pay from the research effort:

Suzy V. Torti, Peter Alexander, Erik Carboni, Grant Bouchillon, Lia Tesfay, Heather Hatcher, Ben Wertz, Michael Gorczynski, Rachel R. Tenney, Rebeca Romero Aburto, Chardutta C. Galande

7. INVENTIONS, PATENTS, LICENSES – none to report
8. REPORTABLE OUTCOMES

D5-conjugated MWCNTs, a material that in the future may be commercialized as an agent for photothermal tumor ablation.

9. OTHER ACHIEVEMENTS

The optimal use of nanomaterials for treatment of cancer following systemic delivery would benefit from a detailed understanding of the passage of nanomaterials through the bloodstream. Since we were contemplating the systemic delivery of D5-nanomaterials, Eric Carboni, a student supported by this award, performed some experiments to understand the passage of nanomaterials in flowing liquids. This work was described in an earlier progress report and is reproduced here.

Specific Aim 3 is directed at the delivery of nanoparticles to tumor sites in vivo. While awaiting approval to conduct these experiments in mice, we conducted microfluidic studies to simulate the passage of these nanoparticles in blood vessels. This should be of enormous assistance in planning effective in vivo experiments.

When injected intravenously, nanoparticles must be able to tolerate flow in blood vessels and resist aggregation, and must also penetrate and stay within the tumor region. These particles are believed to accumulate in tumor cells due to the Enhanced Permeability and Retention (EPR) effect, as a direct result of the irregular and "leaky" vascular structures typically found in tumor sites.[1,2]. Normal endothelial cell interstitial spacing is on the order of 1-2 nm, whereas tumor-affected vasculature exhibits a pore size of anywhere from 100 to 780 nm. Many studies postulate that this abnormally large pore size will allow for enhanced uptake of small, drug-containing

nanoparticles by the tumor, as compared to regular tissue. However, the interstitial fluid pressure in a tumor is higher than the capillary pressure of blood vessels as a result of protein buildup in the tumor, thereby creating a pressure gradient that leads to an outward convection and low hydraulic conductivity, both of which oppose inward diffusion. As a result, it is questionable as to the exact nature of the EPR effect and whether even small particles, such as drug-containing solid lipid nanoparticles, will be able to successfully diffuse into and remain in the *tumor.*

However, there also exists the possibility that nanoparticles may exhibit margination, wherein they are moved closer to the periphery of the blood vessels as a result of the forces resulting from blood flow. Margination is responsible for the movement of white blood cells towards the blood vessel periphery and red blood cells towards the center of the blood vessel and is a result of hydrodynamic forces, inertial forces, and particle shape and size. It is vital to better understand this phenomena before exploring the EPR effect, as margination has an enormous impact in drug delivery because it affects the proximity of drug carriers to the periphery of blood vessels and, by extension, the diffusion of the drug into tissue cells from the blood stream.

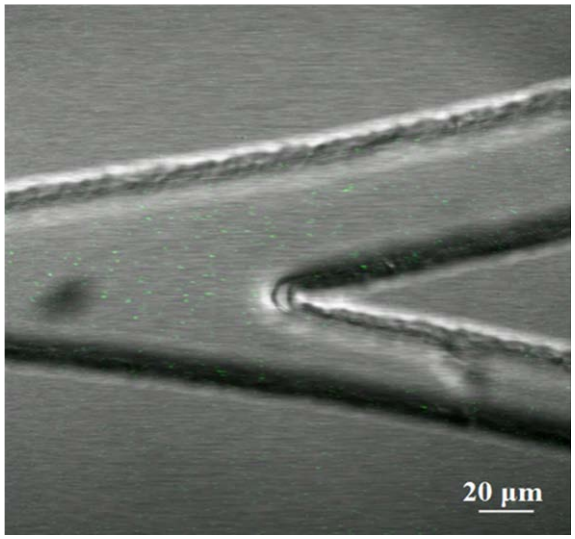

Figure 9. Confocal image of 0.1 micron (100 nm) polymer beads (Fluoresbrite® YG Microspheres 0.10 µm, Polysciences Inc.) in a polydimethylsiloxane microfluidic device. The device's main channel has 50 micron width and 62 micron depth and bifurcates into a channel of identical dimensions (top channel in figure) and a channel of 30 micron width and 62 micron depth (bottom channel).

Because of their large aspect ratio, it is unknown how nanotubes will behave in blood flow and whether or not they will exhibit margination. We therefore investigated margination behavior of various shapes and sizes of particles through the use of microfluidics. Microfluidics utilizes micron-scale devices, typically fabricated using polydimethylsiloxane polymer via soft lithography techniques. By creating such a device, a simulated channel can be created and the margination of carbon nanotubes in a flowing media, such as blood, can be observed and studied. The goal is to achieve a better understanding by observing the margination effect in vitro and to ultimately characterize and accurately predict and model this effect via experimental trials and the use of image-analysis and particle tracking software.

To begin, a procedure for making microfluidic devices was developed with the help of the Shor lab at UConn. Once devices were easily reproducible, a simple system was used consisting of spherical 100 nm diameter polystyrene beads (Fluoresbrite® YG beads; Polysciences Inc.) in water in a microfluidic device (**Figure 9**). These particles were imaged using a confocal microscope but they were very difficult to track as an initial, model system. For this reason, 0.5 micron beads were used in order to develop particle tracking procedures.

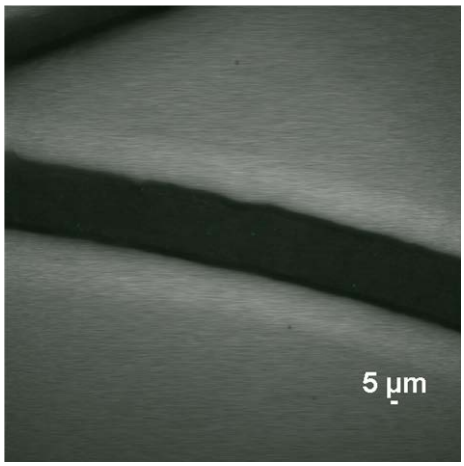

Figure 10 Confocal image of fluorescent, 0.5 micron polystyrene beads (Fluoresbrite® Carboxylated YG Microspheres 0.5 µm, Polysciences Inc.) diluted 1:3000 times in bovine blood and flowing through a 50 micron wide and 62 micron deep channel in the microfluidic device.

It was important to ensure a physiologically relevant flow rate before introducing blood into the system. A flow rate of 0.6 microliters per minute was calculated, in order to achieve the physiologically relevant flow rate of 0.328 mm/s. This flow rate was achieved via the use of a syringe pump, which was hooked up to the microfluidic device while the device was imaged via the use of the confocal microscope. In order to check that the pump was working properly, beads were tracked using ImageJ software and an average velocity of 0.623 mm/s was calculated, which is comparable to the expected syringe pump flow rate of 0.328 mm/s.[3]. This flow rate istherefore physiologically relevant.

Finally, a trial was conducted using 0.5 micron beads in bovine blood. As can be seen in **Figure 10**, the beads can be easily visualized in blood and, therefore, are trackable. By using the capability of the confocal microscope to image only a very thin depth of the device, margination near the walls of the device can be observed and particle motion and margination propensity can be quantified. Future trials will observe particle behavior at the bifurcation of the device and also the effects of size, shape, and other properties on nanoparticle margination propensity.

REFERENCES

1. Maeda, H.; Greish, K.; Fang, J. The EPR effect and polymeric drugs: A paradigm shift for cancer chemotherapy in the 21st century. *R. Satchi-Fainaro and R. Duncan (ed.)*. **2006**, Springer Berlin, 103-121.
2. Fang, J.; Nakamura, H.; Maeda, H. The EPR effect: Unique features of tumor blood vessels for drug delivery, factors involved, and limitations and augmentation of the effect. *Adv. Drug Deliv. Rev*. **2011**, 63, 136-151.
3. Gentile, F. et al. The margination propensity of spherical particles for vascular targeting in the microcirculation. J. Nanobio. 2008, 6, 1-9.

10. APPENDICES

Publications:

- Narayanan TN, Gupta BK, Vithayathil SA, Taha-Tijerina J, Xie B, Torti SV, Kaipparettu BA and Ajayan PM. Hybrid 2D Nanomaterials as Dual-mode Contrast Agents in Cellular Imaging. Advanced Materials 24:2992-8, 2012. PMID:22573478.
- Ravi N. Singh*, Peter Alexander*, Andrew R. Burke, Frank M. Torti, Suzy V. TortiCarbon Nanotubes for Thermal Therapy. In Cancer Nanotechnology: Principles and Applications in Radiation Oncology. Edited by Sang Hyun Cho, Ph.D., Georgia Institute of Technology and Sunil Krishnan, M.D., The University of Texas M. D. Anderson Cancer Center CRC Press, Taylor & Francis Group, Boca Raton, FL, 2013.
- Singh R, Torti SV. Carbon Nanotubes in hyperthermia therapy. Adv Drug Deliv Rev 2013 Aug 8. doi:pii: S0169-409X(13)00184-1. 10.1016/j.addr.2013.08.001. [Epub ahead of print] PMID: 23933617
- Romero-Aburto R, Narayanan TN, Nagaoka Y, Hasumura T, Mitcham TM, Fukuda T, Cox PJ, Bouchard RR, Maekawa T, Kumar DS, Torti SV, Mani Sa, Ajayan PM. Fluorinated graphene oxide: a new multimodal material for biological applications. Adv Mater 2013; 25(39):5632-7.

11. OPPORTUNITIES FOR TRAINING AND PROFESSIONAL DEVELOPMENT OF TRAINEES

One benefit of the relocation that occurred during the course of this research was that I was able to expose three trainees to research in the field of kidney cancer and nanomaterials. All of these students are still in training at the time of writing of this report. In addition, the sub-awardees on this proposal conducted their research with support of graduate students, so that the total number of students exposed to this type of research as a result of this award is at least four. Since the students came from diverse backgrounds, they each learned something quite different: Peter Alexander, a graduate student in the Cancer Bioogy Program, learned a considerable amount about materials science and nanoparticles, whereas Erik Carboni and Grant Bouchillion, graduate students in Engineering and Materials Science, were exposed to kidney cancer biology and models of kidney

cancer. All students profited from studying the use of nanoparticles in anti-cancer therapy. As a mentor, I in turn learned a great deal from each of these students, including how to make concepts accessible to students from diverse scientific backgrounds.

Specific training for all trainees included one-on-one work with me and senior research personnel in my laboratory, participation and presentation in group meetings, and formal presentations in Departmental seminars. In addition, Peter Alexander attended the Nano Conference in January 2011 sponsored by the American Association for Cancer Research. He also attended the NCL Lessons Learned Workshop sponsored by the National Cancer Institute NanoCharacterization Laboratory in June 2011. He formally presented his research at in an invited seminar at Wistar Institute in Pennsylvania in 2011. In 2012, he attended the national meeting of the American Association for Cancer Research. Erik Carboni presented an abstract at the 84th Annual Meeting of the Society of Rheology in 2013.

Fluorinated Graphene Oxide; a New Multimodal Material for Biological Applications

Rebeca Romero-Aburto, Tharangattu. N. Narayanan, Yutaka Nagaoka, Takashi Hasumura, Trevor M. Mitcham, Takahiro Fukuda, Paris J. Cox, Richard R. Bouchard, Toru Maekawa, D. Sakthi Kumar, Suzy V. Torti, Sendurai A. Mani, and Pulickel M. Ajayan**

Recent advancement in drug delivery using nanotechnology achieves enhanced circulation half-life and controllable drug release. Some of the newer drug delivery approaches utilize a combination of materials to achieve multimodality, such as, one material serves as a biocompatible photothermal near infra-red (NIR) laser inducible agent that can be loaded with drug, while the second material in the system might work as a clinical contrast agent for magnetic resonance imaging (MRI) or ultrasound. However, few single materials with such multimodal capabilities are reported.[1,2]

Among the known multimodal composites, the most widely used consists of gold nanoparticles (AuNPs) that are color tunable from the visible to NIR region. In addition to inducing hyperthermia and/or drug release due to their plasmonic properties.[3–7] Carbon materials, such as carbon nanotubes (CNTs), graphene and specifically graphene oxide (GO) have been studied for biological applications including drug delivery, and biosensing.[8–22] The presence of diverse functional groups in GO allow chemical incorporation of targeting agents, or therapeutically relevant molecules,[23–26] such as physical adsorption via π–π stacking interactions.[27] Due to the excellent charge transfer properties of CNTs and GO, they have been used to achieve hyperthermia.[28] However, for MRI, either gold nanoparticles or carbon nanomaterials are not sufficient to perform as contrast agents. Therefore, super-paramagnetic iron oxide nanoparticles (SPION) have been assorted with approaches containing AuNPs,[29,30] CNT's or GO[31–34] to create composites that serve as MRI contrast agents. MRI is desirable due to the ability to resolve physiological and anatomical details without utilizing ionizing radiation. Until now, there are no reports that show carbon materials conferring MRI contrast without the incorporation of magnetic nanoparticles.

In addition to the above mentioned agents, fluorinated (^{19}F) contrast agents are highly desirable due to the scarce distribution of fluorine in the human body and their ability to be detected by magnetic resonance imaging (MRI)[35] as well as ultrasound.[36] Moreover, several fluorine (F) containing compounds have also been widely used in medicine as therapeutic drugs.[37] At present, to achieve combined MRI and ultrasonography, perfluorocarbon microbubbles (PFCMB), the state of the art in contrast agents for ultrasonography,[38,39] have been combined with SPIONs to confer MRI detection.[40]

Recently, we developed a novel method to synthesize large quantities of fluorinated graphene oxide (FGO), and extensive characterization of the material has been reported.[41,42] In this manuscript we demonstrate FGO as a multimodal material for biological applications. In fact, we found FGO being the first carbon material to confer MRI without the addition of magnetic nanoparticles. Similar to GO, synthesized FGO has several functional groups in its lattice thus allowing for the same diverse chemical functionalization and loading capabilities as GO. Moreover, FGO like other carbon materials is proven to absorb NIR-laser energy and efficiently transform it into heat. MRI studies conducted on FGO phantoms were seen to exhibit higher negative contrast than GO phantoms. Under a rotational magnetic field FGO is responsive to a 12 mT field. Ultrasound showed FGO to be hyperechoic in comparison to anechoic agar. In summary, we report FGO as a single multimodal material capable of serving as a contrast agent for MRI, ultrasound and photoacoustic imaging. Furthermore, FGO serves as a targetable drug carrier and NIR laser inducible hyperthermic material that can ablate thermosensitive cancer cells.

Although GO has been extensively reported for its biomedical applications, including in vivo strategies, recent reports suggest

R. Romero-Aburto, Dr. T. N. Narayanan, Dr. P. J. Cox, Prof. P. M. Ajayan
Department of Mechanical Engineering & Materials Science
Rice University
6100 Main St. Houston, TX, 77005, USA
E-mail: ajayan@rice.edu
R. Romero-Aburto, Prof. S. A. Mani
Department of Translational Molecular Pathology
MD Anderson Cancer Center
7435 Fannin Street, Houston, TX, 77054, USA
Email: smani@mdanderson.org
Dr. Y. Nagaoka, Dr. T. Hasumura, Dr. T. Fukuda, Prof. T. Maekawa, Prof. D. S. Kumar
Bio-Nano Electronics Research Center
Toyo University
2100, Kujirai, Kawagoe, Saitama, 350 8585, Japan
T. M. Mitcham, Prof. R. R. Bouchard
Department of Imaging Physics
MD Anderson Cancer Center
1881 East Rd. Houston, TX, 77054, USA
Prof. S.V. Torti
Department of Molecular Microbial and Structural Biology
University of Connecticut Health Center
263 Farmington Ave, Farmington, CT06030, USA
Dr. T. N. Narayanan
CSIR-Central Electrochemical Research Institute
Karaikudi, 630 006, Tamilnadu, India

DOI: 10.1002/adma201301804

that various negatively charged functional groups present in GO can induce thromboembolism (aggregation of platelets in blood).[43] Singh et al. reported that surface charge of graphene could play a key role in the interaction between graphene and platelets. Furthermore, they demonstrated that amine functionalized graphene is a better candidate for biomedical applications due to its positive surface charge, hence avoiding thrombotic and hemolytic predisposition.[44] This can be due to the $-NH_3^+$ formation of $-NH_2$ with the adjacent proton in solution or at the interface with biomolecules. Fluorine also modifies the electronic properties of graphene by reducing the charge in the conducting π orbitals.[45] Hence low level inhomogeneous doping of highly electronegative F can induce partial positive surfaces on graphene. However, complete spatial charge separation is unlikely due to the high charge mobility of graphene. The hydrophobic centers in FGO (or fluorinated graphene in the case of reduced FGO) may also act as energetic barriers between platelet membrane and FGO, hence preventing thromboembolism. Moreover, F doping can greatly increase the lipophilicity of drug carrier/molecule, an important consideration when designing drug delivery systems/molecules that are designed to be active in vivo.[46]

Similar to oxidizing chemical exfoliation of the graphite basal plane, which introduces functional groups generating GO,[47,48] we exfoliated fluorinated graphite and produced FGO. The resulting FGO is composed of alkyl fluorides, epoxy, carbonyl, carboxylic and hydroxyl groups covalently bonded to the carbon lattice.[41] Most importantly, addition of these oxygen functionalities makes FGO hydrophilic.[41] Further characterization of FGO suggested a sheet like morphology evidenced by atomic force microscopy (AFM) (**Figure 1**A, Figure S1A, Supporting Information), transmission electron microscopy (TEM) (Figure 1B) and scanning electron microscopy (SEM) (Figure S1B, Supporting Information), corresponding to traditional 2D graphene material. The AFM results suggest that the thickness of a typical FGO sheet is <1 nm, indicating the presence of 1–2 layered FGO. The lateral width seems to be around 1 µm and it correlates with the TEM data.

Incubation of FGO with cells from the human breast cancer cell line, MCF-7, did not show any cytotoxicity even after 3 days with a concentration of up to 576 µg mL^{-1} (Figure 1C). This clearly shows that FGO is potentially nontoxic similar to the previous finding for GO using various other cell lines, predominantly due to the availability of various oxygen containing functional groups.[49–51]

Functional groups in FGO permit π–π stacking interactions or covalent bonding of therapeutic and targeting agents. To load chemotherapeutics, such as Doxorubicin (DOX) by means of π–π stacking interactions, DOX was mixed with FGO-COOH (1:1 v/v) overnight at 4 °C and after centrifugal washes to separate the unbound drug UV–vis spectroscopic analysis was performed to identify the interaction between DOX molecule and FGO. DOX (≈480 nm)[52] as well as FGO (≈230 nm)[24] displayed their characteristic peaks in UV–vis spectra consistent with earlier reports. Besides, an additional peak is observed at ≈490 nm in FGO loaded with doxorubicin (FGO-DOX) indicative of DOX interaction with FGO through non-covalent attractive forces (Figure 1D).[53] Moreover, using photoluminescence, we found a reduction in DOX fluorescence due to quenching mediated

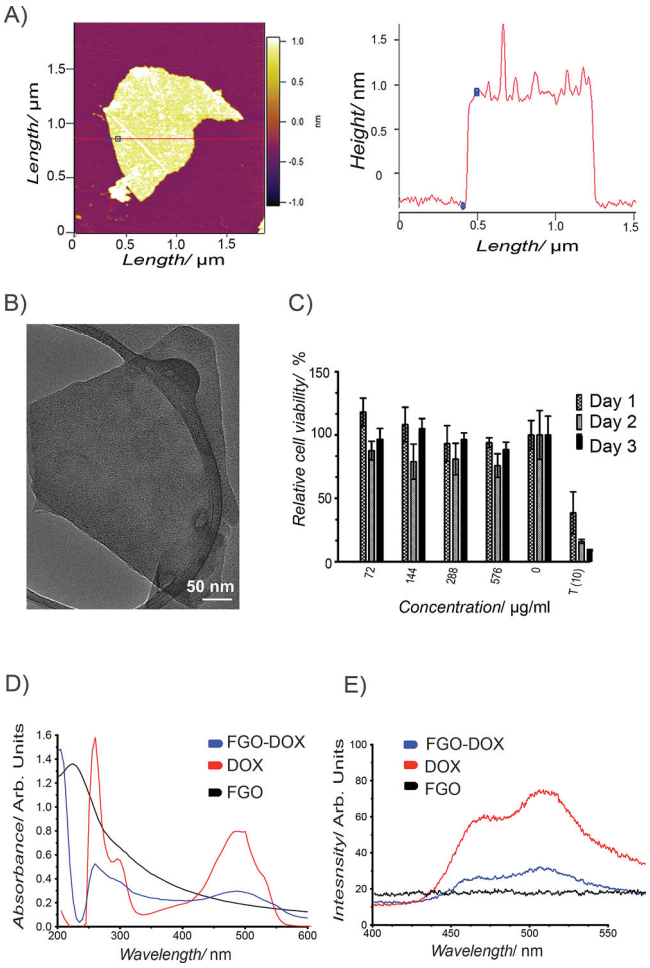

Figure 1. FGO Characterization. A) AFM analysis of FGO including height profile. B) TEM image of FGO. C) Concentration and time dependent MTT assay to determine cell viability after incubation with FGO, T(10) is the positive control (taxol 10 µg mL^{-1}). Bars denote mean standard deviation error. D) Absorption spectra of FGO-DOX (blue), DOX (red) and FGO (black). E) Photoluminescence spectra of FGO-DOX (blue), DOX (red), FGO (black).

by the interaction with FGO (Figure 1E). Collectively, these data suggest that FGO could be used to non-covalently load therapeutic agents.

The presence of fluorine in FGO's basal plane (dipolar C–F bonds) can introduce paramagnetic centers. In fact, using superconducting quantum interference device (SQUID) characterization at 300 K, we found a linear dependency to the magnetic field, proving that FGO exhibits paramagnetic behavior (**Figure 2**A). Since FGO is responsive to a 5 T magnetic field (Figure 2A), we scanned MRI phantoms on a 4.7 T Biospec System (Figure 2B) to determine if FGO could serve as an MRI contrast agent. Due to structural similarities between FGO and GO, we compared them for their ability to serve as MRI contrast agents. As predicted, FGO exhibits contrast in T_2 mode (Figure 2B) while GO did not. We used relaxed water (0.5 mg mL^{-1} of magnevist) as a positive control. This suggest that the paramagnetic behavior in FGO is attributed to the presence of fluorine (C–F bonds), therefore in biological environments,

ADVANCED MATERIALS
www.advmat.de

www.MaterialsViews.com

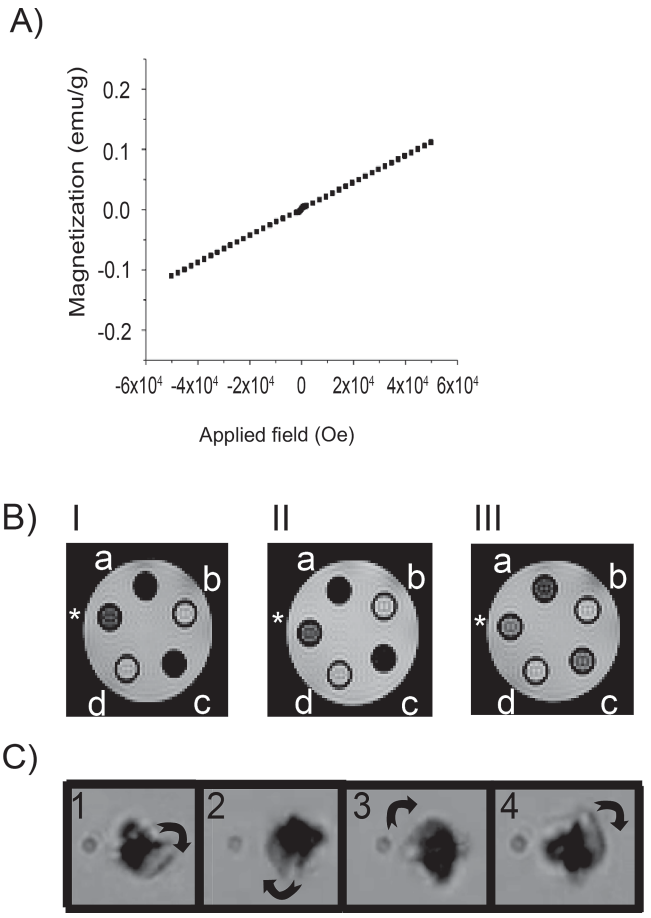

Figure 2. Magnetic properties of FGO. A) SQUID magnetization curve. B) Spin-spin (T_2) relaxation measurements acquired on a 4.7 T MRI of FGO (I: $a = 625$, $c = 500$; II: $a = 313$, $c = 250$; III: $a = 156$, $c = 125\mu g\ mL^{-1}$) and GO (I: $b = 625$, $d = 500$; II: $b = 313$, $d = 250$; III: $b = 156$, $d = 125\mu g\ mL^{-1}$). The positive control (*) consists of diluted magnevist ($0.5mg\ mL^{-1}$). C) Rotational magnetic field snapshots of FGO under a field of 12 mT, rotation is clockwise.

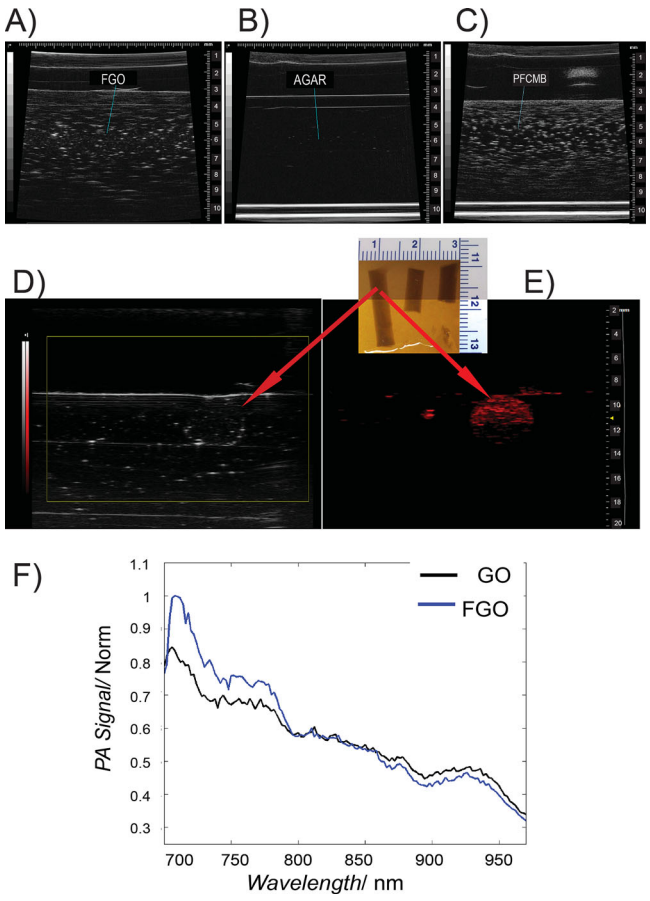

Figure 3. Ultrasound and photoacoustic behavior of FGO. A) Ultrasound imaging of FGO, B) Agar and C) perfluorocarbon microbubbles (PFCMB) in a 40 MHz linear array transducer. D,E) Photoacoustic FGO gelatin phantom under a 21 MHz ultrasound equipment coupled with a VisualSonics Vevo LAZR system at 720 nm. F) Photoacoustic normalized signal spectrum of FGO (blue) and GO (black).

materials like FGO will have higher signal to noise ratio because of the scarce distribution of ^{19}F as opposed to protons (^{1}H) in the body. To further test FGO's magnetic response, rotational magnetic field experiments were performed under an optical microscope (details are provided in the supporting information) and snapshots taken from the recorded video fragments (Figure 2C). The results show that FGO can be magnetically triggered, even with a small system of electromagnets having a magnetic field of 12 mT, which is further evident in the video (Supporting Information, Video 1). This emphasizes the dramatic change in physical properties of GO due to the presence of small amounts of F in its lattice.

Earlier experiments conducted to compare diagnostic techniques to detect breast cancer revealed that the combination of MRI and ultrasound yields the best results.[54] Since FGO has been proven to confer MRI contrast; we also investigated its ability as an ultrasound detection agent. FGO was imaged at a 40 MHz center frequency and generated appreciable acoustic backscattering, as demonstrated by the hyperechoic regions in **Figure 3**A. As expected, pure agar without added scatterers, which served as the negative control, presented as entirely anechoic (Figure 3B), while the positive control PFCMB, generated a strong backscatter signal (Figure 3C). Most importantly, we observed a strong backscatter signal using FGO's ($291.2\ \mu g\ mL^{-1}$), which is qualitatively significantly stronger than pure agar. These results suggest that FGO could be used as an ultrasound contrast agent. The spectroscopic imaging of FGO and GO generated similar photoacoustic signal spectrum (Figure 3F), which peaked at 720 nm. When evaluated at a preclinical frequency (21 MHz), FGO was well visualized with PA imaging (Figure 3E), while it was poorly visualized when relying on ultrasound alone (Figure 3D). The inability of FGO to provide a better ultrasound signal is probably due to the reduction in frequency from 40 to 21 MHz.

The value of a drug carrier like FGOs can be maximized if this material can be photoheated, due to its applicability as a cancer photothermal therapy.[55–57] Cell culture conditions were used to investigate the hyperthermic ability of FGO when irradiated with an 800 nm NIR laser (Chameleon Ultra, Coherent Inc.), with a power of 1.6 W (details are given in experimental

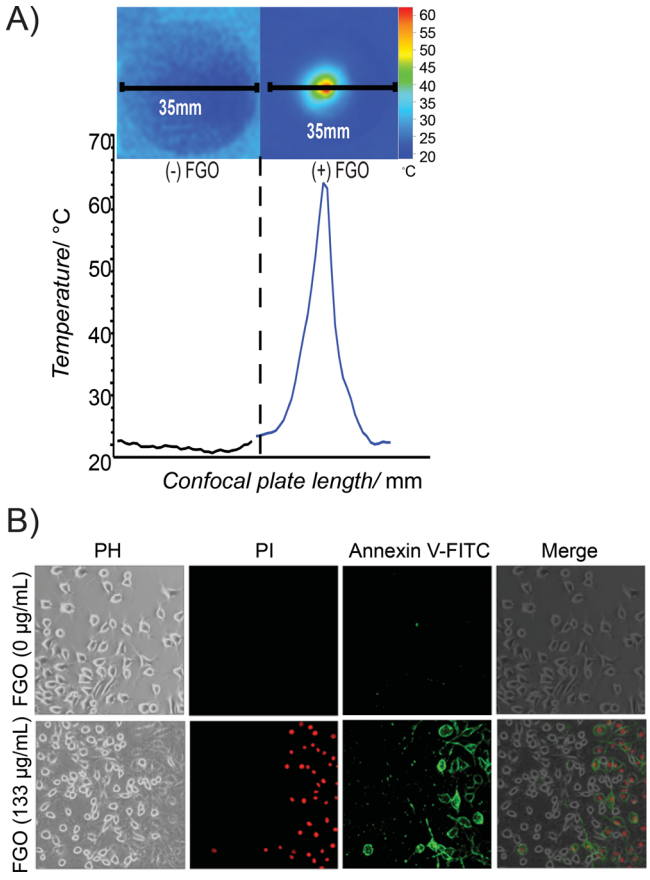

Figure 4. Hyperthermia cell ablation facilitated by FGO. A) NIR-laser-induced hyperthermia of DMEM (-) FGO and of (+) FGO. Each confocal plate length is 35 mm. B) In vitro NIR-laser induced differential photothermal ablation of glioma cells (GI-1) incubated with 0 µg mL^{-1} of FGO (top) or 133 µg mL^{-1} of FGO (bottom) using an apoptotic/necrotic staining and observed by optical microscopy.

section). Temperature of the tissue culture sample containing FGO increased to 62.3 °C within 1 min of irradiation, relative to control culture media without FGO, which remained at ≤25.0 °C following irradiation (**Figure 4**A). To test, whether NIR laser energy transformed to heat by FGO could induce cell death, we exposed glioma cancer cells (GI-1), in the presence and absence of FGO and irradiated them with NIR laser. The cells containing FGO exhibited significant cell death evidenced by an increase in staining for necrosis related to propidium iodide as well as apoptosis related annexin-5-fluorescein isothiocyanate (annexin-V-FITC) (bottom panel of Figure 4B) compared to the cells without FGO (top panel of Figure 4B). Collectively, these findings indicate that FGO could be used to increase the local temperature and induce cell death. Since we observed that heat dissipation occurs within 1 min after laser irradiation and there are no indicatives of apoptosis or necrosis outside the irradiation radial zone; suggesting that FGO can be used to specifically ablate cancer tissues without damaging nearby healthy tissues (top panel of Figure 4B).[58]

The results presented here indicate that FGO is a theranostic material that exhibits multimodal imaging, including MRI, ultrasound and photoacoustic. Furthermore, drug loading as well as the ability to induce hyperthermia via NIR laser can be achieved with FGO. A strong backscattering signal from FGO was observed under ultrasonography, opening the possibility for a second imaging modality. One limitation of using FGO in ultrasonography is the requirement of micron-size scatterers, which would tend to limit the agent to the vasculature. Nevertheless, for photoacoustic imaging, the scatterer's size is no longer a requirement. Therefore, FGO's ability to absorb NIR laser energy makes it suitable for photoacoustic imaging, thus enabling micro or nanoscopic FGO to be employed in strategies that seek crossing the vasculature. Additionally, the ability to convert the absorbed NIR laser energy into heat to increase the local temperature could serves as an excellent therapeutic agent against cancer cells that are sensitive to higher temperatures. The induced hyperthermia can potentially be employed as a release mechanism for therapeutic agents that have been conjugated to FGO. Moreover, attaching a targeting entity to the loaded nano-FGO will facilitate selective targeting to the tumor environment or tissue of interest.

In conclusion, we found that FGO is a novel carbon material with clinically translatable multimodal capabilities. These include, the ability to serve as MRI, ultrasound and photoacoustic contrast agents, as well as having the potential to load hydrophobic therapeutic agents to the hydrophilic FGO basal plane. Notably, it can serve as a photothermal ablation agent when irradiated with a NIR laser. Future refinement and differential size selection of FGO as well as testing targeted nano-FGO for its synergistic hyperthermia and drug release in vitro and in vivo will make FGO a more attractive agent for various diseases including cancer.

Experimental Section

Preparation of Fluorinated Graphene Oxide (FGO): Briefly, graphite fluorinated polymer (2 g) (Alfa Aesar, Ward Hill, MA, USA) was exfoliated using the modified Hummer's method. A detailed synthesis protocol has been reported elsewhere.[41,47]

Particle Shape and Morphology: Drop-cast powder FGO morphology was obtained by field emission SEM (FEI Quanta 400) with a working voltage of 10 kV. A JEOL 2100 field emission gun transmission electron microscope was used to image the drop-cast FGO solution on a copper holey carbon grid with a working voltage of 200 kV. AFM images were obtained at ambient conditions using an Asylum Research model MFP-3D instrument.

Cytotoxicity Studies: Cells were cultured and maintained in Dulbecco's modified Eagle medium (DMEM) (Invitrogen) containing fetal bovine serum (FBS) (10%) and penicillin/streptomycin (P/S) (1%) antibiotics. The same medium was used as a solvent for the serial dilutions of FGO. Cells from a human breast cancer cell line, MCF-7 (from ATCC), were seeded in a 96-well plate (1×10^3 cells/well; 100 µL/well) and incubated for 1 day to allow cell adhesion to the plate. On the following day, different concentrations of FGO (50 µL) were added to each well giving final concentrations of 72, 144, 287, and 575 µg mL^{-1} respectively and incubated for 24, 48 and 72 h. At the end of the study, 3-(4,5-dimethyl-2-thiazolyl)-2,5-diphenyltetrazolium bromide (MTT) (5 mg mL^{-1}, 50 µL/well) was added and incubated for 4.5 h. After MTT removal, dimethyl sulfoxide (DMSO) (200 µL/well) was added; the reagent was left for 10 min before optical density of solubilized formazan salts was assessed at 570 nm in a µQuantplate reader (Bio-Tek Instruments Inc.)

Drug-Loading Characterization: Room-temperature absorbance measurements were carried out in a Beckman Coulter DU730

spectrophotometer from 200 to 700 nm. Photoluminescence experiments were done in a Hitachi F-4500 fluorescence spectrometer with a 150 W Xe lamp as a light source (λ_{ex} = 300 nm) and a step of 0.2nm.

Magnetization Measurements: A superconducting quantum interference device (SQUID) (Quantum Design) was used to measure the room-temperature magnetic properties of the FGO powders.

Magnetic Resonance Imaging (MRI) Phantoms: All the relaxation measurements were performed using a 4.7 T Biospec system (Bruker Biospin MRI, Billerica, MA) with a 30 cm bore, imaging gradients with an inner diameter of 60 mm, and a volume resonator with 35 mm inner diameter. Serial dilutions of the contrast agent were sealed in NMR spectroscopy tubes and suspended in relaxed water in order to minimize the effects of susceptibility differences between the samples and their surroundings. Spin-spin (T_2) relaxation times were measured using a multiecho spin-echo sequence (TEmin = 8.5 ms, with 8.5 ms echo spacing over 24 echoes; T_R = 5000 ms). All the images were acquired with matching slice geometry (1 mm axial sections, 32 mm x 32 mm field-of-view over a 64 × 64 image matrix).

Ultrasound and Photoacoustic Phantoms: Photoacoustic and ultrasound imaging were performed using VisualSonics Vevo LAZR-2100 high-frequency photoacoustic and VisualSonics VEVO 770 B-mode ultrasound system. In the ultrasound imaging study, acoustic coupling was achieved through ultrasound gel. Ultrasound phantom plates were scanned using a 40 MHz linear array transducer, to acquire a cross-sectional image. The gain was set to 10 dB, and all the samples were scanned under the same experimental conditions. In the photoacoustic imaging study, FGO was imaged spectroscopically with a 21 MHz linear array from 680 to 970 nm to determine the peak signal produced by FGO and GO. FGO gelatin phantoms were then imaged at 720 nm to acquire a cross-sectional image; acoustic coupling was achieved through a distilled water bath.

NIR Laser-Induced Photoheating: The irradiation power of the NIR laser was 1.6 W, determined by a power meter (VEGA, OPHIR Japan, Ltd.). In situ samples where exposed for 1 min to the NIR-laser and the thermal profiles were measured. The sample preparation consisted of aqueous solution of FGO (1 mg mL^{-1}, 100 µL) added to a confocal plate (35 mm) containing DMEM (50 µL). The negative control consisted of DMEM (150 µL) added into a confocal plate (35 mm). To measure the thermal gradient we used a thermal imager test 881–2 (Testo AG, Germany). All the thermal data was analyzed with Testo IR software.[59]

In Vitro Hyperthermia Induced by NIR Laser: Glioma (GI-1) cells (from Riken Bio Resource Center, Japan) (5 × 10^4 cells per well) were seeded on a confocal plate (35 mm) with DMEM and incubated overnight at 37 °C and 5% CO_2. Sample preparation consisted of washing the cells with warm PBS and adding FGO (0, 400 µg mL^{-1}, 50 µL) respectively to the confocal plate that already had fresh warm DMEM (100 µL). The experimental conditions were the same as the in situ experiment. After laser exposure, cells were washed and stained using Annexin V-FITC apoptosis detection kit and its protocol. After incubation in darkness, the cells were observed at a magnification of 20× under an inverted confocal microscope IX81 (Olympus Corp.) with a confocal scanning unit CSU-X1 (Yokogawa Electric Corp.) and coupled to an iXon DU897 CCD camera (Andor Technology) utilizing laser wavelengths of 488 and 561 nm as well as phase contrast acquisition.

Supporting Information

Supporting Information is available from the Wiley Online Library or from the author.

Acknowledgements

The authors acknowledge Dr. Srivani Veeranarayanan, Dr. Athulya Aravind, Dr. Aby C. Polouse, and Dr. M Sheikh Mohamed for their help provided in the course of this research. This work was supported by the US Army Medical Research Acquisition Act (USAMRAA), award number W81XWH-10–1–0434, and partially supported by the IMI Program of the National Science Foundation under Award No. DMR 0843934. S.A.M. lab is supported by George and Barbara Bush Endowment for Innovative Cancer Research. The authors would also like to acknowledge Charles Kingsley and Keith A. Mitchel at the small-animal ultrasound and MRI facility at MD Anderson Cancer Center, which is funded by the Cancer Center Support Grant from the National Cancer Institute (CA16672).

Received: April 23, 2013
Revised: July 11, 2013
Published online: August 27, 2013

[1] J.-A. A. Ho, L.-S. Wang, M.-C. Chuang, *Int. J. Nanomed.* **2012**, 4679.
[2] Y. Xia, W. Li, C. M. Cobley, J. Chen, X. Xia, Q. Zhang, M. Yang, E. C. Cho, P. K. Brown, *Acc. Chem. Res.* **2011**, *44*, 914–924.
[3] S. Luo, E. Zhang, Y. Su, T. Cheng, C. Shi, *Biomaterials* **2011**, *32*, 7127–7138.
[4] A. M. Gobin, M. H. Lee, N. J. Halas, W. D. James, R. A. Drezek, J. L. West, *Nano Lett.* **2007**, *7*, 1929–1934.
[5] D. Pissuwan, S. M. Valenzuela, M. B. Cortie, *Trends Biotechnol.* **2006**, *24*, 62–67.
[6] J. You, G. Zhang, C. Li, *ACS Nano* **2010**, *4*, 1033–1041.
[7] 2009 pilot study of AuroLase therapy sponsored by Nanospectra Biosciences, Inc., http://clinicaltrials.gov/ct2/show/NCT00848042?term=aurolase&rank=2, Accessed: November 2012.
[8] Y. Wang, Z. Li, D. Hu, C.-T. Lin, J. Li, Y. Lin, *J. Am. Chem. Soc.* **2010**, *132*, 9274–9276.
[9] L. Feng, Z. Liu, *Nanomedicine* **2011**, *6*, 317–324.
[10] S. Bi, T. Zhao, B. Luo, *Chem. Commun.* **2012**, *48*, 106–108.
[11] V. Singh, D. Joung, L. Zhai, S. Das, S. I. Khondaker, S. Seal, *Prog. Mater. Sci.* **2011**, *56*, 1178–1271.
[12] K. Yang, L. Feng, X. Shi, Z. Liu, *Chem. Soc. Rev.* **2012**,*42*, 530–547.
[13] H. Shen, *Theranostics* **2012**, 283.
[14] F. Schedin, A. K. Geim, S. V. Morozov, E. W. Hill, P. Blake, M. I. Katsnelson, K. S. Novoselov, *Nat Mater* **2007**, *6*, 652–655.
[15] G. Gollavelli, Y.-C. Ling, *Biomaterials* **2012**, *33*, 2532–2545.
[16] Z. Liu, *Theranostics* **2012**, 235.
[17] E. Katz, *ChemPhysChem* **2004**.
[18] H. Bao, Y. Pan, L. Li, *Nano LIFE* **2012**, *02*, 1230001.
[19] A. Bahrami, *Ph.D. Thesis*, University of Cambridge, January 2011.
[20] X. Luo, C. Matranga, S. Tan, N. Alba, X. T. Cui, *Biomaterials* **2011**, *32*, 6316–6323.
[21] S. Park, N. Mohanty, J. W. Suk, A. Nagaraja, J. An, R. D. Piner, W. Cai, D. R. Dreyer, V. Berry, R. S. Ruoff, *Adv. Mater.* **2010**, *22*, 1736–1740.
[22] Y. Wang, Z. Li, J. Wang, J. Li, Y. Lin, *Trends Biotechnol.* **2011**, *29*, 205–212.
[23] L. Zhang, J. Xia, Q. Zhao, L. Liu, Z. Zhang, *Small* **2009**.
[24] W. Zhang, Z. Guo, D. Huang, Z. Liu, X. Guo, H. Zhong, *Biomaterials* **2011**, *32*, 8555–8561.
[25] K. P. Loh, Q. Bao, G. Eda, M. Chhowalla, *Nat. Chem.* **2010**, *2*, 1015–1024.
[26] L. Zhou, H. Jiang, S. Wei, X. Ge, J. Zhou, J. Shen, *Carbon* **2012**, *50*, 5594–5604.
[27] V. Georgakilas, M. Otyepka, A. B. Bourlinos, V. Chandra, N. Kim, K. C. Kemp, P. Hobza, R. Zboril, K. S. Kim, *Chem. Rev.* **2012**, *112*, 6156.
[28] M. P. Melancon, M. Zhou, C. Li, *Acc .Chem. Res.* **2011**, *44*, 947–956.
[29] X. Ji, R. Shao, A. M. Elliott, R. J. Stafford, E. Esparza-Coss, J. A. Bankson, G. Liang, Z. P. Luo, K. Park, J. T. Markert, C. Li, *J. Phys. Chem. C* **2007**, *111*, 6245–6251.
[30] T. A. Larson, J. Bankson, J. Aaron, K. Sokolov, *Nanotechnology* **2007**, *18*, 325101.

[31] X. Ma, H. Tao, K. Yang, L. Feng, L. Cheng, X. Shi, Y. Li, L. Guo, Z. Liu, *Nano Res.* **2012**, *5*, 199–212.
[32] T. N. Narayanan, B. K. Gupta, S. A. Vithayathil, R. R. Aburto, S. A. Mani, J. Taha-Tijerina, B. Xie, B. A. Kaipparettu, S. V. Torti, P. M. Ajayan, *Adv. Mater.* **2012**, *24*, 2992–2998.
[33] E. Vermisoglou, G. Pilatos, G. Romanos, E. Devlin, N. K. Kanellopoulos, G. N. Karanikolos, *Nanotechnology* **2011**, *22*, 1–10.
[34] F. He, J. Fan, D. Ma, L. Zhang, C. Leung, H. L. Chan, *Carbon* **2010**, *48*, 3139–3144.
[35] J. Ruiz Cabello, B. P. Barnett, P. A. Bottomley, J. W. M. Bulte, *NMR Biomed.* **2011**, *24*, 114–129.
[36] R. Díaz-López, N. Tsapis, E. Fattal, *Pharm. Res.* **2009**, *27*, 1–16.
[37] A. Strunecka, J. Patočka, P. Connett, *J. Appl. Biomed.* **2004**, *2*, 141–150.
[38] J. Riess, *Curr. Opin. Colloid Interface Sci.* **2003**, *8*, 259–266.
[39] F. Forsberg, N. Rawool, D. Merton, *Ultrasonics* **1996**.
[40] Z. Liu, T. Lammers, J. Ehling, S. Fokong, J. Bornemann, F. Kiessling, J. Gätjens, *Biomaterials* **2011**, *32*, 6155–6163.
[41] A. Mathkar, T. N. Narayanan, L. B. Alemany, P. Cox, P. Nguyen, G. Gao, P. Chang, R. Romero-Aburto, S. A. Mani, P. M. Ajayan, *Part. Part. Syst. Charact.* **2013**, *30*, 266–272.
[42] P. Chantharasupawaong, R. Philip, T. N. Narayanan, P. M. Sudeep, A. Mathkar, P. M. Ajayan, J. Thomas, *J. Phys. Chem. C* **2012**, *116*, 25955–25961.
[43] S. K. Singh, M. K. Singh, M. K. Nayak, S. Kumari, S. Shrivastava, J. J. A. Grácio, D. Dash, *ACS Nano* **2011**, *5*, 4987–4996.
[44] S. K. Singh, M. K. Singh, P. P. Kulkarni, V. K. Sonkar, J. J. A. Grácio, D. Dash, *ACS Nano* **2012**, *6*, 2731–2740.
[45] F. Karlicky, K. K. R. Datta, M. Otyepka, R. Zbořil, *ACS Nano* **2013**, DOI:10.1021/nn4024027.
[46] C. Heidelberger, D. Morren, L. Griesbach, B. J. Montag, R. Duschinsky, E. Pleven, R. Schnitzer, *Proc. Am. Assoc. Cancer Res.* **1957**, *2*, 212.
[47] D. C. Marcano, D. V. Kosynkin, J. M. Berlin, A. Sinitskii, Z. Sun, A. Slesarev, L. B. Alemany, W. Lu, J. M. Tour, *ACS Nano* **2010**, *4*, 4806–4814.
[48] W. Gao, L. B. Alemany, L. Ci, P. M. Ajayan, *Nat. Chem.* **2009**, *1*, 403–408.
[49] X. Sun, Z. Liu, K. Welsher, J. T. Robinson, A. Goodwin, S. Zaric, H. Dai, *Nano Res.* **2008**, *1*, 203–212.
[50] J. Peng, W. Gao, B. K. Gupta, Z. Liu, R. Romero-Aburto, L. Ge, L. Song, L. B. Alemany, X. Zhan, G. Gao, S. A. Vithayathil, B. A. Kaipparettu, A. A. Marti, T. Hayashi, J.-J. Zhu, P. M. Ajayan, *Nano Lett.* **2012**, *12*, 844–849.
[51] Z. Liu, J. T. Robinson, X. Sun, H. Dai, *J. Am. Chem. Soc.* **2008**, *130*, 10876–10877.
[52] G. Eda, Y. Y. Lin, C. Mattevi, H. Yamaguchi, *Adv. Mater.* **2010**, *22*, 505–509.
[53] X. Yang, X. Zhang, Z. Liu, Y. Ma, Y. Huang, Y. Chen, *J. Phys. Chem. C* **2008**, *112*, 17554–17558.
[54] T. Hata, H. Takahashi, K. Watanabe, M. Takahashi, K. Taguchi, T. Itoh, S. Todo, *J. Am. Coll. Surgeons* **2004**, *198*, 190–197.
[55] B. Tian, C. Wang, S. Zhang, L. Feng, Z. Liu, *ACS Nano* **2011**, *5*, 7000–7009.
[56] K. Yang, S. Zhang, G. Zhang, X. Sun, S.-T. Lee, Z. Liu, *Nano Lett.* **2010**, *10*, 3318–3323.
[57] J. T. Robinson, S. M. Tabakman, Y. Liang, H. Wang, H. Sanchez Casalongue, D. Vinh, H. Dai, *J. Am. Chem. Soc.* **2011**, *133*, 6825–6831.
[58] E. Moros, *Physics of Thermal Therapy*, CRC Press, Boca Raton, FL, USA **2012**.
[59] Testo AG 881-1 Thermal Imager (2011), http://www.testo.com, Accessed: July 2012

17

Carbon Nanotubes for Thermal Therapy

Ravi N. Singh
Wake Forest School of Medicine

Peter Alexander
Wake Forest School of Medicine

Andrew R. Burke
Wake Forest School of Medicine

Frank M. Torti
Wake Forest School of Medicine

Suzy V. Torti
Wake Forest School of Medicine

17.1 Introduction

Carbon nanotubes (CNTs) have generated enormous interest for a wealth of applications including field emission (Saito et al. 2002; Milne et al. 2004), energy storage (Patchkovskii et al. 2005), molecular electronics (Javey et al. 2003; Keren et al. 2003; Weisman 2003), and atomic force microscopy (Wong et al. 1998). These nanoparticles exhibit a number of novel properties including extraordinary strength, unique electrical properties, and a specific heat and thermal conductivity that are among the highest known for any material (Iijima 1991; Dresselhaus et al. 1995; Berber et al. 2000).

CNTs were first characterized by Ijima (1991) more than two decades ago. Initially, they were described as cylindrical molecules of pure carbon ranging from 1.4 nm in diameter for a single-walled nanotube (SWNT) to 30–50 nm for concentrically arranged, multiwalled nanotubes (MWNT) and possessed widely variable lengths on the order of several microns. Advances in the synthesis and processing of nanotubes have now made it possible to produce nanotubes with both well-defined wall numbers and narrow length distributions ranging from tens of nanometers (ultrashort nanotubes) to several microns. Methods to synthesize CNTs include arc discharge (Ebbesen and Ajayan 1992), laser vaporization of graphite (Puretzky et al. 2000), magnetic field synthesis (Doherty et al. 2006), chemical vapor deposition using gaseous metal catalysts such as cobalt, nickel, molybdenum, or iron (Cassell et al. 1999; Nobuhito et al. 2007), or water-assisted chemical vapor deposition (Hata et al. 2004).

CNTs possess high aspect ratios (the ratio of the longer dimension to the shorter dimension). The large surface area allows conjugation of multiple moieties including peptides, proteins, nucleic acids, radionuclides, other nanoparticles, and drugs to the surface of these nanoparticles (Pantarotto et al. 2003; Pantarotto et al. 2004a, 2004b; Kam et al. 2005; Singh et al. 2005; Kam and Dai 2005a; Lacerda et al. 2006) and permits a strong amplification of signals generated from these agents (Ajayan et al. 2002; Patri et al. 2004; Talanov et al. 2006). Because of these exploitable properties, it is not surprising that CNTs have been studied for applications to enhance the treatment of human malignancies (Kim 2007). Over the past decade, investigations into the use of CNTs for biomedical applications have greatly increased. Of particular interest is their ability to act as delivery vehicles for anticancer agents, including chemotherapeutic agents (Feazell et al. 2007; Liu et al. 2008), radionuclides (McDevitt et al. 2007), and nucleic acids (Wang et al. 2008). Furthermore, they have been shown to be effective as antitumor vaccine delivery systems (Meng et al. 2008) and as cancer imaging and diagnostic agents in animal models (Yu et al. 2006). The attractiveness of CNTs for use in these applications derives from their ability to easily cross cell membranes (Shi Kam et al. 2004; Kostarelos et al. 2007; Selvi et al. 2008) as well as their ability to be functionalized with target-specific molecules that preferentially target cancer cells (Liu et al. 2007; Chen et al. 2008; Kostarelos et al. 2009).

Another feature of CNTs that renders them particularly well suited for anticancer therapy is their ability to act as high-efficiency absorbers of near-infrared radiation (NIR) to promote

the generation of therapeutic heat specifically in tumors (Torti et al. 2007; Chakravarty et al. 2008; Klingeler et al. 2008; Biris et al. 2009; Burke et al. 2009; Day et al. 2009; Marches et al. 2009; Zhou 2009; Boldor et al. 2010; Burlaka et al. 2010; Fisher et al. 2010; Picou et al. 2010). CNTs are amenable to stimulation by a range of energy sources including NIR, microwave (MW), and radio-frequency (RF) radiation emitters directed at the site of the CNTs from outside the body. Following exposure to electromagnetic radiation, CNTs release vibrational energy and deliver substantial heat to the tumor site. Because of their potential to deliver multiple rounds of heat therapy in a noninvasive manner and their imaging capabilities, which permits more precise localization of heat delivery (Ding et al. 2011), CNTs have potential to improve the thermal treatment of cancer. Although other nanomaterials share some of these properties, CNTs offer perhaps the best combination of attributes for the development of a noninvasive, thermal therapy.

In this chapter, we will examine the rationale for using CNTs for photothermal cancer therapy. The differences in heating properties between carbon nanomaterials and various sources of radiation will be discussed below. We will consider current knowledge that could be used to optimize the design of CNTs for heat generation and localization, and analyze the current state of CNT-based anticancer photothermal therapy (PTT). Finally, we will examine at the prospects of translating CNT-based photothermal therapeutics to the clinic.

17.2 Photothermal Properties of CNTs

The interaction of light with CNTs is important for a number of applications, including biomedical use in PTT. For PTT, a photothermal sensitizer delivered to cancer cells is excited by a specific wavelength of light, generally in the NIR region of the electromagnetic spectrum (700–1100 nm), which in turn causes the photosensitizer to enter an excited state and release vibrational energy that is transformed into heat, leading to cell death (Kam et al. 2005; Torti et al. 2007). Because biological systems largely lack chromophores that absorb in the NIR region, transmission of NIR light through the body is poorly attenuated (Konig 2000; Weissleder 2001). As noted earlier, CNTs possess an extremely broad electromagnetic absorbance spectrum, covering not only the NIR window, but both the RF and MW bands as well (Gannon et al. 2007). This suggests that, in conjunction with an appropriate energy source, CNTs can be used to treat deeply seated lesions without the need for direct access to the tumor site. Although the photophysical effects governing the interaction of CNTs with electromagnetic energy have been studied through Raman scattering, fluorescence, and nonlinear optical analysis (Avouris et al. 2008; Biris et al. 2011; Kanemitsu 2011; Lehman et al. 2011; Saito et al. 2011; Yin et al. 2011), more research is needed to develop a clear understanding of these properties. It appears that CNTs act as ballistic conductors due to lack of energy dissipation through electron movement and quantized resistance, which are related to low dimensionality and quantum confinement of electrons within the carbon lattice of the nanotube wall (Brigger et al. 2002; Schonenberger and Forro 2000). Because of this, the specific structure of the nanotube, especially the number of walls, has a great effect on the efficiency of this material for use in photothermal applications. In the following section, we will examine the role nanotube structure plays in determining the photothermal heat transduction efficiency of CNTs.

17.2.1 Effect of Nanotube Structure on Photothermal Properties

After excitation by electromagnetic energy, CNTs exhibit a wide variety of vibrational (phonon) modes created by phonon–phonon and phonon–electron interactions (Kempa 2002; Hagen et al. 2004; Liu et al. 2011). These phonon interactions are dominant in determining the thermal properties of CNTs. In general, more phonon modes appear as the nanotube diameter and the size of the unit cell increases, meaning that the heat capacity and ability to generate and transport heat are unique to each nanotube structure. In one sense, phonons can be considered as quanta of heat. Thus, a basic understanding of the specific thermal conductivity properties of different types of nanotubes is essential to understanding the photothermal heating behavior of these materials. Here, we will briefly examine the thermal conductivity and the interaction of electromagnetic radiation with SWCNTs, MWCNTs, and related nanostructures, focusing on exposure to NIR.

SWCNTs. Measurements of bulk samples of SWNTs indicate a room-temperature thermal conductivity over 200 W/(m K) (Hone et al. 2000). This is far less than measurements of the room temperature thermal conductivity of an individual SWCNT along its axis which range from 2200 W/(m K) (Hone 2000) to about 3500 W/(m K) (Pop et al. 2006) because of the disorganized orientation of nanotubes in bulk samples. The phonon thermal conductivity displays a peak around 100 K and decreases with increasing temperature (Hone et al. 2000). At higher temperatures, thermal conductivity is predicted to decrease in a generally linear fashion because of the increased phonon–phonon and electron–phonon scattering interactions (known as the Umklapp processes) (Hone 2000; Osman and Srivastava 2001).

SWNHs. SWCNTs can be modified by sealing one end. These nanoparticles are called single-wall nanohorns (SWNHs) and form aggregate structures with typical diameters from 50 to 100 nm. SWNHs are produced without the use of metal catalysts by laser ablation of pure graphite (Whitney et al. 2011). The diameter can be adjusted by modifying the laser pulse length during production, and the size can be adjusted by modifying growth time (Geohegan et al. 2007). Nanohorns have been studied less extensively than either SWCNTs or MWCNTs for photo thermal applications. However, Whitney et al. found a linear relationship between the optical attenuation coefficient and concentration of SWNHs. They also demonstrated that the attenuation coefficient increased with shorter wavelengths, indicating that SWNHs likely will heat most efficiently when exposed to shorter wavelength NIR (Zhang et al. 2008; Whitney et al. 2011).

Because tissue penetrance is significantly better at longer NIR wavelength (Konig 2000), the use of SWNH for photothermal applications may be limited to the treatment of superficial diseases. The few studies to examine the use of SWNH for PTT have required significantly higher SWNH concentrations and longer NIR exposure times than needed for SWCNTs or MWCNTs to generate enough heat to be effective for photothermal ablation of cancer (Zhang et al. 2008; Whitney et al. 2011).

MWCNTs. Similar to SWCNTs, the large number of phonon modes in MWCNTs indicates that these structures also are exceptional heat conductors. The thermal conductivity of a single MWCNT along its axis at room temperature appears to be greater than that of comparable SWCNTs, with measured conductivities in the range of 3000 W/(m K) (Kim, Shi et al. 2001) to 6600 W/m K (Berber et al. 2000). However, other research groups have reported somewhat lower thermal conductivity with a range from 1500 to 3500 W/m K depending on the diameter of the tube (Fujii, Zhang et al. 2005). It is not clear if these differences are due to variations in the methods used to measure conductance, differences in the MWCNT preparations used, or some other cause. A study using bundles of bulk MWCNTs found a far lower room temperature thermal conductivity of only 20 W/m K (Yi, Lu et al. 1999). This lower value may be due to defects in the CNTs, but also suggests a potential inhibition of heating due to aggregation-induced resistive thermal junctions. As expected, the thermal conductivity of MWCNTs increases as diameter decreases, suggesting that interactions of photons and electrons between the walls affect conductivity (Osman and Srivastava 2001).

MWCNTs possess a broader absorption spectra compared to SWNTs and other plasmonic nanoparticles including nanoshells (Dresselhaus 2004; Torti et al. 2007; Burke et al. 2009). In contrast to SWNTs, the larger number of electrons available in the MWNT for transport, together with a smaller electronic bandgap or metallic behavior, suggests that the most efficient optical coupling of light and CNTs occurs when the nanotube length is comparable to half that of the wavelength of the incident radiation (Hanson 2005), which is consistent with the classic behavior of dipole antennae (Wang 2004; Hanson 2005). Accordingly, in response to illumination with a 1064-nm laser, MWCNTs with lengths of approximately one (1100 nm) or one-half (700 nm) that of the laser wavelength readily heated (Torti et al. 2007). In contrast, MWNTs with a length of one-third that of the laser (330 nm) failed to generate appreciable heat. As a further indication of this antenna effect, MWCNTs also demonstrate polarization effects, meaning that the antenna response of the CNTs is suppressed when the electric field of the incoming radiation is polarized perpendicular to the dipole axis of the CNTs (Wang 2004).

In practice, MWCNTs appear to be far more efficient at heat production than SWCNTs following exposure to electromagnetic radiation, possibly due to increased numbers of electrons (carriers) available for photon interactions and a greater mass per particle (Burke et al. 2009; Fisher et al. 2010). Furthermore, most SWCNTs act as semiconductors, and only a fraction of the as-produced tubes exhibit the metallic behavior shown in MWCNTs (Burlaka et al. 2010). This means that the electrons in MWNCTs can more easily become excited than those in most SWCNTs and begin releasing excess energy in the form of heat. Experimental studies comparing the NIR absorbance at 1064 nm of aqueous dispersions of MWCNTs to similarly dispersed SWCNTs indicate that MWCNTs absorb approximately three times more light per particle than SWCNTs (Fisher et al. 2010). Interestingly, the heat-generating capacity of MWCNTs following exposure to an equivalent dose of NIR has been shown to be up to 20-fold higher than that of SWCNTs (Burke et al. 2009; Levi-Polyachenko et al. 2009). This effect is far greater than the optical absorbance data would indicate, and the mechanism by which this occurs remains to be explained. However, the difference in heating between SWCNTs and MWCNTs may be an important feature because a smaller dose of MWCNTs could be used to achieve an equivalent temperature rise following NIR exposure. Thus, MWCNTs could potentially achieve equivalent clinical responses at doses less likely to engender systemic toxicity and off-target effects than SWCNTs.

17.2.2 Effect of Doping on Photothermal Properties of CNTs

Doping of non-carbon atoms into CNTs represents a method to control the photoelectronic properties of the tubes by chemistry rather than through alterations in specific geometry (Esfarjani et al. 1999). Doping can be used to alter the electronic band structure to increase the overall conductivity (hence the antenna behavior) of the nanotubes. Numerous types of dopants can be introduced into CNT walls through methods such as intercalation of electron donors such as alkali metals or acceptors such as halogens, substitutional doping, encapsulation in the interior space, coating on the surface, molecular absorption, and covalent sidewall functionalization (Terrones et al. 2008; Stoyanov et al. 2009; Ayala et al. 2010; Kong et al. 2010).

Doping CNTs with other atoms can have a dramatic effect on their photothermal properties, potentially enhancing their optical absorption and heat transductance capability. Substitutional doping (replacing carbon in the lattice with a non-carbon atom) of the tubes alters the Fermi level of the valence band: the greater the doping, the stronger is the shift of the Fermi level. For pure CNTs, the valence and conduction bands appear to be symmetric about the Fermi level. By comparison, nitrogen doping introduces an impurity located 0.27 eV below the bottom of the conduction bands and boron doping induces a level that is 0.16 eV above the top of the valence bands found in undoped CNTs (Schonenberger and Forro 2000). The lowering of the Fermi level by boron dopants increases the number of conduction channels without introducing strong carrier scattering (Dai 2002). Thus, boron-doped nanotubes show metallic behavior with weak electron–phonon coupling. In contrast to undoped CNTs, which even in idealized conditions show a small bandgap (semiconducting or semimetallic behavior), the valence band of boron-doped MWNTs is filled with a prominent acceptor-like peak near the Fermi level. Although there is only limited

experimental evidence, one effect of doping appears to be an increased optical coupling of MWNTs to NIR due to increasing the number of free carriers available, leading to the generation of higher temperatures following exposure to NIR when compared to equivalent undoped tubes (Liu and Fan 2005; Liu and Gao 2005; Torti et al. 2007).

The effect of incorporation of non-carbon atoms into the interior of CNTs on photothermal properties is less explored. Experimental studies have demonstrated that MWCNTs produced with a high concentration of the iron-based catalyst ferrocene in their lumen appear to heat more efficiently than iron-free MWCNTs, achieving temperatures of up to 5–7°C greater following exposure to an equivalent dose of NIR (Levi-Polyachenko et al. 2009). On the other hand, others have found that increasing concentrations of ferrocene in the lumen of MWCNTs has no effect on heating properties (Ding et al. 2011). Although the mechanism accounting for this difference remains poorly understood, it should be noted that the enhanced heating effect observed by Levi-Polyachenko occurred when heating ferrocene-containing MWCNTs at nanotube concentrations greater than 100 μg/mL, whereas Ding et al. only investigated the heating of 100 μg/mL MWCNT samples.

17.3 RF and MW Heating of CNTs

In addition to efficiently absorbing NIR, CNTs are also capable of generating heat upon irradiation with MW or RF radiation. The MW spectrum ranges from 300 MHz to 300 GHz, whereas the broader RF spectrum overlaps and extends from 3 kHz to 300 GHz. MW heating of CNTs causes polarization, producing a similar antenna effect as seen by NIR heating (Wang 2004). Experiments performed with CNTs in viscous dense environments found decreased heating, attributed to reduced photon–photon and photon–electron interactions due to inhibited vibrations (Ye et al. 2006). CNTs irradiated by MWs can induce heat by conduction and dipolar polarization, enabling localized heating (Vazquez and Prato 2009). The modes of CNT heat generation using MW/RF are similar to NIR, as MW irradiation transforms electromagnetic energy into mechanical vibrations and ultimately heat. Residual metals in CNTs may also donate free charges that help expedite MW coupling. Because of the overlap in wavelengths, the heating properties of MW and RF irradiation of CNTs will be discussed together.

Based on theoretical modeling, Dumitricia et al. (2004) found that SWCNTs blended in polycarbonate should absorb MW radiation at a 6- to 20-GHz range. In this study, capped SWCNTs treated with ~100-fs pulses are predicted to remain intact with 8% of valence electrons promoted to antibonding states. Irradiation would also result in opening of the caps without damaging the cylindrical structure. In contrast, heating of bulk (noncapped) SWCNTs is predicted to promote 10% of valence electrons and result in fragmentation to the particles. With both types of NTs, the maximum temperature predicted was 800 K, which stabilized to 300 K. In a separate study, SWCNTs heated with 700 W at 2.45 GHz were observed to spread to twice their original volume during heating before contracting again. Many of the SWCNTs fused after heating and formed junctions (Imholt et al. 2003). A temperature of at least 1500°C must be reached for this phenomenon to occur, suggesting that tremendous temperature increases were achieved in this experiment (Ajayan et al. 2002). Another factor that can influence heating of CNTs is their purity. Unpurified SWCNTs (containing Fe catalyst impurities) reached a temperature of 1850°C upon heating, whereas purified SWCNTs only reached 650°C (Wadhawan 2003). Both types of SWCNTs had diameters of 1.1 nm and were irradiated with 1000-W MW radiation at 2.45 GHz. This suggests that residual metals may play an important role in CNT heating.

Reulet et al. found that RF irradiation at 100 MHz–10 GHz of a single SWCNT (1 nm diameter and several different lengths) caused electron heating by dissipation of mechanical energy. No change was seen in the resonance spectrum upon heating, suggesting that the electrostatic forces on the tube and Coulomb force produced by the RF field are responsible for excitation and vibrations. Different resonant frequencies were seen depending on the length of the NT (Reulet et al. 2000). SWCNTs irradiated with 800 W by a 13.56-MHz RF field produced a temperature increase of 30–40°C (1.6 K/s rate). The heating rate is higher than predicted, and may be due to spontaneous self-assembly of SWCNTs into longer antennae. The total thermal power deposition was found to be 130,000 W/g, with over half specifically from the NTs (75,000 W/g). RF heating of CNTs does not appear to be due to excitement of electronic transitions or resonance because of the long wavelengths (Gannon et al. 2007).

Table 17.1 summarizes cellular effects of stimulation of nanotubes with RF radiation. RF-mediated heating of hepatocellular and pancreatic cancer cell lines *in vitro* using 250–500 μg/mL

TABLE 17.1 Thermal Ablation Using Radiofrequency Radiation to Heat Carbon Nanomaterials

Nanomaterial/ Functionalization	Power Input	NT Dose	Temperature Change	Cancer Model and Therapeutic Efficacy	Ref.
SWNT; coated in Kentera polymer	13.56 MHz RF field (400–1000 W)	50–500 μg/mL	33–45°C linear increase with power, exponential increase of heat when fixed power with increasing conc. Enhanced bulk heating at 5 μg/mL	Hep3B, HepG2 and Panc-1 human liver and pancreatic cancer cells; 60–70% cell death FACS with 50 μg/mL, ~90% with 100 μg/mL and 100% with 500 μg/mL. Treated for 2 min 800 W.	Gannon et al. (2007)
SWNTs; coated in Kentera polymer	13.56 MHz RF field (600 W)	500 μg/mL	Not reported	Rabbits with VX2 liver xenografts, intratumoral injection. 2 min RF treatment. Complete thermal necrosis	Gannon et al. (2007)

concentration of SWCNTs killed almost all the treated cells, with dose-dependent increases in cell death observed. About 25% of cells that were heated in media alone (without SWCNTs) were killed, suggesting the potential impact of nonspecific ion stimulation in heat generation upon treatment (Gannon et al. 2007) *in vivo* treatment of a VX2 hepatocellular carcinoma xenograft in rabbits resulted in complete thermal necrosis of the tumor. No toxicity was seen, but there was a 2- to 5-mm zone of thermal injury to the surrounding liver (Gannon et al. 2007). This demonstration indicates that SWNTs may be capable of noninvasively treating tumors in any part of the body, a capability currently not shared by NIR laser-based treatments. However, little research has been conducted on the efficacy of this type of therapy both *in vitro* and *in vivo*, possibly because of the risk of significant off-target heating. Therefore, we will focus only on NIR-mediated therapies for the remainder of this chapter.

17.4 Strategies to Localize Heat Distribution and Monitor Photothermal Heating of CNTs

Control of the spatial and temporal distribution of heat used for thermal ablation is essential for localizing heat to a target and reducing collateral damage to normal cells and tissues (Boldor et al. 2010).

Simply viewed, heat delivery for photothermal applications is dependent on the total laser energy incident upon the target and the efficiency of the CNT target at converting that energy into heat. Thus, heat generations is limited only by the maximum laser output and achievable nanomaterial concentration. Conversely, heat dissipation away from the CNTs is a complex process that is dependent on tube environment, tube proximity to heat absorbers, solvent, and the substrate into which the tubes are dispersed. As discussed in more detail below, it is unlikely that continuous heating of nanoscale sources can produce a significant temperature increase adjacent to the surface of a nanoparticle, nanowire, or nanotube because of heat transfer away from the site of irradiated nanomaterials, unless the heating power is extremely large (Keblinski et al. 2006).

Several studies have reported that nanoscale temperature localization following NIR heating of isolated nanoparticles can be achieved through use of high-powered, rapidly (femto- to nanosecond time scales) pulsed lasers (Plech et al. 2003; Hartland et al. 2004; Pustovalov and Babenko 2004; Ge et al. 2005). Ultrashort laser pulses of approximately 100 fs are believed to immediately promote electrons in CNTs to antibonding states, whereas pulses that are greater than a picosecond transfer energy from the promoted electrons to atomic thermal motion, resulting in potentially uncontrolled structural changes in the material (Dumitrica et al. 2004). Nanosecond NIR pulses have been reported to produce temperature increases of 150–300°C in samples containing gold nanoparticles because there was insufficient time for heat dissipation from the several micrometer heated area (Zharov et al. 2005). Similar strategies using nanosecond pulsed lasers have been successfully applied for the treatment of scattered cancer cells following uptake of CNTs (Zharov et al. 2005; Biris et al. 2009; Vitetta et al. 2011).

Unfortunately, nanosecond or picosecond pulsed lasers are not commonly available in clinical environments, and as noted, temperature increases over larger volumes tend to be very small following such brief exposures. However, the use of somewhat longer (millisecond to tens of seconds) NIR pulses to irradiated CNTs may offer a few opportunities for cancer therapy that are not dependent on macroscale temperature increases (Panchapakesan et al. 2005; Kang et al. 2009). In one study, cancer cells that had taken up bundles of SWCNTs were exposed to low intensity NIR (800 nm; 50–200 mW/cm^2) for 60 s. An insignificant temperature rise was measured following treatment. Instead, water molecules entrapped inside and between the bundled SWCNTs boiled; as the water molecules evaporated, extreme pressures developed in SWCNT bundles causing them to explode and kill nearby cancer cells (Panchapakesan et al. 2005). The key to this strategy is the use of bundles of SWCNTs, as the nanobomb effect is not observed for well-dispersed samples. In a different study, Kang et al. (2009) heated cancer cells that had taken up CNTs with a millisecond pulsed laser (1064 nm; 200 mW/cm^2) for 20 s, resulting in the death of 85% of the treated cancer cells. Significantly, almost no temperature change was detected, and it is believed that the mode of cell killing was a photoacoustic explosion induced by photon–electron interactions that generated a shockwave, physically disrupting the cells' membranes.

Although there may be some benefit to other treatment strategies as noted above, in general, continuous NIR treatment may be best suited for treating bulky tumors, as the generated heat can effectively spread throughout the tumor (Biris et al. 2009). Moreover, sustained heating of a large number of nanoparticles dispersed across a tumor volume under conditions typically used for *in vivo* thermal ablation produces a global temperature rise that is far larger than the localized temperature rise near each particle, allowing for substantial heating across the entire volume to be treated, which is necessary for anticancer therapy (Keblinski et al. 2006; Boldor et al. 2010). The problem is that for long heating times (several seconds or greater), heat transfer away from the target area is significant and not only reduces the effectiveness of the therapy, but may result in collateral damage to healthy tissue surrounding the treatment area.

To reduce the spread of heat from the tumor target to the surrounding tissue, the total electromagnetic energy deposited into the tissue should be minimized such that only the amount of heat needed for treatment is delivered to the targeted area. This requires real-time monitoring of spatiotemporal changes in temperature resulting from NIR irradiation of CNTs. There are several ways to monitor the temperature distribution in a tumor volume following CNT delivery and NIR irradiation, including the use of infrared cameras (Huang et al. 2010; Picou et al. 2010) and magnetic resonance imaging (MRI)-based methods (Burke et al. 2009; Ding et al. 2011). Infrared cameras have proven useful for optimizing both CNT concentration and NIR

irradiation parameters needed to generate specific temperature profiles in model tissue (Picou et al. 2010) and in tumor-bearing mice (Huang et al. 2010). However, NIR cameras do not offer the possibility of noninvasively imaging temperature changes deep within tissue.

A noninvasive method of temperature mapping that also allows for superposition of temperature information over high-resolution anatomical images taken at any depth is an MRI-based thermometry method known as proton resonance frequency (PRF) MR temperature mapping (reviewed by Rieke and Pauly 2008). This technique is based on the principle that when the temperature rises, hydrogen bonds break between water molecules in tissue and this causes a PRF shift that varies linearly with temperature changes. Clinically, PRF MR temperature mapping is used to provide control over the treatment outcome by relating the treatment temperature to actual thermal tissue damage. With regard to CNT enhanced photothermal cancer therapy, Burke et al. (2009) demonstrated that this technique could be used to both locate the tumor target in a mouse model of kidney cancer and to calculate the delivered thermal dose to that same tissue following NIR exposure. PRF MRI thermometry showed that a maximum temperature of 76°C was achieved in the tumors injected with 100 μg of MWCNTs following a 30-s NIR exposure (1064 nm; 3 W/cm^2). In the absence of CNTs, the maximum temperature rose to only 46°C after the same NIR treatment.

The demonstration that CNTs are compatible with PRF MR temperature mapping is a key step toward future clinical applications, as this technique helps to monitor whether thermal ablative temperatures are reached, and also aids in reducing the risk of collateral damage to neighboring normal tissue. However, this technique could further be refined; optimally, CNTs used for thermal therapy should also be capable of MR contrast enhancement, which would allow for accurate monitoring of nanomaterial distribution in the tumor and image guided placement of the NIR source (Salvador-Morales et al. 2009). Several studies have shown that elements that enhance magnetic resonance (MR) contrast, such as iron (Ding et al. 2011) or gadolinium (Gd) (Sitharaman et al. 2005; Hartman et al. 2008; Richard et al. 2008; Ananta et al. 2010; Zhang et al. 2010), can be incorporated into CNTs to enable their detection by noninvasive imaging.

As a step toward this goal, MWCNTs containing iron were studied for their potential as dual-modality agents for both MR contrast enhancement and photothermal energy transduction (Ding et al. 2011). In this study, MR imaging provided an accurate picture of the distribution of iron-containing MWCNTs inside the tumor, which is essential information for pretreatment planning and determination of laser positioning for MR image guided PTT of tumors in mice. The contrast and heating properties of such MWCNTs did not change upon multiple rounds of NIR exposure, even after reaching thermal ablative temperatures. Thus, the distribution of the MWCNTs could be monitored over time, and multiple or fractionated laser treatments could be targeted to the tumor as necessary without the need for additional injections.

However, a potential limitation of iron-containing MWCNTs is their propensity to attenuate MR signals. Although this enables iron-containing MWCNTs to act as highly effective T2 contrast agents, extensive MR signal attenuation can potentially interfere with temperature mapping by PRF MR thermometry. Ideally, a CNT specifically engineered for the clinical application of nanoparticle-assisted photothermal cancer therapy will both be compatible with an imaging modality such as MRI to spatially define the margins of the target lesion and assess the distribution of injected nanoparticles within the tumor, and also compatible with a noninvasive temperature mapping technique to ensure that the appropriate thermal dose was achieved in the target area. The optimization of such a material will be a critical step toward the realization of the full potential of nanoparticle enhanced PTT.

17.5 Anticancer Efficacy of CNT-Enhanced PTT

In vitro and *in vivo* tests of the antitumor efficacy of CNTs have been highly encouraging. The first study describing the use of SWNTs for PTT of cancer cells was published in 2005 by Kam et al. (2005); subsequently, MWCNTs were also shown to be effective (Torti et al. 2007). Although there are many variables that will be discussed in detail below, the general therapeutic approach involves exposing adherent cancer cells, cancer cells in suspension, or tumors grown in mice to CNTs followed by irradiation with an external NIR laser (Figure 17.1). This technique, which can be termed nanotube-enhanced PTT, has proven to be an effective treatment in a wide variety of human cancer models including cervical carcinoma (Kam et al. 2005), renal carcinoma (Torti et al. 2007; Burke et al. 2009), mouth carcinoma (Moon et al. 2009), prostate adenocarcinoma (Fisher et al. 2010), breast adenocarcinoma (Ding et al. 2011), ascitic carcinoma (Burlaka et al. 2010), and lymphoma (Chakravarty et al. 2008; Marches et al. 2009) *in vitro* as summarized in Table 17.3. Efficacy also has been demonstrated *in vivo* in numerous syngeneic mouse models of cancer (Huang et al. 2010; Robinson et al. 2010) and in human xenografts grown in mice (reviewed by Iancu and Mocan 2011 and summarized in Table 4). Q1

The clinical model for the use of nanomaterials as heat transduction agents is based on laser-induced thermotherapy (LITT) (O'Neal et al. 2004), a photothermal ablation technique in which an NIR laser is used to directly heat a target tissue, such as a tumor, above the thermal ablation temperature threshold of approximately 55°C (Kangasniemi et al. 2004; O'Neal et al. 2004; Nikfarjam et al. 2005). As a result, protein denaturation, membrane lysis, and coagulative necrosis occur, leading to cell death. A major limitation of LITT has been an inability to consistently achieve thermoablative temperatures throughout the target lesion and to confine treatment exclusively to the tumor (Chen et al. 2005; Gnyawali et al. 2008). Therefore, to be of clinical benefit, CNTs must greatly improve the deposition of heat following NIR exposure.

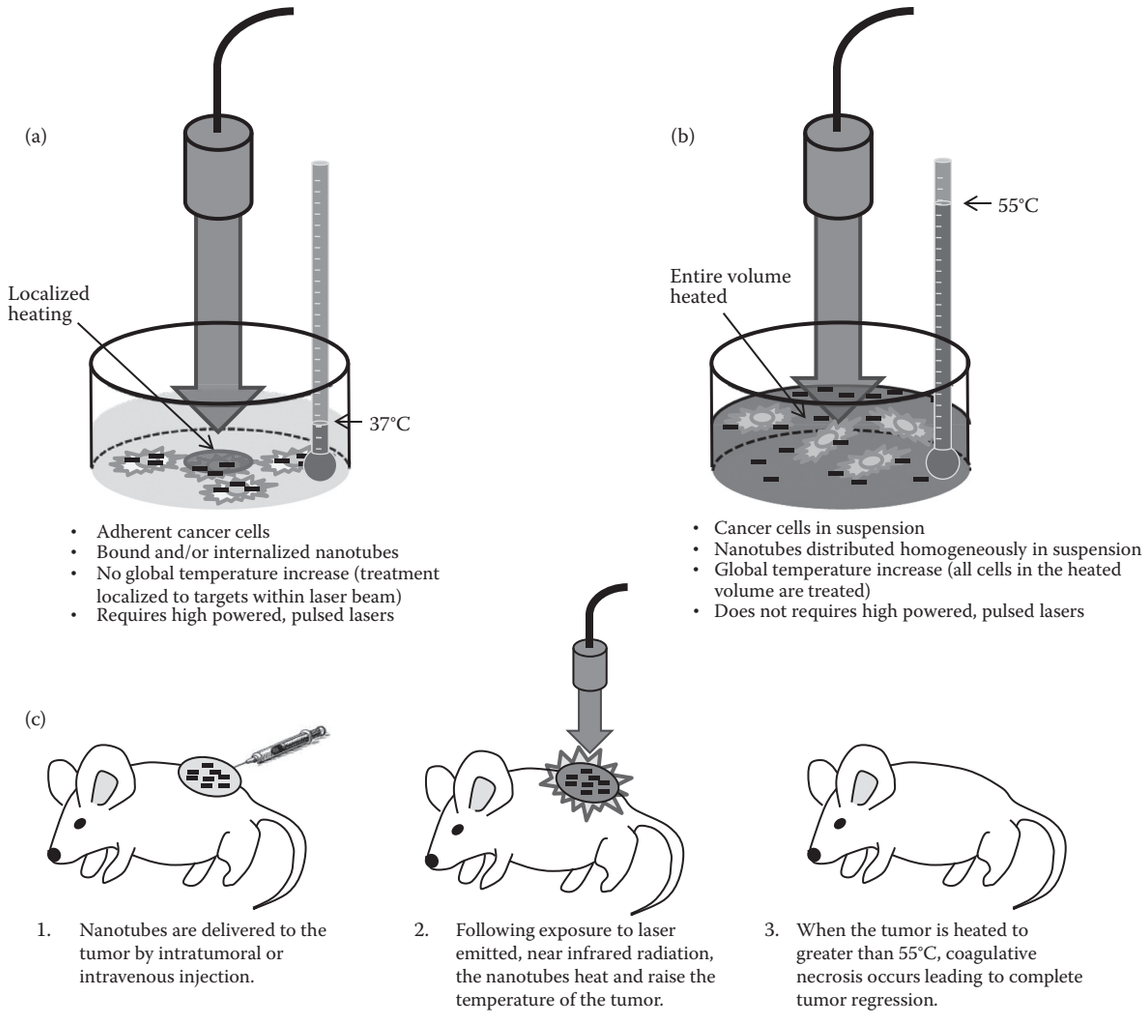

FIGURE 17.1 Schematic illustration nanotube enhanced photothermal therapy. (a) Selective photothermal heating of cancer cells. Adherent cancer cells readily take up carbon nanotubes following coincubation. Excess unbound nanotubes are washed away. Following exposure to laser emitted near-infrared radiation (NIR), cells that have taken up nanotubes rapidly heat and die. The amount of heat generated is insufficient to significantly raise the temperature of the surrounding media, making treatment localized to the cellular level. (b) Volumetric photothermal heating of cancer cells. Cells are dispersed in aqueous media containing well suspended nanotubes. After exposure to NIR, the entire volume heats significantly, causing cancer cell death. (c) Heating of tumors *in vivo*. Typical *in vivo* studies generally have taken a volumetric approach to therapeutic heating mediated by nanotube enhanced photothermal therapy. Nanotubes can be directly injected into the tumor or delivered via the tumor vasculature. After exposure to NIR via an external laser, the nanotube containing tumor rapidly heats up, causing coagulative necrosis and cancer cell death.

Several studies have explored the potential of CNTs to improve LITT by enhancing deposition of heat following NIR exposure. Kam et al. (2005) first described the use of SWCNTs for PTT. After 60 s of exposure to 808-nm laser radiation, little heat was generated in the absence of SWCNTs. However, in the presence of SWCNTs, the absorbance was robust, raising the temperature of the solution to more than 55°C (i.e., into the established thermoablative range). This temperature increase was sufficient to kill HeLa cells (a well-characterized cervical carcinoma cell line) that previously had internalized SWNTs following incubation period of a few hours. Efficient conversion of tissue penetrating wavelengths of NIR into heat is fundamental to the application of this and other nanomaterials that seek to treat nonsuperficial cancerous lesions *in vivo*.

After this initial study, further testing of the heating of cancer cells with SWCNTs upon NIR irradiation was conducted *in vitro* and *in vivo*. Huang et al. (2010) observed that the quantity of heat generated and the efficacy of the therapy improved with both increasing SWCNT concentration and increased laser exposure (energy deposition). In the same study, both tumor reduction and a modest survival benefit were seen in a subcutaneous syngeneic murine squamous cell carcinomas model

following intratumoral injection of 1 mg/mL of SWCNTs and irradiation with a low power (200 mW/cm^2) NIR laser for 10 min. The treatment resulted in a maximum temperature increase in the tumor of 18°C as measured by IR thermometry, indicating that the thermal ablation threshold was reached. However, this treatment failed to achieve a durable cancer remission. Uneven tumor ablation and tumor recurrence were observed, and necrosis was seen in nearby normal tissue, indicating significant heat transfer away from the tumor site and into the surrounding nontumor region.

By comparison, Moon et al. (2009) demonstrated that heat localization and therapeutic efficacy of SWCNT-mediated PTT could be greatly improved through the use of higher powered laser irradiation (3 W/cm^2) for a shorter irradiation time (3 min). Following intratumoral injection of SWNCTs (120 μg/mL) into mice bearing subcutaneous xenografts of human mouth carcinoma cells and NIR irradiation, the tumors were completely destroyed, with no apparent toxicity, side effects, or tumor recurrence during several months of follow-up. Nearby normal tissue was spared, whereas tumor sections stained positively for TUNEL, suggesting apoptosis as the mode of cell death. However, even in the absence of SWCNTs the irradiation procedure itself resulted in significant burning of the target region. Ideally, the total energy needed to induce thermal ablation should be minimized to reduce off-target damage.

In this regard, MWCNTs may offer a significant potential advantage over SWCNTs: as previously noted, because of the unique structure of MWCNTs, they absorb NIR far more efficiently than SWCNTs, thus requiring only a fraction of the incident radiation or concentration SWCNTs needed to generate an equivalent increase in temperature (Torti et al. 2007; Burke et al. 2009). Analysis of the literature suggests that in most studies, the total energy needed to achieve thermal ablation *in vitro* with SWCNTs typically is on the order of 100 to several hundred Joules and the required SWCNT concentrations are greater than 100 μg/mL (see Tables 17.2 and 17.3). Using MWCNTs, thermal ablative temperatures could be achieved *in vitro* following exposure of 10 μg/mL of MWCNTs to as little as 4 J, resulting in the death of 99% of treated cancer cells (Biris et al. 2009). Although Ghosh et al. (2009) conducted detailed experiments to examine the influence of nanotube concentration, laser power, and duration of laser exposure on the heating of SWCNTs and MWNCTs, no systematic effort has been made to determine the ideal combination of CNT type, concentration, and NIR needed to minimize the required energy dose for therapeutic heat generation. Thus, treatment parameters still vary widely (see Tables 17.2 and 17.3).

For example, effective treatment of Erlich ascitic carcinoma cells *in vitro* was achieved following incubation of the cells with MWCNTs at a 100 μg/mL concentration and irradiation with an NIR laser (780–1400 nm range) at 3.5 W/cm^2 for 1.5–2 min, heating the culture media to between 50°C and 70°C (Burlaka et al. 2010). Fisher et al. treated renal adenocarcinoma cells (RENCA) and PC-3 human prostate cancer cell lines with 100 μg/mL MWCNTs and 5 min by exposure to NIR (15.3 W/cm^2 at 1064 nm). The resulting 42°C temperature increase in the culture media surrounding the cells was sufficient to kill (Fisher et al. 2010). In this latter study, cell internalization of MWCNTs was measured using fluorescence and transmission electron microscopy. Consistent with previous reports (Kostarelos et al. 2007), MWCNTs were taken up by cells and translocated to the nucleus. With increasing incubation duration, a greater number of MWNTs were observed in cellular vacuoles and nuclei. In Section 17.5, the role cell binding and internalization of CNTs play in the efficacy of treatment will be discussed in more detail. Q2

The number of MWCNTs needed per cell for effective thermal therapy has been studied (Torti et al. 2007). Human CRL1932 renal adenocarcinoma cells grown in a monolayer were incubated with increasing concentrations of nitrogen-doped MWCNTs corresponding to estimated MWCNT to cell ratios of 1:1, 100:1, and 1000:1. Following exposure to NIR (3 W/cm^2 of 1064 nm NIR with for 4 min), a 23°C temperature rise was observed in the culture media of cells exposed to MWCNTs at the 1000:1 ratio, with near-complete cell death. No significant heating differences of cell death was observed in cells exposed to MWCNTs at the 1:1 or 100:1 ratios as compared to control heated cells heated in the absence of MWCNTs.

In a follow-up study, Burke et al. (2009) demonstrated that cellular uptake of MWCNTs before NIR exposure was not necessary for *in vitro* cancer cell killing. Murine RENCA were homogeneously dispersed in phosphate buffered saline containing 100 μg/mL of MWCNTs (Burke et al. 2009). Following a brief exposure to NIR (3 W/cm^2 of 1064 nm NIR with for 30 s), 98% of cancer cells were killed, whereas 45 s of treatment killed 100% of the cells. *In vivo* studies demonstrated that intratumoral injection of increasing doses of MWCNTs (10, 50, or 100 μg) into RENCA tumors implanted in the flanks of nude mice significantly decreased tumor growth and increased survival in a dose-dependent manner following exposure to NIR (3 W/cm^2 of 1064 nm NIR with for 30 s). In the absence of MWCNTs, this laser treatment resulted in minimal superficial burning. Durable remission was observed in 80% of mice receiving the 100 μg MWCNT dose combined with NIR for the length of the 6-month study. Although MWCNTs remained at the injection site, no toxicity was detected. In contrast, all mice administered MWCNTs in the absence of NIR did not survive beyond 3 months, and no difference in tumor growth was observed between these animals and untreated controls.

This study presented a key demonstration of the capability of MWNTs coupled with laser irradiation to enhance the *in vivo* treatment of tumors through more controlled thermal deposition leading to increased tumor injury. Furthermore, Burke et al. examined the induction of heat shock proteins (HSPs) 27, 70, and 90 as an indirect measure of heat generation in full-depth tissue sections taken from tumors of mice 16 h after NIR exposure. HSPs are induced by elevated temperatures (typically in excess of 43°C) and serve as endogenous cellular markers of thermal stress. They observed minimal expression for all HSPs in untreated tumors, but in tumors treated with NIR in the absence of MWCNTs, significant HSP expression was observed.

TABLE 17.2 Photothermal Cancer Therapy Using Near-Infrared Radiation to Heat Carbon Nanomaterials *In Vitro*

Nanomaterial	Functionalization	Cancer Model	Optimal Nanotube Conc.	NIR Paramenters: Wavelength; Irradiance; Duration; Laser Mode	Radiant Exposure (Total Energy)[a]	Maximum Temp.[b]	Therapeutic Efficacy	Reference
SWCNH (nanohorn)	Acid oxidized; bovine serum albumen coated	5RP7 rat fibroblasts cells transformed by the c-Ha-ras oncogene	20 μg/mL	670 nm; 160 mW/cm^2; 5 min; continuous	48 J/cm^2 (38 J)	>41°C	Nanohorns were incubated with cell monolayer for 24 h then irradiated. 68% of cells killed following treatment.	Zhang et al. (2008)
	Pluronic F127 coated	RENCA murine kidney cancer cells	85 μg/mL	1064 nm; 40 W/cm^2; 1 min; continuous	2400 J/cm^2 (300 J)	up to 85°C	Nanohorns were incubated with cell monolayer for 24 h then irradiated;. >90% cell death following treatment.	Whitney et al. (2011)
SWCNT	Acid oxidized	BT474 breast cancer	100 μg/mL	800 nm; 200 mW/cm^2; 1 min; continuous	12 J/cm^2 (Energy: N/A – spot size unknown)	minimal temp. increase	Nanotubes mixed with suspended cells then irradiated. No temperature increase was measured. Cell death attributed to photoacoustic shock wave rather than thermal effect. Cell death rate not quantified.	Panchapakesan et al. (2005)
	DNA coated	U251 human glioblastoma	10 μg/mL	808 nm; 2 W/cm^2; 5 min; continuous	600 J/cm^2 (226 J)	up to 50°C	Nanotubes were mixed with suspended cells then irradiated. Near 100% cell death following treatment.	Markovic et al. (2011)
	Acid oxidized; PEG coated; antibody targeted	MCF-7 human breast cancer cells	Not reported	808 nm; 800 mW/cm^2; 3 min; continuous	144 J/cm^2 (113 J)	55–60°C	Nanotubes were mixed with suspended cells and incubated for 30 min. Then irradiated. Near 100% cell death following treatment. Highly selective for targeted population.	Ning et al. (2007)
	Acid oxidized; antibody targeted	SK-BR-3 human breast cancer cells	4 μg/mL	808 nm; 5 W/cm^2; 3 min; continuous	900 J/cm^2 (137 J)	>38°C	Nanotubes were incubated for 24 h with cell monolayer, washed, then irradiated. Near 100% cell death following treatment with targeted SWCNTs. Highly selective for targeted population.	Xiao et al. (2009)
	Chitosan coated; folic acid targeted	Hep G2 human hepatocellular carcinoma cells	20 μg/mL	1064 nm; 200 mW/cm^2 average; 20 s; Q-switched, millisecond pulsed	4 J/cm^2 (28 J)	minimal temp. increase	Nanotubes were incubated for 3–5 h with cell monolayer then irradiated. >85% cell death following treatment. Cause of death attributed to photoaccoustic shock wave rather than thermal effect. Highly selective for targeted population.	Kang et al. (2009)
	Phospholipid-PEG coated; antibody targeted	Daudi human Burkitt's lymphoma cells	90 μg/mL	808 nm; 5 W/cm^2; 7 min; continuous	2100 J/cm^2 (Energy: N/A –spot size unknown)	temp. not reported	Nanotubes were mixed with suspended cells for 20 min, washed, then irradiated; >90% cell death following treatment with targeted SWCNTs. Highly selective for targeted population.	Chakravarty et al. (2008)
	DNA coated or; phospholipid-PEG coated; folic acid targeted	HeLa human cervical carcinoma cells	25 μg/mL	808 nm; 1.4 W/cm^2; 2 min; continuous	168 J/cm^2 (approx. 1187 J)	>70°C	Nanotubes were mixed with suspended cells, washed, then irradiated. Extensive cell death reported but not quantified following treatment. Highly selective for targeted population.	Kam et al. (2005)

(*continued*)

TABLE 17.2 Photothermal Cancer Therapy Using Near-Infrared Radiation to Heat Carbon Nanomaterials *In Vitro* (Continued)

Nanomaterial	Functionalization	Cancer Model	Optimal Nanotube Conc.	NIR Paramenters: Wavelength; Irradiance; Duration; Laser Mode	Radiant Exposure (Total Energy)[a]	Maximum Temp.[b]	Therapeutic Efficacy	Reference
	Acid oxidized; antibody targeted	BT-474 human breast carcinoma cells	approx. 5–10 μg/mL	808 nm; 9.5 W/cm^2; 9 min; continuous	5130 J/cm^2 (Energy: N/A – spot size unknown)	temp. not reported	Nanotubes were incubated with cell monolayer for 24 h, washed, then irradiated. Approx. 40% of targeted cells were killed. Highly selective for targeted population.	Marches et al. (2011)
	Phospholipid-PEG; folate targeted	EMT6 murine breast carcinoma cells	3.5 μg/mL	980 nm; 1 W/cm^2; 2 min; continuous	120 J/cm^2 (Energy: N/A – spot size unknown)	up to 70°C	Nanotubes were incubated with cell monolayer for 2 h, washed, then irradiated. >85% cell death observed after treatment. Highly selective for targeted population.	Zhou et al. (2011)
	Chitosan coated; antibody targeted	Glioblastoma cells expressing high or low levels of CD133, isolated from patient samples	2.5 μg/well of 24 well plate	808 nm; 2 W/cm^2; 5 min; continuous	600 J/cm^2 (678 J)	temp. not reported	Nanotubes were incubated 6 h with cell monolayer then washed away and irradiated; >95% cell death following treatment. Highly selective for targeted population.	Wang et al. (2011)
MWCNT	Nitrogen-doped; Pluronic F127 coated	CRL 1932 human kidney cancer cells	approx. 83	1064 nm; 3 W/cm^2; 4 min; continuous	720 J/cm^2 (171 J)	46°C	Nanotubes were incubated for 24 h with cell monolayer then irradiated. >95% of cells dead after treatment.	Torti et al. (2007)
	Raw (as produced)	Erlich ascitic murine carcinoma cells	100	780–1400 nm; 3.5 W/cm^2; 1.5 min; continuous	315 J/cm^2 (Energy: N/A– spot size unknown)	Up to 50°C	Nanotubes were mixed with suspended cells then irradiated. >95% cell death following treatment.	Burlaka et al. (2010)
	HCl cleaned	HeLa human cervical cancer cells	10	1064 nm; approx. 32 W/cm^2; 4 s; continuous	128 J/cm^2 (4 J)	temp. in laser beam >75°C	Nanotubes were incubated for 48 h with cell monolayer then irradiated. >98% cell death following treatment.	Biris et al. (2009)
	Pluronic F127 coated	RENCA murine kidney carcinoma cells alone	100	1064 nm; 3 W/cm^2; 45 s; continuous	135 J/cm^2 (26 J)	>53°C	Nanotubes were mixed with suspended cells then irradiated. Near 100% cell death following treatment.	Burke et al. (2009)
	Pluronic F127 coated	RENCA murine kidney carcinoma and PC3 human prostate carcinoma cells	100	1064 nm; 15.3 W/cm^2; 5 min; continuous	4590 J/cm^2 (900 J)	66°C	Nanotubes were mixed with suspended cells then irradiated. Near 100% cell death following treatment. Note: Cells were maintained at 25°C before treatment. Heating curves indicate that 30–60 s NIR should be sufficient to kill cells maintained at 37°C.	Fisher et al. (2010)
	Oxidized, human serum albumen coated	HepG2 and CRL-4020 human hepatocellular carcinoma cells	1–50	808 nm; 64 W/cm^2; 2 min; continuous	7680 J/cm^2 (approx. 240 J)	temp. not reported	Nanotubes were Incubated for 1 min to 24 h with cell monolayer then irradiated; >95% cell death at all conc. MWCNTs after 5 h or longer incubation.	Iancu et al. (2011)
	Acid oxidized; antibody targeted	Human stNB-V1 neuroblastoma cells; PC12 Neuron-derived rat pheochromocytoma cells	5–10 μg/mL	808 nm; 0.6–6 W/cm^2 for 10 min followed by 6 W/cm^2 for 5 min; continuous	approx. 3000 J/cm^2 (Energy: N/A – spot size unknown)	temp. not reported	Nanotubes were incubated 6 h with cell monolayer then washed and irradiated; All treated cells died. Highly selective for targeted population.	Wang et al. (2011)

[a] Radiant exposure was calculated from the product of the NIR irradiance and the exposure time. For dosimetry calculations (total energy), the radiant exposure was multiplied by the surface area of the laser beam (laser spot size) incident upon the surface of the tumor or cancer cell target as reported in the cited reference.

[b] Maximum temperature indicates the maximum temperature achieved following laser irradiation as reported by the cited references. Depending on the technique used to measure temperature, this may be a local (cellular) temperature measurement or a macroscale (averaged over a volume of several milliliters) temperature measurement.

Q3

TABLE 17.3 Photothermal Cancer Therapy Using Near-Infrared Radiation to Heat Carbon Nanomaterials *In Vivo*

Nanomaterial	Nanotube Functionalization	Cancer Model	Nanotube Dose/ Route	NIR Paramenters: Wavelength; Irradiance; Duration; Mode	Radiant Exposure (Total Energy)[a]	Maximum Temp.[b]	Therapeutic Efficacy	Ref.
SWCNH (nanohorn)	Acid oxidized; bound to BSA	RAS-transformed 5RP7 rat fibroblast cells implanted in nude mice	30 μg; intratumoral	670 nm; 160 mW/ cm^2; treatment given in 5 locations per tumor, 3 min each day for 10 days; continuous	28.8J/cm^2 per treatment × 5 locations for 10 days; (5.7 J per site per treatment (cumulative dose approx. 280 J/tumor))		Significant tumor regression observed in nanotube treated mice following irradiation, although no complete regression observed.	Zhang et al. (2008)
SWCNT	PEG coated	SCCVII murine squamous carcinoma cells implanted in C_3H/ HeN mice	60–100 μg; intratumoral	785 nm; 200 mW/ cm^2; 10 min; continuous	120 J/cm^2	590 J; 48°C	Complete tumor regression for 5/8 nanotube treated mice for at least 45 days following irradiation.	Huang et al. (2010)
	Phospholipid-PEG coated	4T1 murine breast cancer cells implanted in BALB/c mice	70 μg; intravenous	808 nm; 600 mW/ cm^2; 5 min; continuous	180 J/cm^2	approx. 90 J (assuming 5 mm tumor diameter)	Complete tumor regression in 10/10 nanotube treated mice for at least 60 days following irradiation.	Robinson et al. (2010)
	Phospholipid-PEG coated	KB human epidermoid mouth carcinoma cells implanted in nude mice	12 μg; intratumoral	808 nm; 3.8 W/cm^2; 3 min; continuous	684 J/cm^2	435 J; Up to 70°C in solution – *in vivo* temp. not reported	Complete tumor regression in 4/4 nanotube treated mice for at least 25 days following irradiation.	Moon et al. (2009)
	PEG-grafted poly(maleic anhydride-octadecene) coated	4T1 murine breast carcinoma cells implanted in BALB/c mice	100 μg; intravenous	808 nm; 1 W/cm^2; 5 min; continuous	300 J/cm^2	N/A – spot size not reported	Tumor regression observed in 5/7 treated mice following irradiation. No tumor regrowth observed in 3/7 treated mice for at least 2 weeks following irradiation.	Liu et al. (2011)

(*continued*)

TABLE 17.3 Photothermal Cancer Therapy Using Near-Infrared Radiation to Heat Carbon Nanomaterials *In Vivo* (Continued)

Nanomaterial	Nanotube Functionalization	Cancer Model	Nanotube Dose/ Route	NIR Paramenters: Wavelength; Irradiance; Duration; Mode	Radiant Exposure (Total Energy)[a]	Maximum Temp.[b]	Therapeutic Efficacy	Ref.
	phospholipid-PEG coated; folate targeted	EMT6 murine breast carcinoma cells inplanted in BALC/c mice	Dose estimated to be 20–25 μg based on typical mouse weight of 20–25 g; intratumoral	980 nm; 1 W/cm^2; 5 min; continuous	300 J/cm^2	Estimated to be 60 J based on 5 mm tumor diameter; Up to 65°C	Tumor growth was not evaluated. However, >85% tumor cell death observed in nanotube treated mice 3 h after irradiation.	Zhou (2009)
MWCNT	Pluronic F127 coated	MDA-MB-231 human breast cancer implanted in nude mice	100 μg; intratumoral	1064 nm; 3 W/cm^2; 30 s; continuous	90 J/cm^2	21.6 J; temp. not reported	Complete tumor regression in 4/4 nanotube treated mice for at least 30 days following irradiation.	Ding et al. (2011)
	DNA coated	PC3 human prostate cancer cells in nude mice	50 μg; intratumoral	1064 nm; 2.5 W/cm^2; pulsed 5 s on, 3 s off for 14 repetitions (70 s exposure time); pulsed	175 J/cm^2	Energy: N/A – spot size not reported	Tumor regression observed in 4/4 nanotube treated mice with indication of recurrence in some animals 3 weeks after irradiation.	Ghosh et al. (2009)
	Pluronic F127 coated	RENCA murine kidney carcinoma cells alone or implanted in nude mice	100 μg; intratumoral	1064 nm; 3 W/cm^2; 30 s; continuous	90 J/cm^2	18 J; >70°C	Complete tumor regression in 8/10 nanotube treated mice for at least 300 days following irradiation.	Burke et al. (2009)
	Chitosan coated; antibody targeted	Glioblastoma cells expressing high or low levels of CD133, isolated from patient samples, implanted in nude mice	10 μg; cells incubated with nanotubes *in vitro* then implanted in mice	808 nm; 2 W/cm^2; 5 min; continuous	600 J/cm^2	678 J; temp. not reported	Complete tumor regression in 3/3 nanotube treated mice without metastasis for at least 5 weeks following irradiation.	Wang et al. (2011)

[a] Radiant exposure was calculated from the product of the NIR irradiance and the exposure time as reported in the cited reference. For dosimetry calculations (total energy), the radiant exposure was multiplied by the surface area of the laser beam (laser spot size) incident upon the surface of the tumor or cancer cell target as reported in the cited reference.

[b] Maximum temperature indicates the maximum temperature achieved following laser irradiation as reported by the cited references. Depending on the technique used to measure temperature, this may be a surface temperature measurement or an internal temperature measurement.

Maximal HSP27, HSP70, and HSP90 expression was induced proximal to the incident laser (near the skin) and then gradually diminished with increasing depth. In contrast, in tumors treated with NIR plus MWCNTs, the temperature elevation was sufficient to induce coagulative necrosis in much of the tumor, thus preventing significant HSP induction. However, HSPs were seen at deeper tissue levels, near the interface between tumor and normal tissue. These results demonstrate that NIR irradiation combined with MWCNTs can be used to extend the depth of thermal therapy.

Similar observations were made *in vitro* by Fisher et al. (2010), again demonstrating the combination of MWNTs and NIR can dramatically decrease cell viability without inducing HSP expression—possibly indicating a necrotic rather than apoptotic cell death mechanism. A necrotic mode of cell death offers a significant advantage over many conventional therapies that rely on induction of pro-death signal transduction pathways (Gottesman 2002; Bergamaschi et al. 2003; Pommier et al. 2004), because it does not provide selective pressure to induce the evolution of treatment-resistant cancer cell clones. However, necrosis has not been universally observed as the mechanism of cell death following treatment with NIR and MWCNTs; Kratz (2010) reported a dramatic increase in apoptosis in Hep G2 human hepatocellular carcinoma cells following exposure to MWCNTs and NIR. To date, no extensive research has been conducted to factors that may influence the mechanism(s) of cell death induced by the combination of CNTs and NIR, and this is clearly an area where more knowledge is needed.

The thermal effects generated by CNTs may have benefits in addition to direct thermal ablation of cancer cells. For example, hyperthermia can increase the permeability of tumor vasculature. This can enhance the delivery of drugs into tumors, as well as synergistically enhance cytotoxicity when combined with chemotherapy or radiotherapy (Falk and Issels 2001). In this regard, the use of mild NIR irradiation of MWCNTs to rapidly heat cancer cells to temperatures below the thermal ablation threshold has been shown to increase the uptake of codelivered chemotherapeutic drugs and enhance cancer cell death both *in vitro* and *in vivo* in a murine ascites tumor model (Levi-Polyachenko et al. 2009). Similarly, it was also demonstrated that photothermal heating of SWNTs chemically conjugated with platinum-based chemotherapeutics was significantly more effective than either therapy alone (Feazell et al. 2007). Such strategies may allow increased cancer selectivity of chemotherapeutic agents or reduce the dose necessary for efficacy and thus reduce the toxicity of such treatments.

17.6 Tumor Selective Nanotube Binding and Uptake for Enhanced Anticancer PTT

Once CNTs come into contact with cells, they can easily pass through cell membranes (Kostarelos et al. 2007). The mechanism of CNT internalization is still not completely understood and is greatly influenced by the physicochemical properties of the tubes themselves (Raffa et al. 2010). It is believed that they can enter the cell both passively by diffusion across the lipid membrane and are transported actively by endocytosis or receptor-mediated endocytosis (Shi Kam et al. 2004; Cai et al. 2005; Chen et al. 2008). Internalization of CNTs by cells offers an opportunity for extremely confined heating effects. For example, Kam et al. demonstrated that brief NIR excitation (six pulses, each 10 s long, at 1.4 W/cm^2) of SWCNTs taken up by endocytosis can trigger endosomal rupture with no apparent adverse toxicity (Kam et al. 2005; McDevitt et al. 2007; Welsher et al. 2008). Moreover, the combination of NIR and SWCNTs was shown to selectively release noncovalent molecular cargoes (DNA in this case) from nanotube carriers. In contrast to the nontoxic effect observed following brief, pulsed exposure to NIR, extensive cell death was observed after cells with internalized SWNTs were continuously exposed to NIR for 2 min of radiation under a 1.4 W/cm^2 power (Kam et al. 2005).

This result hinted that if SWNTs could be selectively internalized into cancer cells, NIR radiation of the nanotubes could then selectively activate or trigger cell death without harming normal cells. One strategy to allow for more selective therapy would be to specifically (or actively) target CNTs to tumors. This can be accomplished by conjugation of peptides, proteins, or antibodies to the surface of CNTs, which has been shown to increase the specificity of tumor targeting (Kam et al. 2005; McDevitt et al. 2007; Welsher et al. 2008). The addition of targeting ligands involves modifying CNT surface chemistry (functionalizing), which could affect the optical absorbance and thermal properties of CNTs. Several studies have shown that under limited experimental conditions, the optical properties of SWCNTs were retained after adding targeting moieties (Chakravarty et al. 2008; Marches et al. 2009). To date, no detailed studies have been conducted to compare the photothermal behavior of such functionalized tubes to their nonfunctionalized precursors over a broad set of conditions.

An early approach to selective targeting adopted by several groups was to use folic acid (FA) as a targeting ligand to direct CNTs to FA receptors (FR), which are overexpressed on many tumors (Kamen and Smith 2004). In one such study conducted *in vitro*, SWCNTs (average length 150 nm) were conjugated to FA, and directed toward human cervical cancer cells with low FR expression, or HeLa cells overexpressing FR. The FR overexpressing cells internalized the targeted SWCNTs (as verified by fluorescent labeling), whereas normal cells with low FR expression did not take up the NTs. After the cells were heated using 808-nm laser at 1.4 W/cm^2 continuously for 2 min, extensive cell death was observed for the FR overexpressing cells, whereas cells with low FR expression remained intact and exhibited normal proliferation behavior (Kam et al. 2005). Similar results were observed by Zhou (2009), and by Kang et al. (2009), who targeted FA conjugated SWCNTs to human hepatocellular carcinoma cells (HepG2) overexpressing FR. In the latter study, the effect of NIR combined with FA-targeted SWCNTs on FR overexpressing HepG2 cells was found to be dependent on the

nanotube concentration, with cell death rising from 50% in cells treated with CNTs at a concentration of 2 μg/mL, to greater than 85% cell death at a concentrations of 20 μg/mL and higher. In contrast, similar treatment of HepG2 cells with low FR expression resulted in less than 10% cell death at SWCNT concentrations of 20 μg/mL and less. However, selectivity of this treatment was greatly reduced at higher nanotube concentrations; significant cell death (35–40%) was observed in HepG2 expressing low levels of FR following treatment with 50 μg/mL SWCNT dispersions, indicating that nonspecific binding and uptake of CNTs may reduce the selectivity of this treatment.

Although homogeneous upregulation of FR is found in up to 90% of some cancers including ovarian and brain cancers, other solid tumors, such as those found in the breast, have more variable folate receptor expression with only about 50% showing overexpression (Leamon and Reddy 2004). Therefore, folate is useful as a targeting modality in only a fraction of cancers. The versatility of CNTs as a platform allows for display of many types of ligands other than small molecules such as folate including antibodies with binding affinity for the breast cancer associated receptor Her2 (Marches et al. 2011; Xiao et al. 2009). In one such study, anti-Her2 conjugated SWCNTs were seen to bind to Her2 expressing, SK-BR-3 human breast adenocarcinoma cells, but remained at the surface without internalizing (Xiao et al. 2009). Little binding was observed in Her2 negative MCF-7 breast adenocarcinoma cells following exposure to anti-Her2 conjugated SWCNT. After washing away unbound CNTs and adding fresh media to the cells, treatment with an NIR laser at 5 W/cm^2 for 2 min killed 97% of SK-BR-3 cells. Strikingly, minimal cell death was observed using nontargeted SWCNTs combined with NIR, and the Her2 antibody alone had no effect. Similarly, MCF-7 cells, to which the anti-Her2 conjugated SWCNTs did not bind, were spared from thermal ablation upon identical treatment conditions.

Further refinement of this treatment strategy was achieved by Marches et al. (2011), who also conjugated SWCNTs to an anti-Her2 antibody. In this case, the anti-Her2 targeting moiety induced internalization of the SWCNTs following binding to Her2 expressing cancer cells. By tracking the relative cell binding and internalization of the anti-Her2 conjugated SWCNTs over time, Marches et al. determined that cells containing internalized CNTs were more sensitive to NIR-mediated thermal ablation than cells that bind to, but do not internalize, the CNTs. Moreover, in a mixed population of cells expressing or not expressing Her2, NIR-mediated cell damage was restricted primarily to Her2 expressing cells that bound and internalized the CNTs (Marches et al. 2011), demonstrating the possibility of tailoring this type of therapy to differentiate between targets on a cell by cell basis.

One significant advantage of CNTs over other nanoparticles is that because of the large surface area/volume ratio, CNTs can effectively display more than one targeting ligand on their surface. This allows CNTs to be engineered to bind to multiple receptors overexpressed on cancer cells, a strategy that can be used to expand both the tropism and specificity of cancer-targeted CNTs. For example, antibodies targeting Her2 and another receptor overexpressed in breast cancers, insulin-like growth factor 1 receptor (IGF1R) were attached to SWCNTs (Ning et al. 2007). In cell culture studies, the binding of each targeting ligand did not affect the other, allowing specific binding to both MCF-7 cells (which express IGF1R but not Her2) and BT474 cells (a human breast ductal carcinoma cell line that expresses Her2 but not IGF1R). Following NIR irradiation, almost all of the cells with targeted SWCNTs were killed. NIR irradiation of cells exposed to nonspecifically targeted SWCNTs killed fewer cells (less than 50%). Significantly, the estimated power used to kill each cell was calculated to be approximately 200 nW (an order of magnitude less than other protocols) (Ning et al. 2007).

Perhaps the most striking example of the possibility of selective thermal cancer ablation mediated by CNTs was recently demonstrated through the use of SWCNTs designed to accumulate at an intracellular target. In 2010, Zhou et al. demonstrated that, following coating with a phospolipid modified to contain polyethylene glycol (PEG) in the head group, SWCNTs selectively accumulate intracellularly at the mitochondrial membrane. When exposed to NIR, these SWCNTs selectively destroy the target mitochondria, thereby inducing mitochondrial depolarization, cytochrome *c* release, and caspase 3 activation. *In vivo*, treatment with these modified SWCNTs suppressed tumor growth in a murine breast cancer model, resulting in complete tumor regression in some cases (Zhou et al. 2011).

Strategies to selectively target CNTs to cancer cells for thermal ablation therapy are not limited to the use of SWCNTs. Several studies have demonstrated that similar approaches to those described above for SWCNTs can be applied to MWCNTs, allowing for the greater heat transduction capability of MWCNTs to be used for targeted PTT. In one study, MWCNTs were conjugated to monoclonal antibody directed GD2, a carbohydrate antigen overexpressed in neuroblastomas (Wang et al. 2009). Binding and internalization was found to be specific for GD2 expressing neuroblastoma cells, whereas control rat neuroendocrine tumor cells that did not express GD2 did not take up these MWCNTs. Cells were heated using an 808-nm laser that gradually increased from 0.6 to 6 W/cm^2 over 10 min and was maintained at 6 W for 5 min more. This treatment caused necrosis in nearly all GD2+ cancer cells (as determined by calcein staining) but not in control cells. Only the cells within the laser zone were killed, and a clear boundary of living cells delineated the border between the treatment zone and cells that were not illuminated by the laser (Wang et al. 2009).

A second example of selectively targeting MWCNTs involved functionalizing the surface of MWCNTs with human serum albumin in order to target the albumin-binding Gp60 receptor expressed in hepatocellular carcinoma cells (Kratz 2010). Specific internalization was seen in Gp60 expressing HepG2 cells, but not in normal hepatocytes. Uptake was shown to be mediated by receptor binding, followed by caveolin-dependent endocytosis. Following NIR irradiation (808 nm; 2 W/cm^2 for 2 min) cell death directly correlated with increased concentrations of CNTs and increased CNT exposure time. There was a

5- to 6-fold increase in apoptosis of cancer cells compared to hepatocytes. Treatment with nonfunctionalized MWCNTs produced no significant differences in cell death between the cancer and non-cancer cell lines.

Targeted thermal ablation therapies based on CNTs are being tested for the treatment of cancers that are highly resistant to current therapies, including glioblastomas (Wang et al. 2011). In glioblastomas and other brain tumors, the CD133 receptor appears to be a cancer stem cell marker associated with malignancy, tumor recurrence, and poor survival. (Singh et al. 2004; Beier et al. 2008; Zeppernick et al. 2008). Cancer stem cells have been putatively identified as self-renewing therapy-resistant populations in many types of tumors (Jordan et al. 2006). In glioblastomas, CD133+ subpopulations are enriched following radiotherapy, are radio- and chemotherapy-resistant, and are responsible for restoring tumor cells after treatment (Singh et al. 2004; Bao et al. 2006; Lee et al. 2006). Treatment strategies based on targeting this subpopulation may be able to prevent the development of resistance to therapy.

Recently, Wang et al. used MWCNTs chemically conjugated to a monoclonal antibody directed against CD133 to target these cells. In cell culture experiments, they observed specific internalization of these targeted MWCNTs via endocytosis in glioblastoma cells that expressed CD133, but not in cells that did not. Importantly, these were not immortalized cells, but were cells that had been freshly isolated from patients. To test the selectivity of nanotube-enhanced PTT, mixed populations of both cell types were incubated with 2.5 mg of the MWCNTs for 6 h and then were irradiated with an 808-nm laser at 2 W/cm^2 for 5 min. Flow cytometry confirmed that CD133+ cells were killed, whereas CD133– cells were spared. These effects were further recapitulated by an *in vivo* xenograft model in which CD133 expressing glioblastoma cells were pretreated with targeted MWCNTs before injection into mice. The cells took up the MWCNTs, and xenograft growth was abolished and no metastases were detected after NIR exposure (Wang et al. 2011). This was a key demonstration of the potential of CNTs to treat glioblastomas and other currently untreatable cancers.

Cancer stem cells are particularly well described in breast cancer, where they have been shown to be highly resistant to standard chemotherapy and radiotherapy (Al-Hajj et al. 2003; Diehn and Clarke 2006). Recent work by Burke et al. (2012) describes the utility of MWCNT-mediated thermal ablation in treating this otherwise therapy-resistant cell population. Initially, bulk (non-stem) and stem breast cancer cells were treated with hyperthermia delivered by incubation in a circulating water bath to mimic conventional clinical hyperthermic therapy, and changes in cell viability were determined. By this method, breast cancer stem cells were significantly more resistant to hyperthermia than bulk breast cancer cells across the entire treatment range. In contrast, when both cell types were heated to the same final temperature using 50 μg/mL amidated MWCNTs and NIR laser radiation (1064 nm; 3 W/cm^2), stem and bulk breast cancer cells were equally sensitive to MWCNT-mediated thermal therapy. The authors demonstrated that this was due to the induction of rapid and robust necrotic cell death following MWCNT-mediated thermal therapy that was largely absent after conventional hyperthermia. Collectively, these findings demonstrate that nanotube-mediated hyperthermia is functionally distinct from hyperthermia delivered by other means, and may represent a significant therapeutic advance for the treatment of refractory, stem cell-driven cancers.

17.7 Systemic Delivery and Biocompatibility of CNTs for PTT

In order for CNT enhanced PTT to spare normal tissue from heating, it is important for the CNTs to be selectively taken up by tumor cells and not by normal cells. Ideally, this could be achieved following systemic administration of tumor targeted CNTs. Significant effort has been made to achieve selective targeting of nanoparticles to tumor sites based on both passive and active targeting (Brannon-Peppas and Blanchette 2004; You et al. 2006; Li and Huang 2008; Ruenraroengsak et al. 2010; Van Lehn et al. 2010; Yoo et al. 2010). Passive targeting refers to strategies that attempt to achieve tumor delivery without utilizing specific biological (ligand–receptor) interactions by correlating the physicochemical and surface characteristics of the nanoparticle with the pathophysiology and anatomy of the target site. Active delivery is inherently dependent on passive delivery to reach the tumor site, but also adds to nanoparticles the ability to associate or interact with specific biological moieties by attachment of ligands with an enhanced binding affinity for complementary cellular receptors, as discussed above.

For the past 20 years, passive strategies to selectively deliver nanoparticles to tumor sites have relied on the enhanced permeability and retention effect. First reported by Maeda et al., the strategy proposes that tumor specificity of nanoparticles that remain in circulation for long periods can be achieved because of the nanoparticles' ability to extravasate through the leaky vasculature surrounding the tumor and enter the tumor site (Maeda et al. 2000; Liu et al. 2008). Long blood circulation frequently is achieved through coating nanoparticles with steric stabilizers such as PEG, which inhibit blood clearance by reducing the uptake of nanoparticles by macrophages and other components of the mononuclear phagocyte system. Several groups have demonstrated that PEG coating can greatly improve the tumor localization of CNTs following intravenous injection in mice (Cato et al. 2008; Liu et al. 2009; Bhirde et al. 2010).

Recently, this strategy for passively targeting nanotubes to tumors intravenously was shown to be effective for nanotube-enhanced PTT (Robinson et al. 2010). Short (140 nm), PEG-coated SWCNTs at a dose of 3.6 mg/kg were injected via the tail vein into mice bearing 4T1 murine breast tumors. Three days later, SWCNT accumulation at the tumor site was confirmed by detection of the inherent NIR photoluminescence of the SWCNTs (1100–1400 μm wavelength) using an optical imaging system. The tumors were heated for 5 min at 0.6 W/cm^2 with 808 nm laser, resulting in complete tumor ablation. All treated mice survived

without recurrence for the duration of the 6-month study, and no toxicity was seen. This was an extremely significant step toward the development of a tumor-selective, systemically delivered photothermal ablation agent. It is important to note that in this experiment, the nanotubes were not modified to display a specific targeting ligand, nor were they internalized by the cancer cells themselves. More research is needed to determine if active targeting will offer an additional benefit *in vivo*.

Although these results indicate the CNTs offer great promise for targeted hyperthermia of cancer, the translation of CNTs from an interesting nanomaterial to an effective pharmaceutical product is still in its nascence. The toxicity, and therefore the ability to analyze the potential risk–benefit balance for these materials, will ultimately determine their long-term clinical fate. Unfortunately, the development of an accurate toxicity profile of CNTs is a complicated matter. Not only do structural characteristics, such as diameter and length, greatly influence biological and toxicological responses following injection of CNTs (Donaldson, Aitken et al. 2006), but also changes in surface functionalization, which alter adsorption properties, electrostatic interactions, hydrophobicity/hydrophilicity, and influence the stability of CNT dispersions, also affect CNT toxicity (Dyke and Tour 2004; Lacerda et al. 2006). Finally, toxicity may also be due to by-products from CNT manufacturing, including residual catalysts such as Co, Fe, Ni, and Mo (Lacerda et al. 2006).

The toxicity of CNTs has been reviewed extensively elsewhere (Ai et al. 2011; Beg et al. 2011; Donaldson et al. 2011; Kaiser et al. 2011; Stella 2011; Uo et al. 2011; Zhang et al. 2011). Therefore, only a few key studies will be highlighted here. It should be noted that most toxicity studies have focused on environmental exposure following inhalation of pristine CNTs that have not been modified from their "as produced" state (Jia et al. 2005; Lam et al. 2006; Smart et al. 2006; Warheit 2006; Kolosnjaj et al. 2007; Wick et al. 2007; Kostarelos 2008; Koyama et al. 2009). For example, concerns have been raised regarding the possibility of very long (10–20 μm) nanotubes to induce an asbestos-like reaction (Schipper et al. 2008), or for inhalation of nanotubes to cause dose-dependent granulomatous pneumonia, oxidative stress, and acute inflammatory and cytokine responses, with fibrosis and decrease in pulmonary function (Shvedova et al. 2005), and the possibility that CNTs may elicit an immune or allergic response (Park et al. 2009; Ryman-Rasmussen et al. 2009).

CNTs are inherently hydrophobic, and the toxicity of the pristine CNTs may be largely due to their hydrophobicity (Sayes et al. 2006). CNTs used for biomedical applications must be modified in some way from their pristine, as-produced, condition in order to render them suitable for dispersion in aqueous environments (Burke et al. 2011). Typical modifications include acid oxidation of the CNT exterior to introduce carboxyl groups (reviewed by Tasis et al. 2003), "wrapping" CNTs in long-chain surfactants (reviewed by Nakashima and Fujigaya 2007), and as noted above, linking antibodies or other targeting moieties to the CNT surface both to aid in their dispersion and promote their accumulation in tumor tissue (Liu et al. 2007; McDevitt et al. 2007). Such chemical modifications can improve the overall toxicity profile of CNTs and enhance their body clearance (Dyke and Tour 2004; Lacerda et al. 2006; Sayes et al. 2006).

The use of CNTs as nanomedicines will necessitate bypassing the body's natural defenses, possibly through intravenous delivery, where alternative toxicities might be observed. Because of the ability of intravascularly delivered particulates to induce undesired thrombotic events (Radomski et al. 2005; Dobrovolskaia et al. 2008; Mayer et al. 2009; Semberova et al. 2009), demonstration that CNTs are compatible with blood is particularly critical. Recently, the role played by chemical functionalization of CNTs on blood toxicity following intravenous injection into mice was examined (Burke et al. 2011). It was found that pristine MWCNTs were substantially more thrombogenic than chemically functionalized MWCNT following intravenous injection in mice. At a dose of 250 μg, pristine MWCNT were acutely lethal, inducing blockage of the pulmonary vasculature. In contrast, an equivalent dose of covalently functionalized MWCNTs exerted little effect on coagulation *in vivo*, with their sole measurable effect being a transient depletion of platelets. Consistent with this, the majority of studies in which mice were injected with CNTs that have been chemically functionalized to improve aqueous dispersion have not shown any long-term or chronic toxicity (Lacerda et al. 2006; Singh et al. 2006; Liu et al. 2008; Yang et al. 2008; Deng et al. 2009; Qu et al. 2009). Although larger and longer-term studies must be undertaken before the toxicity profile of CNTs is fully understood, it appears that CNTs can be designed to be biocompatible and suitable for systemic delivery.

17.8 Perspectives on Translational Potential of CNT-Enhanced PTT

CNTs have the potential to play a key role in the next generation of photothermal agents. They offer a unique capacity for designing and tuning optical, thermal, and cancer-selective properties that are not possible with other types of therapeutic vectors. Clinical applications of CNT-enhanced photothermal ablation could not only provide rapid and localized heating in response to NIR, but also be compatible with noninvasive imaging to spatially define the margins of the target lesion, assess the distribution of injected CNTs within the tumor, ensure the that the appropriate thermal dose is achieved in the target area, and track the response of the treated area to therapy over time. This combined functionality allows CNTs to overcome many of the drawbacks of traditional thermotherapy and may allow for expanded clinical use of image-guided LITT and improved therapeutic outcomes for cancer patients following such treatment.

Conceptually, benefits to patients offered by CNTs could be safely achieved using minimally invasive methods. For example, CNTs could be infused directly into a tumor or the main blood supply of a tumor could be identified intraoperatively by ultrasound to allow for intra-arterial infusion of CNT dispersions followed by laser irradiation using a mini-laser–guided

by a videoscopic or other real-time imaging modality. As noted by Iancu and Mocan (2011), the potential benefits of such a treatment strategy include reduced postoperative pain, more rapid recovery and decreased hospitalization, fewer surgical or wound complications, and improved cosmetics. Additionally, the next era of thermal therapy could include not only the use of nanoparticles for ablation of tissues, but the evaluation of nanoparticles for codelivery of chemotherapeutic agents to cancer cells. Efficient strategies for selectively targeting CNTs to tumors following intravenous or arterial injection may further enhance treatment efficacy.

Further research will be required to critically assess the potential for toxicity as well as evaluate pharmacologic properties of newly designed targeted CNTs. Since these properties will depend on the precise particle under evaluation, extensive materials assessment will be a critical preamble to successful clinical development. The encouraging results obtained to date with a variety of CNTs suggest that we have only begun to plumb their therapeutic potential.

Acknowledgments

This study was supported in part by National Institutes of Health grants RO1CA12842 and R01CA128428-02S1, and National Institutes of Health training and career development grants T32CA079448 and K99CA154006.

References

Biris, A. S., D. Boldor et al. 2009. Nanophotothermolysis of multiple scattered cancer cells with carbon nanotubes guided by time-resolved infrared thermal imaging. *Journal of Biomedical Optics* 14(2):021007.

Burke, A., X. Ding et al. 2009. Long-term survival following a single treatment of kidney tumors with multiwalled carbon nanotubes and near-infrared radiation. *Proceedings of the National Academy of Sciences of the United States of America* 106(31):12897–12902.

Burlaka, A., S. Lukin et al. 2010. Hyperthermic effect of multiwalled carbon nanotubes stimulated with near infrared irradiation for anticancer therapy: *In vitro* studies. *Experimental Oncology* 32(1):48–50.

Chakravarty, P., R. Marches et al. 2008. Thermal ablation of tumor cells with antibody-functionalized single-walled carbon nanotubes. *Proceedings of the National Academy of Sciences of the United States of America* 105(25):8697–8702.

Ding, X., R. Singh et al. 2011. Development of iron-containing multiwalled carbon nanotubes for MR-guided laser-induced thermotherapy. *Nanomedicine (London)*.

Fisher, J. W., S. Sarkar et al. 2010. Photothermal response of human and murine cancer cells to multiwalled carbon nanotubes after laser irradiation. *Cancer Research* 70(23):9855–9864.

Gannon, C. J., P. Cherukuri et al. 2007. Carbon nanotube-enhanced thermal destruction of cancer cells in a noninvasive radiofrequency field. *Cancer* 110(12):2654–2665.

Ghosh, S., S. Dutta et al. 2009. Increased heating efficiency and selective thermal ablation of malignant tissue with DNA-encased multiwalled carbon nanotubes. *ACS Nano* 3(9):2667–2673.

Huang, N., H. Wang et al. 2010. Single-wall carbon nanotubes assisted photothermal cancer therapy: Animal study with a murine model of squamous cell carcinoma. *Lasers in Surgery and Medicine* 42(9):638–648.

Iancu, C., L. Mocan et al. 2011. Enhanced laser thermal ablation for the *in vitro* treatment of liver cancer by specific delivery of multiwalled carbon nanotubes functionalized with human serum albumin. *International Journal of Nanomedicine* 6:129–141.

Kam, N. W., M. O'Connell et al. 2005. Carbon nanotubes as multifunctional biological transporters and near-infrared agents for selective cancer cell destruction. *Proceedings of the National Academy of Sciences of the United States of America* 102(33):11600–11605.

Kang, B., D. Yu et al. 2009. Cancer-cell targeting and photoacoustic therapy using carbon nanotubes as bomb agents. *Small* 5(11):1292–1301.

Liu, X. W., H. Q. Tao et al. 2011. Optimization of surface chemistry on single-walled carbon nanotubes for *in vivo* photothermal ablation of tumors. *Biomaterials* 32(1):144–151.

Marches, R., C. Mikoryak et al. 2011. The importance of cellular internalization of antibody-targeted carbon nanotubes in the photothermal ablation of breast cancer cells. *Nanotechnology* 22(9):095101.

Markovic, Z. M., L. M. Harhaji-Trajkovic et al. 2011. In vitro comparison of the photothermal anticancer activity of graphene nanoparticles and carbon nanotubes. *Biomaterials* 32(4):1121–1129.

Moon, H. K., S. H. Lee et al. 2009. In vivo near-infrared mediated tumor destruction by photothermal effect of carbon nanotubes. *ACS Nano* 3(11):3707–3713.

Ning, S., S. Lu et al. 2007. Integrated molecular targeting of IGF1R and HER2 surface receptors and destruction of breast cancer cells using single wall carbon nanotubes. *Nanotechnology* 18(31):315101.

Panchapakesan, B., S. Lu et al. 2005. Single-wall carbon nanotube nanobomb agents for killing breast cancer cells. *NanoBioTechnology* 1(2):133–139.

Robinson, J. T., K. Welsher et al. 2010. High performance *in vivo* near-IR (>1 mu m) imaging and photothermal cancer therapy with carbon nanotubes. *Nano Research* 3(11):779–793.

Torti, S. V., F. Byrne et al. 2007. Thermal ablation therapeutics based on CN(*x*) multi-walled nanotubes. *Int J Nanomedicine* 2(4):707–714.

Wang, C. H., S. H. Chiou et al. 2011. Photothermolysis of glioblastoma stem-like cells targeted by carbon nanotubes conjugated with CD133 monoclonal antibody. *Nanomedicine* 7(1):69–79.

Whitney, J. R., S. Sarkar et al. 2011. Single walled carbon nanohorns as photothermal cancer agents. *Lasers in Surgery and Medicine* 43(1):43–51.

Xiao, Y., X. Gao et al. 2009. Anti-HER2 IgY antibody-functionalized single-walled carbon nanotubes for detection and selective destruction of breast cancer cells. *BMC Cancer* 9:351.

Zhang, M., T. Murakami et al. 2008. Fabrication of ZnPc/protein nanohorns for double photodynamic and hyperthermic cancer phototherapy. *Proceedings of the National Academy of Sciences of the United States of America* 105(39):14773–14778.

Zhou, F. 2009. Cancer photothermal therapy in the near-infrared region by using single-walled carbon nanotubes. *Journal of Biomedical Optics* 14(2):021009.

Zhou, F. F., S. N. Wu et al. 2011. Mitochondria-targeting single-walled carbon nanotubes for cancer photothermal therapy. *Small* 7(19):2727–2735.

Bibliography

Ai, J., E. Biazar et al. 2011. Nanotoxicology and nanoparticle safety in biomedical designs. *International Journal of Nanomedicine* 6:1117–1127.

Ajayan, P. M., M. Terrones et al. 2002. Nanotubes in a flash— ignition and reconstruction. *Science* 296(5568):705.

Al-Hajj, M., M. S. Wicha et al. 2003. Prospective identification of tumorigenic breast cancer cells. *Proceedings of the National Academy of Sciences of the United States of America* 100(7):3983–3988.

Ananta, J. S., B. Godin et al. 2010. Geometrical confinement of gadolinium-based contrast agents in nanoporous particles enhances T(1) contrast. *Nature Nanotechnology* 5(11):815–821.

Avouris, P., M. Freitag et al. 2008. Carbon-nanotube photonics and optoelectronics. *Nature Photonics* 2(6):341–350.

Ayala, P., R. Arenal et al. 2010. The physical and chemical properties of heteronanotubes. *Reviews of Modern Physics* 82(2):1843–1885.

Bao, S., Q. Wu et al. 2006. Glioma stem cells promote radioresistance by preferential activation of the DNA damage response. *Nature* 444(7120):756–760.

Beg, S., M. Rizwan et al. 2011. Advancement in carbon nanotubes: Basics, biomedical applications and toxicity. *Journal of Pharmacy and Pharmacology* 63(2):141–163.

Beier, D., J. Wischhusen et al. 2008. CD133 Expression and cancer stem cells predict prognosis in high-grade oligodendroglial tumors. *Brain Pathology* 18(3):370–377.

Berber, S., Y. K. Kwon et al. 2000. Unusually high thermal conductivity of carbon nanotubes. *Physical Review Letters* 84(20):4613–4616.

Bergamaschi, D., M. Gasco et al. 2003. p53 polymorphism influences response in cancer chemotherapy via modulation of p73-dependent apoptosis. *Cancer Cell* 3(4):387–402.

Bhirde, A. A., S. Patel et al. 2010. Distribution and clearance of PEG-single-walled carbon nanotube cancer drug delivery vehicles in mice. *Nanomedicine* 5(10):1535–1546.

Biris, A. R., S. Ardelean et al. 2011. Studies on near infrared optical absorption, Raman scattering, and corresponding thermal properties of single- and double-walled carbon nanotubes for possible cancer targeting and laser-based ablation. *Carbon* 49(13):4403–4411.

Biris, A. S., D. Boldor et al. 2009. Nanophotothermolysis of multiple scattered cancer cells with carbon nanotubes guided by time-resolved infrared thermal imaging. *Journal of Biomedical Optics* 14(2):021007.

Boldor, D., L. Picou et al. 2010. Spatio-temporal thermal kinetics of *in situ* MWCNT heating in biological tissues under NIR laser irradiation. *Nanotechnology* 21(43). Q5

Brannon-Peppas, L., and J. O. Blanchette. 2004. Nanoparticle and targeted systems for cancer therapy. *Advanced Drug Delivery Reviews* 56(11):1649–1659.

Brigger, I., C. Dubernet et al. 2002. Nanoparticles in cancer therapy and diagnosis. *Advanced Drug Delivery Reviews* 54(5):631–651.

Burke, A., X. Ding et al. 2009. Long-term survival following a single treatment of kidney tumors with multiwalled carbon nanotubes and near-infrared radiation. *Proceedings of the National Academy of Sciences of the United States of America* 106(31):12897–12902.

Burke, A. R., R. N. Singh et al. 2011. Determinants of the thrombogenic potential of multiwalled carbon nanotubes. *Biomaterials* 32(26):5970–5978.

Burke, A. R., R. N. Singh et al. 2012. The resistance of breast cancer stem cells to conventional hyperthermia and their sensitivity to nanoparticle-mediated photothermal therapy. *Biomaterials* 33(10):2961–2970.

Burlaka, A., S. Lukin et al. 2010. Hyperthermic effect of multiwalled carbon nanotubes stimulated with near infrared irradiation for anticancer therapy: *In vitro* studies. *Experimental Oncology* 32(1):48–50.

Cai, D., J. M. Mataraza et al. 2005. Highly efficient molecular delivery into mammalian cells using carbon nanotube spearing. *Nature Methods* 2(6):449–454.

Cassell, A. M., J. A. Raymakers et al. 1999. Large scale CVD synthesis of single-walled carbon nanotubes. *The Journal of Physical Chemistry B* 103(31):6484–6492.

Cato, M. H., F. D'Annibale et al. 2008. Cell-type specific and cytoplasmic targeting of PEGylated carbon nanotube-based nanoassemblies. *Journal of Nanoscience and Nanotechnology* 8(5):2259–2269.

Chakravarty, P., R. Marches et al. 2008. Thermal ablation of tumor cells with antibody-functionalized single-walled carbon nanotubes. *Proceedings of the National Academy of Sciences of the United States of America* 105(25):8697–8702.

Chen, J., S. Chen et al. 2008. Functionalized single-walled carbon nanotubes as rationally designed vehicles for tumor-targeted drug delivery. *Journal of the American Chemical Society* 130(49):16778–16785.

Chen, W. R., M. Korbelik et al. 2005. Enhancement of laser cancer treatment by a chitosan-derived immunoadjuvant. *Photochemistry and Photobiology* 81(1):190–195.

Dai, H. 2002. Carbon nanotubes: Synthesis, integration, and properties. *Accounts of Chemical Research* 35(12):1035–1044.

Day, E. S., J. G. Morton et al. 2009. Nanoparticles for thermal cancer therapy. *Journal of Biomechanical Engineering-Transactions of the Asme* 131(7):–.

Deng, X. Y., F. Wu et al. 2009. The splenic toxicity of water soluble multi-walled carbon nanotubes in mice. *Carbon* 47(6):1421–1428.

Diehn, M., and M. F. Clarke. 2006. Cancer stem cells and radiotherapy: New insights into tumor radioresistance. *Journal of the National Cancer Institute* 98(24):1755–1757.

Ding, X., R. Singh et al. 2011. Development of iron-containing multiwalled carbon nanotubes for MR-guided laser-induced thermotherapy. *Nanomedicine (London)*.

Dobrovolskaia, M. A., P. Aggarwal et al. 2008. Preclinical studies to understand nanoparticle interaction with the immune system and its potential effects on nanoparticle biodistribution. *Molecular Pharmaceutics* 5(4):487–495.

Doherty, S. P., D. B. Buchholz et al. 2006. Semi-continuous production of multiwalled carbon nanotubes using magnetic field assisted arc furnace. *Carbon* 44(8):1511–1517.

Donaldson, K., F. Murphy et al. 2011. Identifying the pulmonary hazard of high aspect ratio nanoparticles to enable their safety-by-design. *Nanomedicine (London)* 6(1):143–156.

Dresselhaus, M. S. 2004. Applied physics: Nanotube antennas. *Nature* 432(7020):959–960.

Dresselhaus, M. S., G. Dresselhaus et al. 1995. Physics of carbon nanotubes. *Carbon* 33(7):883–891.

Dumitrica, T., M. E. Garcia et al. 2004. Selective cap opening in carbon nanotubes driven by laser-induced coherent phonons. *Physical Review Letters* 92(11):117401.

Dyke, C. A., and J. M. Tour. 2004. Overcoming the insolubility of carbon nanotubes through high degrees of sidewall functionalization. *Chemistry* 10(4):812–817.

Ebbesen, T. W., and P. M. Ajayan. 1992. Large-scale synthesis of carbon nanotubes. *Nature* 358(6383):220–222.

Esfarjani, K., A. A. Farajian et al. 1999. Electronic and transport properties of N-P doped nanotubes. *Applied Physics Letters* 74(1):79–81.

Falk, M. H., and R. D. Issels. 2001. Hyperthermia in oncology. *International Journal of Hyperthermia* 17(1):1–18.

Feazell, R. P., N. Nakayama-Ratchford et al. 2007. Soluble single-walled carbon nanotubes as longboat delivery systems for platinum(IV) anticancer drug design. *Journal of the American Chemical Society* 129(27):8438–8439.

Fisher, J. W., S. Sarkar et al. 2010. Photothermal response of human and murine cancer cells to multiwalled carbon nanotubes after laser irradiation. *Cancer Research* 70(23): 9855–9864.

Gannon, C. J., P. Cherukuri et al. 2007. Carbon nanotube-enhanced thermal destruction of cancer cells in a noninvasive radiofrequency field. *Cancer* 110(12):2654–2665.

Ge, Z. B., Y. J. Kang et al. 2005. Thermal transport in Au-core polymer–shell nanoparticles. *Nano Letters* 5(3):531–535.

Geohegan, D. B., A. A. Puretzky et al. 2007. In situ time-resolved measurements of carbon nanotube and nanohorn growth. *Physica Status Solidi (B)* 244(11):3944–3949.

Ghosh, S., S. Dutta et al. 2009. Increased heating efficiency and selective thermal ablation of malignant tissue with DNA-encased multiwalled carbon nanotubes. *ACS Nano* 3(9):2667–2673.

Gnyawali, S. C., Y. Chen et al. 2008. Temperature measurement on tissue surface during laser irradiation. *Medical & Biological Engineering & Computing* 46(2):159–168.

Gottesman, M. M. 2002. Mechanisms of cancer drug resistance. *Annual Review of Medicine* 53(1):615–627.

Hagen, A., G. Moos et al. 2004. Electronic structure and dynamics of optically excited single-wall carbon nanotubes. *Applied Physics A Materials Science & Processing* 78(8):1137–1145.

Hanson, G. W. 2005. Fundamental transmitting properties of carbon nanotube antennas. *Ieee Transactions on Antennas and Propagation* 53(11):3426–3435.

Hartland, G. V., M. Hu et al. 2004. Investigation of the properties of gold nanoparticles in aqueous solution at extremely high lattice temperatures. *Chemical Physics Letters* 391(4–6):220–225.

Hartman, K. B., S. Laus et al. 2008. Gadonanotubes as ultrasensitive pH-smart probes for magnetic resonance imaging. *Nano Letters* 8(2):415–419.

Hata, K., D. N. Futaba et al. 2004. Water-assisted highly efficient synthesis of impurity-free single-walled carbon nanotubes. *Science* 306(5700):1362–1364.

Hone, J. 2000. Electrical and thermal transport properties of magnetically aligned single wall carbon nanotube films. *Applied Physics Letters* 77(5):666.

Hone, J., M. C. Llaguno et al. 2000. Electrical and thermal transport properties of magnetically aligned single walt carbon nanotube films. *Applied Physics Letters* 77(5):666–668.

Huang, N., H. Wang et al. 2010. Single-wall carbon nanotubes assisted photothermal cancer therapy: Animal study with a murine model of squamous cell carcinoma. *Lasers in Surgery and Medicine* 42(9):638–648.

Iancu, C., and L. Mocan. 2011. Advances in cancer therapy through the use of carbon nanotube-mediated targeted hyperthermia. *International Journal of Nanomedicine* 6:1675–1684.

Iijima, S. 1991. Helical microtubules of graphitic carbon. *Nature* 354(6348):56–58.

Imholt, T. J., C. A. Dyke et al. 2003. Nanotubes in microwave fields: Light emission, intense heat, outgassing, and reconstruction. *Chemistry of Materials* 15(21):3969–3970.

Javey, A., J. Guo et al. 2003. Ballistic carbon nanotube field-effect transistors. *Nature* 424(6949):654–657.

Jia, G., H. F. Wang et al. 2005. Cytotoxicity of carbon nanomaterials: Single-wall nanotube, multi-wall nanotube, and fullerene. *Environmental Science & Technology* 39(5):1378–1383.

Jordan, C. T., M. L. Guzman et al. 2006. Cancer stem cells. *New England Journal of Medicine* 355(12):1253–1261.

Kaiser, J. P., M. Roesslein et al. 2011. Carbon nanotubes — curse or blessing. *Current Medicinal Chemistry* 18(14): 2115–2128.

Kam, N. W., and H. Dai. 2005. Carbon nanotubes as intracellular protein transporters: Generality and biological functionality. *Journal of the American Chemical Society* 127(16):6021–6026.

Kam, N. W., M. O'Connell et al. 2005. Carbon nanotubes as multifunctional biological transporters and near-infrared agents for selective cancer cell destruction. *Proceedings of the National Academy of Sciences of the United States of America* 102(33):11600–11605.

Kamen, B. A., and A. K. Smith. 2004. A review of folate receptor alpha cycling and 5-methyltetrahydrofolate accumulation with an emphasis on cell models in vitro. *Advanced Drug Delivery Reviews* 56(8):1085–1097.

Kanemitsu, Y. 2011. Excitons in semiconducting carbon nanotubes: Diameter-dependent photoluminescence spectra. *Physical Chemistry Chemical Physics* 13(33):14879–14888.

Kang, B., D. Yu et al. 2009. Cancer-cell targeting and photoacoustic therapy using carbon nanotubes as bomb agents. *Small* 5(11):1292–1301.

Kangasniemi, M., R. J. McNichols et al. 2004. Thermal therapy of canine cerebral tumors using a 980 nm diode laser with MR temperature-sensitive imaging feedback. *Lasers in Surgery and Medicine* 35(1):41–50.

Keblinski, P., D. G. Cahill et al. 2006. Limits of localized heating by electromagnetically excited nanoparticles. *Journal of* Q5 *Applied Physics* 100(5).

Kempa, K. 2002. Gapless plasmons in carbon nanotubes and their Q5 interactions with phonons. *Physical Review* B66(19).

Keren, K., R. S. Berman et al. 2003. DNA-templated carbon nanotube field-effect transistor. *Science* 302(5649):1380–1382.

Kim, K. Y. 2007. Nanotechnology platforms and physiological challenges for cancer therapeutics. *Nanomedicine* 3(2): 103–110.

Klingeler, R., S. Hampel et al. 2008. Carbon nanotube based biomedical agents for heating, temperature sensoring and drug delivery. *International journal of hyperthermia* 24(6):496–505.

Kolosnjaj, J., H. Szwarc et al. 2007. Toxicity studies of carbon nanotubes. *Bio-Applications of Nanoparticles* 620:181–204.

Kong, L. B., S. Li et al. 2010. Electrically tunable dielectric materials and strategies to improve their performances. *Progress in Materials Science* 55(8):840–893.

Konig, K. 2000. Multiphoton microscopy in life sciences. *Journal of Microscopy* 200(Pt 2):83–104.

Kostarelos, K. 2008. The long and short of carbon nanotube toxicity. *Nature Biotechnology* 26(7):774–776.

Kostarelos, K., A. Bianco et al. 2009. Promises, facts and challenges for carbon nanotubes in imaging and therapeutics. *Nature Nanotechnol* 4(10):627–633.

Kostarelos, K., L. Lacerda et al. 2007. Cellular uptake of functionalized carbon nanotubes is independent of functional group and cell type. *Nature Nanotechnol* 2(2):108–113.

Koyama, S., Y. A. Kim et al. 2009. In vivo immunological toxicity in mice of carbon nanotubes with impurities. *Carbon* 47(5):1365–1372.

Kratz, F. 2010. Albumin, a versatile carrier in oncology. *International Journal of Clinical Pharmacology and Therapeutics* 48(7):453–455.

Lacerda, L., A. Bianco et al. 2006. Carbon nanotubes as nanomedicines: From toxicology to pharmacology. *Advanced Drug Delivery Reviews* 58(14):1460–1470.

Lam, C. W., J. T. James et al. 2006. A review of carbon nanotube toxicity and assessment of potential occupational and environmental health risks. *Critical Reviews in Toxicology* 36(3):189–217.

Leamon, C. P., and J. A. Reddy. 2004. Folate-targeted chemotherapy. *Advanced Drug Delivery Reviews* 56(8):1127–1141.

Lee, J., S. Kotliarova et al. 2006. Tumor stem cells derived from glioblastomas cultured in bFGF and EGF more closely mirror the phenotype and genotype of primary tumors than do serum-cultured cell lines. *Cancer Cell* 9(5):391–403.

Lehman, J. H., M. Terrones et al. 2011. Evaluating the characteristics of multiwall carbon nanotubes. *Carbon* 49(8): 2581–2602.

Levi-Polyachenko, N. H., E. J. Merkel et al. 2009. Rapid photothermal intracellular drug delivery using multiwalled carbon nanotubes. *Molecular Pharmaceutics* 6(4):1092–1099.

Li, S. D., and L. Huang. 2008. Pharmacokinetics and biodistribution of nanoparticles. *Molecular Pharmaceutics* 5(4):496–504.

Liu, C. H., and S. S. Fan. 2005. Effects of chemical modifications Q5 on the thermal conductivity of carbon nanotube composites. *Applied Physics Letters* 86(12).

Liu, Y. Q., and L. Gao. 2005. A study of the electrical properties of carbon nanotube-$NiFe_2O_4$ composites: Effect of the surface treatment of the carbon nanotubes. *Carbon* 43(1):47–52.

Liu, Z. W., A. Bushmaker et al. 2011. Thermal emission spectra from individual suspended carbon nanotubes. *ACS Nano* 5(6):4634–4640.

Liu, Z., W. B. Cai et al. 2007. In vivo biodistribution and highly efficient tumour targeting of carbon nanotubes in mice. *Nature Nanotechnology* 2(1):47–52.

Liu, Z., W. Cai et al. 2007. *In vivo* biodistribution and highly efficient tumour targeting of carbon nanotubes in mice. *Nature Nanotechnology* l2:6.

Liu, Z., K. Chen et al. 2008. Drug delivery with carbon nanotubes for *in vivo* cancer treatment. *Cancer Research* 68(16):6652–6660.

Liu, Z., S. M. Tabakman et al. 2009. Preparation of carbon nanotube bioconjugates for biomedical applications. *Nature Protocols* 4(9):1372–1382.

Maeda, H., J. Wu et al. 2000. Tumor vascular permeability and the EPR effect in macromolecular therapeutics: A review. *Journal of Controlled Release* 65(1–2):271–284.

Marches, R., C. Mikoryak et al. 2011. The importance of cellular internalization of antibody-targeted carbon nanotubes in the photothermal ablation of breast cancer cells. *Nanotechnology* 22(9):095101.

Marches, R., P. Chakravarty et al. 2009. Specific thermal ablation of tumor cells using single-walled carbon nanotubes targeted by covalently-coupled monoclonal antibodies. *International Journal of Cancer* 125(12):2970–2977.

Mayer, A., M. Vadon et al. 2009. The role of nanoparticle size in hemocompatibility. *Toxicology* 258(2–3):139–147.

McDevitt, M. R., D. Chattopadhyay et al. 2007. Tumor targeting with antibody-functionalized, radiolabeled carbon nanotubes. *Journal of Nuclear Medicine* 48(7):1180–1189.

Meng, J., J. Meng et al. 2008. Carbon nanotubes conjugated to tumor lysate protein enhance the efficacy of an antitumor immunotherapy. *Small* 4(9):1364–1370.

Milne, W. I., K. B. K. Teo et al. 2004. Carbon nanotubes as field emission sources. *Journal of Materials Chemistry* 14(6):933–943.

Moon, H. K., S. H. Lee et al. 2009. In vivo near-infrared mediated tumor destruction by photothermal effect of carbon nanotubes. *ACS Nano* 3(11):3707–3713.

Nakashima, N., and T. Fujigaya. 2007. Fundamentals and applications of soluble carbon nanotubes. *Chemistry Letters* 36(6):692–697.

Nikfarjam, M., V. Muralidharan et al. 2005. Mechanisms of focal heat destruction of liver tumors. *Journal of Surgical Research* 127(2):208–223.

Ning, S., S. Lu et al. 2007. Integrated molecular targeting of IGF1R and HER2 surface receptors and destruction of breast cancer cells using single wall carbon nanotubes. *Nanotechnology* 18(31):315101.

Nobuhito, I. and et al. 2007. Synthesis-condition dependence of carbon nanotube growth by alcohol catalytic chemical vapor deposition method. *Science and Technology of Advanced Materials* 8(4):292.

O'Neal, D. P., L. R. Hirsch et al. 2004. Photo-thermal tumor ablation in mice using near infrared-absorbing nanoparticles. *Cancer Letters* 209(2):171–176.

Osman, M. A., and D. Srivastava. 2001. Temperature dependence of the thermal conductivity of single-wall carbon nanotubes. *Nanotechnology* 12(1):21–24.

Panchapakesan, B., S. Lu et al. 2005. Single-wall carbon nanotube nanobomb agents for killing breast cancer cells. *NanoBioTechnology* 1(2):133–139.

Pantarotto, D., J. P. Briand et al. 2004b. Translocation of bioactive peptides across cell membranes by carbon nanotubes. *Chemical Communications (Cambridge)* 1:16–17.

Pantarotto, D., C. D. Partidos et al. 2003. Immunization with peptide-functionalized carbon nanotubes enhances virus-specific neutralizing antibody responses. *Chemistry & Biology* 10(10):961–966.

Pantarotto, D., R. Singh et al. 2004a. Functionalized carbon nanotubes for plasmid DNA gene delivery. *Angewandte Chemie. International Edition in English* 43(39):5242–5246.

Park, E. J., W. S. Cho et al. 2009. Pro-inflammatory and potential allergic responses resulting from B cell activation in mice treated with multi-walled carbon nanotubes by intratracheal instillation. *Toxicology* 259(3):113–121.

Patchkovskii, S., J. S. Tse et al. 2005. Graphene nanostructures as tunable storage media for molecular hydrogen. *Proceedings of the National Academy of Sciences of the United States of America* 102(30):10439–10444.

Patri, A. K., A. Myc et al. 2004. Synthesis and *in vitro* testing of J591 antibody–dendrimer conjugates for targeted prostate cancer therapy. *Bioconjugate Chemistry* 15(6):1174–1181.

Picou, L., C. McMann et al. 2010. Spatio-temporal thermal kinetics of *in situ* MWCNT heating in biological tissues under NIR laser irradiation. *Nanotechnology* 21(43):435101.

Plech, A., S. Kurbitz et al. 2003. Time-resolved X-ray diffraction on laser-excited metal nanoparticles. *Europhysics Letters* 61(6):762–768.

Pommier, Y., O. Sordet et al. 2004. Apoptosis defects and chemotherapy resistance: Molecular interaction maps and networks. *Oncogene* 23(16):2934–2949.

Pop, E., D. Mann et al. 2006. Thermal conductance of an individual single-wall carbon nanotube above room temperature. *Nano Letters* 6(1):96–100.

Puretzky, A. A., D. B. Geohegan et al. 2000. Dynamics of single-wall carbon nanotube synthesis by laser vaporization. *Applied Physics A: Materials Science & Processing* 70(2):153–160.

Pustovalov, V. K., and V. A. Babenko. 2004. Optical properties of gold nanoparticles at laser radiation wavelengths for laser applications in nanotechnology and medicine. *Laser Physics Letters* 1(10):516–520.

Qu, G. B., Y. H. Bai et al. 2009. The effect of multiwalled carbon nanotube agglomeration on their accumulation in and damage to organs in mice. *Carbon* 47(8):2060–2069.

Radomski, A., P. Jurasz et al. 2005. Nanoparticle-induced platelet aggregation and vascular thrombosis. *British Journal of Pharmacology* 146(6):882–893.

Raffa, V., G. Ciofani et al. 2010. Physicochemical properties affecting cellular uptake of carbon nanotubes. *Nanomedicine* 5(1):89–97.

Reulet, B., A. Y. Kasumov et al. 2000. Acoustoelectric effects in carbon nanotubes. *Physical Review Letters* 85(13):2829–2832.

Richard, C., B. T. Doan et al. 2008. Noncovalent functionalization of carbon nanotubes with amphiphilic Gd3+ chelates: Toward powerful T-1 and T-2 MRI contrast agents. *Nano Letters* 8(1):232–236.

Rieke, V., and K. B. Pauly. 2008. MR thermometry. *Journal of Magnetic Resonance Imaging* 27(2):376–390.

Robinson, J. T., K. Welsher et al. 2010. High performance *in vivo* near-IR (>1 mum) imaging and photothermal cancer therapy with carbon nanotubes. *Nano Research* 3(11): 779–793.

Ruenraroengsak, P., J. M. Cook et al. 2010. Nanosystem drug targeting: Facing up to complex realities. *Journal of Controlled Release* 141(3):265–276.

Ryman-Rasmussen, J. P., E. W. Tewksbury et al. 2009. Inhaled multiwalled carbon nanotubes potentiate airway fibrosis in murine allergic asthma. *American Journal of Respiratory Cell and Molecular Biology* 40(3):349–358.

Saito, R., M. Hofmann et al. 2011. Raman spectroscopy of graphene and carbon nanotubes. *Advances in Physics* 60(3):413–550.

Saito, Y., K. Hata et al. 2002. Field emission of carbon nanotubes and its application as electron sources of ultra-high luminance light-source devices. *Physica B-Condensed Matter* 323(1–4):30–37.

Salvador-Morales, C., W. W. Gao et al. 2009. Multifunctional nanoparticles for prostate cancer therapy. *Expert Review of Anticancer Therapy* 9(2):211–221.

Sayes, C. M., F. Liang et al. 2006. Functionalization density dependence of single-walled carbon nanotubes cytotoxicity in vitro. *Toxicology Letters* 161(2):135–142.

Schipper, M. L., N. Nakayama-Ratchford et al. 2008. A pilot toxicology study of single-walled carbon nanotubes in a small sample of mice. *Nature Nanotechnology* 3(4):216–221.

Q5 Schonenberger, C., and L. Forro. 2000. Mulitwalled carbon nanotubes. *Physics World* 6(37).

Selvi, B. R., D. Jagadeesan et al. 2008. Intrinsically fluorescent carbon nanospheres as a nuclear targeting vector: Delivery of membrane-impermeable molecule to modulate gene expression in vivo. *Nano Letters* 8(10):3182–3188.

Semberova, J., S. H. De Paoli Lacerda et al. 2009. Carbon nanotubes activate blood platelets by inducing extracellular Ca2+ influx sensitive to calcium entry inhibitors. *Nano Letters* 9(9):3312–3317.

Shi Kam, N. W., T. C. Jessop et al. 2004. Nanotube molecular transporters: Internalization of carbon nanotube–protein conjugates into Mammalian cells. *Journal of the American Chemical Society* 126(22):6850–6851.

Shvedova, A. A., E. R. Kisin et al. 2005. Unusual inflammatory and fibrogenic pulmonary responses to single-walled carbon nanotubes in mice. *American Journal of Physiology-Lung Cellular and Molecular Physiology* 289(5):L698–L708.

Singh, S. K., C. Hawkins et al. 2004. Identification of human brain tumour initiating cells. *Nature* 432(7015):396–401.

Singh, R., D. Pantarotto et al. 2005. Binding and condensation of plasmid DNA onto functionalized carbon nanotubes: Toward the construction of nanotube-based gene delivery vectors. *Journal of the American Chemical Society* 127(12): 4388–4396.

Singh, R., D. Pantarotto et al. 2006. Tissue biodistribution and blood clearance rates of intravenously administered carbon nanotube radiotracers. *Proceedings of the National Academy of Sciences of the United States of America* 103(9):3357–3362.

Sitharaman, B., K. R. Kissell et al. 2005. Superparamagnetic gadonanotubes are high-performance MRI contrast agents. *Chemical Communications* (31):3915–3917.

Smart, S. K., A. I. Cassady et al. 2006. The biocompatibility of carbon nanotubes. *Carbon* 44(6):1034–1047.

Stella, G. M. 2011. Carbon nanotubes and pleural damage: Perspectives of nanosafety in the light of asbestos experience. *Biointerphases* 6(2):P1–P17.

Stoyanov, S. R., A. V. Titov et al. 2009. Transition metal and nitrogen doped carbon nanostructures. *Coordination Chemistry Reviews* 253(23–24):2852–2871.

Talanov, V. S., C. A. Regino et al. 2006. Dendrimer-based nanoprobe for dual modality magnetic resonance and fluorescence imaging. *Nano Letters* 6(7):1459–1463.

Tasis, D., N. Tagmatarchis et al. 2003. Soluble carbon nanotubes. *Chemistry-A European Journal* 9(17):4001–4008.

Terrones, M., A. G. Souza et al. 2008. Doped carbon nanotubes: Synthesis, characterization and applications. *Carbon Nanotubes* 111:531–566.

Torti, S. V., F. Byrne et al. 2007. Thermal ablation therapeutics based on CN(x) multi-walled nanotubes. *Int J Nanomedicine* 2(4):707–714.

Uo, M., T. Akasaka et al. 2011. Toxicity evaluations of various carbon nanomaterials. *Dental Materials Journal* 30(3): 245–263.

Van Lehn, R. C., C. E. Sing et al. 2010. Multidimensional targeting: Using physical and chemical forces in unison. *Current Pharmaceutical Biotechnology* 11(4):320–332.

Vazquez, E., and M. Prato. 2009. Carbon nanotubes and microwaves: Interactions, responses, and applications. *ACS Nano* 3(12):3819–3824.

Vitetta, E. S., R. Marches et al. 2011. The importance of cellular internalization of antibody-targeted carbon nanotubes in the photothermal ablation of breast cancer cells. *Nanotechnology* 22(9). Q5

Wadhawan, A. 2003. Nanoparticle-assisted microwave absorption by single-wall carbon nanotubes. *Applied Physics Letters* 83(13):2683.

Wang, Y. 2004. Receiving and transmitting light-like radio waves: Antenna effect in arrays of aligned carbon nanotubes. *Applied Physics Letters* 85(13):2607.

Wang, X., J. Ren et al. 2008. Targeted RNA interference of cyclin A2 mediated by functionalized single-walled carbon nanotubes induces proliferation arrest and apoptosis in chronic myelogenous leukemia K562 cells. *ChemMedChem* 3(6):940–945.

Wang, C. H., S. H. Chiou et al. 2011. Photothermolysis of glioblastoma stem-like cells targeted by carbon nanotubes conjugated with CD133 monoclonal antibody. *Nanomedicine* 7(1):69–79.

Wang, C. H., Y. J. Huang et al. 2009. In vitro photothermal destruction of neuroblastoma cells using carbon nanotubes conjugated with GD2 monoclonal antibody. *Nanotechnology* 20(31):315101.

Warheit, D. B. 2006. What is currently known about the health risks related to carbon nanotube exposures? *Carbon* 44(6):1064–1069.

Weisman, R. B. 2003. Carbon nanotubes — Four degrees of separation. *Nature Materials* 2(9):569–570.

Weissleder, R. 2001. A clearer vision for *in vivo* imaging. *Nature Biotechnology* 19(4):316–317.

Welsher, K., Z. Liu et al. 2008. Selective probing and imaging of cells with single walled carbon nanotubes as near-infrared fluorescent molecules. *Nano Letters* 8(2):586–590.

Whitney, J. R., S. Sarkar et al. 2011. Single walled carbon nanohorns as photothermal cancer agents. *Lasers in Surgery and Medicine* 43(1):43–51.

Wick, P., P. Manser et al. 2007. The degree and kind of agglomeration affect carbon nanotube cytotoxicity. *Toxicology Letters* 168(2):121–131.

Wong, S. S., E. Joselevich et al. 1998. Covalently functionalized nanotubes as nanometre-sized probes in chemistry and biology. *Nature* 394(6688):52–55.

Xiao, Y., X. Gao et al. 2009. Anti-HER2 IgY antibody-functionalized single-walled carbon nanotubes for detection and selective destruction of breast cancer cells. *BMC Cancer* 9:351.

Yang, S. T., X. Wang et al. 2008. Long-term accumulation and low toxicity of single-walled carbon nanotubes in intravenously exposed mice. *Toxicology Letters* 181(3):182–189.

Ye, Z., W. D. Deering et al. 2006. Microwave absorption by an array of carbon nanotubes: A phenomenological model. *Physical Review B* 74(7):075425.

Yin, L. C., H. M. Cheng et al. 2011. Fermi level dependent optical transition energy in metallic single-walled carbon nanotubes. *Carbon* 49(14):4774–4780.

Yoo, J. W., E. Chambers et al. 2010. Factors that control the circulation time of nanoparticles in blood: Challenges, solutions and future prospects. *Current Pharmaceutical Design* 16(21):2298–2307.

You, C. C., A. Verma et al. 2006. Engineering the nanoparticle-biomacromolecule interface. *Soft Matter* 2(3):190–204.

Yu, X., B. Munge et al. 2006. Carbon nanotube amplification strategies for highly sensitive immunodetection of cancer biomarkers. *Journal of the American Chemical Society* 128(34):11199–11205.

Zeppernick, F., R. Ahmadi et al. 2008. Stem cell marker CD133 affects clinical outcome in glioma patients. *Clinical Cancer Research* 14(1):123–129.

Zhang, M., T. Murakami et al. 2008. Fabrication of ZnPc/protein nanohorns for double photodynamic and hyperthermic cancer phototherapy. *Proceedings of the National Academy of Sciences of the United States of America* 105(39):14773–14778.

Zhang, J. F., J. C. Ge et al. 2010. In vitro and *in vivo* studies of single-walled carbon nanohorns with encapsulated metallofullerenes and exohedrally functionalized quantum dots. *Nano Letters* 10(8):2843–2848.

Zhang, W., Z. Zhang et al. 2011. The application of carbon nanotubes in target drug delivery systems for cancer therapies. *Nanoscale Res Lett* 6:555.

Zharov, V. P., E. N. Galitovskaya et al. 2005. Synergistic enhancement of selective nanophotothermolysis with gold nanoclusters: Potential for cancer therapy. *Lasers in Surgery and Medicine* 37(3):219–226.

Zhou, F. 2009. Cancer photothermal therapy in the near-infrared region by using single-walled carbon nanotubes. *Journal of Biomedical Optics* 14(2):021009.

Zhou, F. F., D. Xing et al. 2010. New insights of transmembranal mechanism and subcellular localization of noncovalently modified single-walled carbon nanotubes. *Nano Letters* 10(5):1677–1681.

Zhou, F. F., S. N. Wu et al. 2011. Mitochondria-targeting single-walled carbon nanotubes for cancer photothermal therapy. *Small* 7(19):2727–2735.

Q1: There is no Table 4 included found in this chapter. Please confirm if there is a fourth table for this chapter and provide the missing data, as necessary

Q2: Citation to Section 16.5 was changed to Section 17.5; please check, or correct as necessary.

Q3: If this footnote has corresponding citation within the Table 17.2, please delete.

Q4: Not found in the Reference list; please provide the complete details for this citation.

Q5: Please provide the page range.

Published in final edited form as:
Adv Mater. 2012 June 12; 24(22): 2992–2998. doi:10.1002/adma.201200706.

Hybrid 2D Nanomaterials as Dual-mode Contrast Agents in Cellular Imaging

Tharangattu N. Narayanan[1], **Bipin K. Gupta**[2], **Sajna A. Vithayathil**[3], **Rebeca R. Aburto**[1,4], **Prof. Sendurai A. Mani**[3], **Jaime Taha-Tijerina**[1], **Bin Xie**[5], **Benny A. Kaipparettu**[4], **Suzy V. Torti**[5], and **Prof. Pulickel M. Ajayan**[1]

Pulickel M. Ajayan: ajayan@rice.edu

[1]Department of Mechanical Engineering and Materials Science, Rice University, 6100 Main Street, Houston, TX 77006, USA

[2]National Physical Laboratory (CSIR), Dr. K. S. Krishnan Road, New Delhi 110012, India

[3]Department of Molecular and Human Genetics, Dan L. Duncan Cancer Center, Baylor College of Medicine, Houston, TX 77030, USA

[4]Department of Molecular Pathology, MD Anderson Cancer Center, 7435 Fannin Street, Unit # 951, Houston, TX 77054, USA

[5]Department of Biochemistry, Wake Forest School of Medicine, Winston-Salem, NC 27157, USA

Keywords

hybrid materials; imaging techniques; magnetic resonance imaging; luminescence; graphene oxide

The design of multifunctional nanofluids is highly desirable for biomedical therapy/cellular imaging applications.[1–4] The emergence of hybrid nanomaterials with specific properties, such as magnetism and fluorescence, can lead to an understanding of biological processes at the biomolecular level.[1] Various hybrid systems have been analyzed in the recent past for several possible biomedical applications.[5–9] Carbon-based hybrid systems such as carbon nanotubes with various nanoparticles are being widely tested for their biological applications because of their ability to cross cell membranes and their interesting thermal and electrical properties.[10,11] Graphene oxide (GO) is a fairly new graphene-based system with a 2D carbon honeycomb lattice decorated with numerous functional groups attached to the backbone: these functional groups make it an excellent platform for further attachment of nanoparticles and synthesis of hybrid materials. Cell viability studies on GO have been recently attempted, showing biocompatibility. [12,13] Moreover, the intrinsic photoluminescence (PL) properties of GO can be utilized for cellular imaging.[13] The large surface area and non-covalent interactions with aromatic molecules make GO an excellent system for biomolecular applications and drug attachment.

On the other hand, magnetic-field-assisted biomolecular imaging, drug delivery, and therapy have received tremendous attention in nano-biotechnology since the proposal of magnetic materials for hyperthermia treatment of cancer, in 1957.[14] Iron oxide (Fe_3O_4) occupies a unique position among the various magnetic materials as a result of its considerable saturation magnetization (87 emu g^{-1}), interesting transport properties, and, above all, high

*Correspondence to: Prof. P. M. Ajayan (ajayan@rice.edu).

Supporting Information
Supporting Information is available from the Wiley Online Library or from the author.

bio-compatibility.[2] Aqueous ferrofluids based on superparamagnetic iron oxide (SPION, ultrafine Fe_3O_4 nanoparticles having size ~10 nm) are well proven for their biomedical applications such as magnetic hyperthermia (using their radio-frequency power loss), magnetic contrast enhancement, enzyme immobilization, and drug targeting and delivery. [10]

The advent of state-of-the-art biomedical imaging tools has helped the development of cell imaging/tracking or gene monitoring with high temporal and spatial resolution.[15,16] Non-invasive multimodality techniques are also rapidly changing the evolving field of experimental imaging based on genetic expression and thus becoming suitable for future clinical practice. Each imaging technique has its own limitations, and multimodality imaging agents can address this hurdle. Magnetic resonance imaging (MRI) is an important diagnostic tool and is unique in its ability to generate 3D images of opaque and soft tissues with high spatial resolution. More interestingly, contrast in MR images arising from the variation in inherent relaxation times can be manipulated using contrast agents. But, despite its competitive molecular imaging capability, the inherent low sensitivity of the MRI technique demands the synthesis of high contrast enhancement agents. This has led to the use of nanoparticles of gadolinium (Gd, paramagnetic) and iron oxide (ferromagnetic/ superparamagnetic) as high relaxivity contrast enhancement agents.

Hybrid materials can also enable non-invasive imaging methods and diagnosis protocols by combining the unique properties of the individual system. Advances in nanotechnology have led to the development of hybrid versions of these nanoparticles, which can improve upon the low sensitivity of MRI by other techniques such as fluorescence. Fluorescence allows bio-imaging with high speed and sensitivity. It has been established that a combination of magnetic and fluorescent imaging techniques with nanostructured systems will be beneficial for in vivo disease diagnosis and in vitro monitoring of living cells.[17] However, the synthesis of highly luminescent biomaterials using ferromagnetic/superparamagnetic Fe_3O_4 is a complicated development owing to the fluorescence quenching property of Fe_3O_4. Researchers have developed lumino-magnetic phosphors for cell imaging applications, [18] but all those nanophosphor materials are paramagnetic in nature, limiting their bio-applications with low magnetic field assistance. Such a multimodality technique can combine the high spatial (50 μm) and temporal resolution of MRI with the high sensitivity of optical imaging probes, and most MRI/optical multimodal agents are based on organic dyes.[1] Though SPIONs have been commercially identified for their applications in T2-weighted MRI contrast enhancement, other imaging modalities using bare SPIONs cannot be realized. Recently, core/shell nanoparticles with SPIONs and polymer-passivated SPION/ metallic hybrid structures have proven their efficacy in other modalities such as optical imaging, magnetomotive photoacoustic imaging, and scattering-based imaging.[19–21]

Here we report the synthesis and demonstration of a single hybrid nanosystem for dual-mode cellular imaging using PL and MRI. An aqueous suspension of 2D nanofillers of GO-Fe_3O_4 (GO-F) at neutral pH (~7) is synthesized by a simple chemical route. Recently, there have been some reports on the synthesis of iron oxide functionalized GO particles by different chemical routes,[22–24] but the material has not been exploited in bio-imaging applications. Here we discuss a detailed PL study conducted on this nanofluid and its in vitro cancer cell imaging, hence demonstrating GO-F as a possible multimodalagent without any cell cytotoxicity. Direct use of iron oxide (Fe_3O_4/γFe_2O_3) for targeted drug delivery is not efficient owing to a “drug burst” effect (quick release of the drug upon injection) before the desired site is reached, and GO-F may be a better candidate since it has been demonstrated using Rhodamine molecules that aromatic drug molecules can be directly attached to the GO lattice. [25–27] In addition, theoretical evaluation of radio frequency power loss by measuring the specific absorption rate (SAR) for Fe_3O_4 nanoparticles having

size ~10 nm shows high values, indicating their suitability for applications in magnetic hyperthermia.[28] However, the heat transfer ability of Fe_3O_4-based ferrofluid is comparatively poor. The high heat transfer ability/thermal conductivity of GO can make GO-F an ideal material for hyperthermia applications.

Development of a GO-SPION-based hybrid system will also help in the investigation of the role of different parameters, such as surface roughness, functional groups, and shape/morphology of nanoparticles, in creating bio/nano interfaces.[29–31] Mahmoudi and Serpooshan proved that SPIONs with jagged surfaces can absorb various biomolecules/proteins much more strongly than SPIONs with smooth surfaces.[29] The GO flake platform also has considerable surface roughness and contains many functional groups, making it a unique material for understanding the biophysical properties at bio/nano interfaces.

We studied nanofluid stability using zeta potential measurements (Malvern Zen 3600 Zetasizer) along with measurements of the hydrodynamic radius of the particles by dynamic light scattering. The zeta potential of GO-F is −48.7 mV, indicating “good stability” of the nanofluid. This guarantees a long shelf-life. The hydrodynamic radius of GO-F was found to be ~583 nm. In situ chemical synthesis allows Fe_3O_4 nanoparticles to be covalently attached on to the GO surface.[16] Hence, the GO-F stable suspension is formed through the oxygen functionalities of GO with Fe_3O_4. Small flakes of GO, after sonication for 3 h, were fully suspended in water for 2 days. A schematic of GO-F is shown in Figure 1a. Epoxy, carboxyl, or hydroxyl groups available in GO make it chemically bond with Fe_3O_4. This was further verified by Fourier transform infrared (FTIR) analysis.

A TEM image of GO-F is shown in Figure 1b. The Fe_3O_4 nanoparticles having a size of approximately 10 nm are uniformly distributed in GO. High-resolution TEM (HRTEM) images and a selected area electron diffraction (SAED) image showing the (311) lattice plane of Fe_3O_4 (with dark contrast) are shown in the Supporting Information (Figure S1). In order to prove the graphitic nature of the nanocomposite sample, micro-Raman studies were conducted with GO-F powder; the result is shown in Figure 1c. Graphitic G (order) and D (disorder) Raman modes are marked in the figure. The higher intensity G peak indicates the extent of graphitization of the sample. The inset in this figure is a photograph of a stable GO-F suspension. The magnetic nature of the powder was verified using a vibrating sample magnetometer (VSM). The room temperature (300 K) magnetization $M(H)$ curve is depicted in Figure 1d. The sample shows a typical superparamagnetic S-like curve, which indicates the contribution of ultrafine Fe_3O_4. The XRD pattern of the GO-F powder is shown in Figure 1e. It consists of broad amorphous-like peaks around 24° and 44°, corresponding to GO having a lattice spacing of ~0.39 nm. The XRD results also indicate the presence of Fe_3O_4 (International Centre for Diffraction Data, ICDD: 750449). FTIR spectra of GO and GO-F are shown in Figure 1f. The presence of different types of oxygen functionalities in GO is evident from peaks corresponding to oxygen stretching vibration (2900–3600 cm^{-1}, –OH vibration), C=O stretching vibration (1720 cm^{-1}), C–OH stretching vibration (1220 cm^{-1}), and C–O stretching vibration (1060 cm^{-1}) in Figure 1f (dark line). Moreover, the signature of aromatic C=C stretching at ~1600 cm^{-1} indicates the presence of the sp^2 hybridized honeycomb lattice. The GO-F also contains these functional groups, but the positions of the bonds are red shifted and the sharpness of the peaks is changed, particularly that of aromatic C=C bonding (Figure 1e; light line). This indicates the change in the coordination environment of various functional groups in GO-F. Peaks between 400 and 700 cm^{-1} correspond to those of Fe-O in Fe_3O_4. The shift in the peak position and modification of C=C bonding is proposed as evidence for covalent bonding in GO with other nanoparticles. The presence of iron oxide in GO-F is further understood from the XPS analysis. The Fe 2p XPS spectrum of GO-F is shown in Figure 1f (the complete XPS spectrum is provided in Figure S2 in the Supporting Information). The peaks of Fe 2p1/2

and Fe 2p3/2 at 710.9 eV and 725 eV, respectively, establish the fact that the iron oxide in the sample is Fe_3O_4. To explore the facets of chemical interactions, interfacial effect, and associated optical properties of GO-F nanofluid, we characterized the pristine GO, Fe_3O_4 ferrofluid, and GO-F suspensions (in water) through UV-visible absorption spectroscopy. Figure 2a shows the absorption spectra of Fe_3O_4, GO, and GO-F. The absorption result reveals that GO-F is optically transparent in the 700–800 nm range. A blue shift of the absorption edge is noticed when the absorption spectrum of GO-F is compared to that of Fe_3O_4 ferrofluid. A higher concentration of Fe_3O_4 nanoparticles in GO strengthens such effects and therefore leads to the blue shift of the absorption spectrum. The blue shift of the absorption edge for GO-F can be attributed to two factors: a) the integration effect in the bandgap due to composite formation between GO (1.70 eV)[32] and Fe_3O_4 (~2.9 eV), [33] and b) the surface interaction and interface formation effect between Fe_3O_4 and functional groups present in GO.[34,35] The absorption peak at ~250 nm throws light onto the fact that a strong interface has formed between GO and Fe_3O_4 (since the absorption peaks of pristine GO and Fe_3O_4 are observed at ~228 nm and ~354 nm, respectively). This has been further confirmed by PL spectroscopy.

Figure 2b exhibits the PL emission spectrum of Fe_3O_4 ferrofluid. An emission peak is observed at 416 nm upon excitation at 365 nm wavelength(3.39 eV) and Figure 2c represents the corresponding PLE (excitation) spectrum for Fe_3O_4 nanoparticles at 416 nm (2.98 eV) emission of Fe_3O_4 nanoparticles. The observed result is consistent with other reports.[36] To investigate further the chemical interaction and the interface formation between GO and Fe_3O_4, rigorous PL studies on the GO-F hybrid system were performed. PL results are shown in Figures 2d–f. In order to confirm the interface formation, we excited the hybrid system at 365 nm wavelength, which will help to make a comparative study with Fe_3O_4. Interestingly, the PL emission spectrum of the GO-F hybrid system shows two strong peaks. One of them can be attributed to Fe_3O_4 and the other to the interface formation between GO and Fe_3O_4, as expected, through oxygen functionalities. In order to ensure that the extra peak represents the interface formation, we performed a PLE experiment. This will compute the actual excitation of the GO-F hybrid system. Figure 2e is the PLE spectrum of GO-F at 469 nm emission. Figure 2f shows strong blue peak emission centered at 469 nm with estimated color coordinates $x = 0.2035$, $y = 0.2427$ of the GO-F nanocomposite at 324 nm excitation wavelength. Moreover, we also performed PL emission spectroscopy of the pristine GO sample at 324 nm excitation to ensure that the additional peak is due to interface formation (Figure 2h). The enhanced luminescence in GO-F arises from the interface between GO and Fe_3O_4 nanoparticles through oxygen functionalities, that is, carboxyl, carbonyl, epoxy, and hydroxyl groups, present in GO nanoparticles. A strong blue emission of the hybrid is ascribed to the integration of surface effects of GO-F and optical emission of Fe_3O_4 nanoparticles.

To know the efficacy of the GO-F nanofluid system as an efficient fluorescent marker, we performed time-resolved photoluminescence (TRPL)spectroscopy. Luminescence decay profiles of GO-F are shown in Figure 2i. Decay was recorded for the GO-F transitions at 469 nm for emission at 371 nm excitation measured at room temperature by a time-correlated single photon counting technique. Lifetime data of the GO-F hybrid were very well fitted to a double-exponential function as shown in Figure 2i. Parameters generated from iterative reconvolution of the decay with the instrument response function (IRF) are listed in Figure 2j. Observed lifetimes of the GO-F are $\tau_1 = 0.70$ ns and $\tau_2 = 4.80$ ns. For double-exponential decay, the average lifetime, τ_{av}, is determined by[15,37,38]

$$\tau_{av}=\frac{A_1\tau_1^2+A_2\tau_2^2}{A_1\tau_1+A_2\tau_2} \quad (1)$$

The average lifetime of this GO-F system is estimated to be τ_{av} ~ 4.65 ns. The observed lifetime of GO-F is in nanoseconds, suggesting that the synthesized GO-F hybrid material is most suitable for biological applications.

As hypothesized, GO-F hybrid nanosuspensions can be used for biological applications such as bioimaging, cell tracking, and drug delivery, if the inherent toxicity of the material allows it. Therefore, the cytotoxicity of GO-F was evaluated using the MTT viability assay with two different human breast cancer cell lines, MDA-MB-231 and T47D, for the indicated period of time. As shown in Figure 3 (Figure S4), no marked cell death or proliferation defects were observed with cells cultured in GO-F suspensions compared to the untreated control cells, suggesting that GO-F does not pose any considerable toxicity problem to the cells.

To determine whether the GO-F hybrid can be used for cellular imaging, we performed in vitro cellular imaging studies using the human breast cancer cell line T47D. Figure 4a shows fluorescent microscopy images of T47D cells treated with GO-F for 24 h (its biocompatibility is shown in Figure S4; cell viability is consistent with the study on the other cell line MDA-MB-231). The blue fluorescent GO-F is distributed inside the cytoplasm as shown in Figures 4aii, iii, v, and vi. The Figures 4aiv–vi show magnified views of individual T47D cells treated with GO-F. The overlap of fluorescence and phase contrast images clearly shows the cellular localization of GO-F (an individual cell staining is shown in Figure S4 in the Supporting Information; it indicates that the nanoparticles are distributed outside the cell nucleus and inside the cell cytoplasm). Another breast cancer cell line named SUM159PT, which is a metastatic breast cancer cell, was also imaged using the fluorescence of GO-F and is shown in Figure S5 in the Supporting Information.

Nowadays, MRI is widely used to aid the diagnosis of many medical disorders. It is a safe non-invasive technique for medical imaging compared to other techniques such as X-ray computer tomography, where ionizing radiations are used. Moreover, owing to subtle physicochemical differences between organs and tissues, MRI is capable of differentiating tissue type and diseases that may not be detected by other imaging techniques. In order to evaluate GO-F as a potential MRI T2 contrast agent, GO-F was suspended in agarose in graded concentrations and T2 values were measured on a 7T MR scanner with a multi-slice multi-echo (MSME) sequence. The results were fitted into a three-parameter spin–spin relaxation equation using Matlab. The T2 value of 2% agarose phantom was greatly reduced from 111.9 to 33.8 and 61.7 ms when doped with 100 $\mu g\ mL^{-1}$ and 10 $\mu g\ mL^{-1}$ GO-F, respectively. T2-weighted MR images are shown in Figure 4b. To calculate molar relaxivity, we used XPS to determine the elemental percentage of iron in GO-F. On a molar basis, GO-F was 63.42% carbon, 35.64% oxygen, and 0.94% iron. Based on GO-F's iron content, its T2 relaxivity was 297.06 $mM^{-1}\ s^{-1}$. As expected, GO-F did not enhance T1 relaxivity. High contrast even with 100 $\mu g\ mL^{-1}$ (with these amounts no cell death has been observed) indicates that GO-F is a unique material for MRI clinical imaging. In order to find applications of this magnetic GO-F in other fields, such as therapy, thermal conductivity measurements have been conducted and details are provided in the Supporting Information. Enhanced thermal conductivity of GO-F also shows its possibilities in magnetic hyperthermia.

In conclusion, we have demonstrated a 2D hybrid nanostructure-based nanofluid that can be used as a contrast agent in a dual mode imaging process, and that allows one to easily

combine two complementary techniques (T2 MRI and optical fluorescence imaging) in cellular imaging. An interfacial energy transfer mechanism has been identified for the PL of GO-F. The time-resolved spectroscopy measurements reveal a nanosecond decay for hybrid GO-F fluid, indicating its potential applications in biological systems. The hybrid GO-F fluid showed good cell viability with different cancer cell lines. This nanofluid exhibited an enhanced thermal conductivity and the nanoparticles of GO-F were found to penetrate the cell cytoplasm, making it viable for intra-cellular magnetic hyperthermia applications. The surface functionalities in GO provide a good platform for large loading of aromatic drug molecules, thereby avoiding “drug burst” effects associated with bare SPIONs.

Experimental Section

GO-F synthesis

GO was synthesized in water using a modified Hummers’ method as previously reported. [39] Uniformly sized Fe_3O_4 nanoparticles were synthesized within the GO suspension using a chemical co-precipitation technique. $FeSO_4{\cdot}7H_2O$ (1 mL, 0.1 M) and $FeCl_3$ (1 mL, 0.2 M) were placed in a conical flask and mixed well using sonication. 1 mL of this solution was added to 10 mL of the GO suspension and magnetically stirred for half an hour. Ammonia solution was dropped into this mixture with constant stirring until the pH of the solution reached 10 and the Fe_3O_4 nanoparticles started to precipitate within the GO. As soon as the pH reached 10, a 3 M citric acid solution was added dropwise while the solution was heated to 75 °C with constant magnetic stirring for 30 min. This solution was filtered (100 nm Teflon filter paper) and washed several times using distilled water until neutral pH was reached. The resultant filtrate was re-dispersed in distilled water using extensive sonication.

Characterization tools

The structural and morphological analyses of GO-F powder were carried out using HRTEM (JEM 2100F transmission electron microscope), and the Raman study was conducted using a micro-Raman spectroscope (Renishaw, inVia). Room temperature magnetic properties were probed using a VSM. XRD studies were conducted using Cu Kα radiation. FTIR studies on the sample were performed using a Nicolet FTIR microscope, while XPS was carried out using a PHI Quantera X-ray photoelectron microscope. UV-vis spectra were collected using a high resolution UV-vis spectrophotometer (Shimadzu, model no. UV-2450) using quartz cells with a 10 mm path length. PL characterization was conducted using a luminescence spectrometer (NanoLog, Horiba Jobin Yvon) with a xenon lamp as the source of excitation. TRPL was recorded using a time-correlated single photon counting technique with an Edinburgh Instruments spectrometer (model No. FLSP-920) and picosecond laser diode as the source of excitation.

Cytotoxicity and cellular imaging methods

The cells were cultured and maintained in Dulbecco’s Modified Eagle’s Medium (DMEM), high glucose 1X (Invitrogen), containing 4.5 g L^{-1} D-glucose, 4 mM L-glutamine, and 110 mg L^{-1} sodium pyruvate, with 10% fetal bovine serum (FBS), 100 IU mL^{-1} penicillin, and 100 μg mL^{-1} streptomycin. For the cytotoxicity assay, MDA-MB231 and T47D cells (5×10^3 cells per well) were cultured in 96-well plates, overnight. Different concentrations of GO-F (0–100 μg mL^{-1}) in culture media were added to each well in triplicate. After24 h and 48 h of culture with GO-F, cells were washed gently with 200 μL warm, sterile phosphate-buffered saline (PBS), and then 200 μL/well of MTT reagent [3-(4,5-dimethyl-2-thiazolyl)-2,5-diphenytetrazolium bromide (4 mg mL^{-1})] was added. After 4 h of incubation, MTT reagent was removed and 200 μL of dimethyl sulfoxide (DMSO) was added per well and incubated for an additional 5 min at room temperature. The optical

density of solubilized formazan salts was assessed at 570 nm in a Tecan Infinite M200 microplate reader (Männedorf, Switzerland).

For imaging, 1×10^4 cells/well were plated in four-well sterile chamber slides (Nunc, Rochester, NY) with 500 μL culture medium. After overnight culture, 50 μg mL^{-1} GO-F suspension was added to the culture medium and incubated under regular cell culture conditions. After 4 h and 24 h of culture, medium with GO-F was removed from the cells and washed two times with 1 mL 1X PBS. Cells were fixed using 1% paraformaldehyde and mounted with Vectashield antifade mounting media (Vector Laboratories, Burlingame, CA). Cellular imaging was carried out using a Nikon Eclipse 90i microscope equipped with the Cool SnaP HQ2 CCD camera (Photometrics, Tucson, AZ). A Nikon Intensilight C-HGFI lamp was used as the fluorescence light source.

Thermal conductivity measurements on GO-F

The effective thermal conductivities of nanofluids were measured using a thermal properties analyzer (Decagon Devices Inc., Pullman, WA, model KD2 Pro). This device is based on the transient hot-wire technique. Here, a finite-length wire is completely immersed in a finite volume of GO-F. While the wire is heating up, the change in resistance (thus its temperature) is measured as a function of time using a Wheatstone bridge circuit. The thermal conductivity (TC) value is determined from the heating power and the slope of the temperature change with logarithmic time scale. The instrument uses a 1.3 mm diameter by 60 mm long stainless steel probe that is immersed in the nanofluids to obtain the thermal conductivity. The instrument was calibrated using glycerin and measurement was verified up to three decimal places.

T2 MRI measurements

In order to evaluate GO-F as a potential MRI T2 contrast agent, agarose phantoms were made with GO-F. Their T2 values were measured on a 7T MR scanner with a MSME sequence and the results were fitted to a three-parameter spin–spin relaxation equation using Matlab.

Supplementary Material

Refer to Web version on PubMed Central for supplementary material.

Acknowledgments

T.N.N. and P.M.A. gratefully acknowledge financial support from Nanoholdings LLC, Rowayton, CT. B.K.G. thanks the Indo-US Science and Technology Forum (IUSSTF) for financial support. S.V.T., B.X., and P.M.A. acknowledge support from RO1CA12842 and R01CA128428-02S1 from the National Institutes of Health.

References

1. Mahmoudi M, Serpooshan V, Laurent S. Nanoscale. 2011; 3:3007. [PubMed: 21717012]
2. Narayanan TN, Reena Mary AP, Swalih PKA, Sakthi Kumar D, Makarov D, Albrecht M, Puthumana J, Anas A, Anantharaman MR. J Nanosci Nanotechnol. 2011; 11:1958. [PubMed: 21449334]
3. Block S, Glöckl G, Weitschies W, Helm CA. Nano Lett. 2011; 11:3587. [PubMed: 21819124]
4. McCarthy JR, Kelly KA, Sun EY, Weisslender R. Nanomedicine. 2007; 2:153. [PubMed: 17716118]
5. Richard C, Doan B-T, Beloeil J-C, Bessodes M, Tóth E, Scherman D. Nano Lett. 2007; 8:232. [PubMed: 18088153]

6. Zhao Y, Vivero-Escoto JL, Slowing II, Trewyn BG, Lin VSY. Expert Opin Drug Deliv. 2010; 7:1013. [PubMed: 20716017]
7. Hoare T, Santamaria J, Goya GF, Irusta S, Lin D, Lau S, Padera R, Langer R, Kohane DS. Nano Lett. 2009; 9:3651. [PubMed: 19736912]
8. Habib AH, Ondeck CL, Chaudhari P, Bokkstaller MR, McHenry ME. J Appl Phys. 2008; 103:07A307.
9. Zhang H, Pan D, Zou K, He J, Duan X. J Mater Chem. 2009; 19:3069.
10. Zhu M, Diao G. Nanoscale. 2011; 3:2748. [PubMed: 21611651]
11. Levi-Polyachenko NH, Merkel EJ, Jones BT, Carroll DL, Stewart JH. Mol Pharmaceutics. 2009; 6:1092.
12. Sun X, Liu Z, Welsher K, Robinson JT, Goodwin A, Zaric S, Dai H. Nano Res. 2008; 1:203. [PubMed: 20216934]
13. Wang K, Ruan J, Song H, Zhang J, Wo Y, Guo S, Cui D. Nanoscale Res Lett. 2011; 6:2.
14. Gilchrist RK, Medal R, Shorey WD, Hanselman RC, Parrott JC, Taylor CB. Ann Surgery. 1957; 146:596.
15. Frullano L, Meade TJ. J Biol Inorg Chem. 2007; 12:939. [PubMed: 17659368]
16. Mulder WJM, Griffioen AW, Strijkers GJ, Cormode DP, Nicolay K, Fayad ZA. Nanomedicine. 2007; 2:307. [PubMed: 17716176]
17. Mulder WJM, Koole R, Brandwijk RJ, Storn G, Chin PTK, Strijkers GJ, de Mello Donegá C, Nicolay K, Griffioen AW. Nano Lett. 2006; 6:1. [PubMed: 16402777]
18. Gupta BK, Rathee V, Narayanan TN, Thanikaivelan P, Saha A, Govind S, Singh P, Shanker V, Marti AA, Ajayan PM. Small. 2011; 7:1767. [PubMed: 21591255]
19. Jin Y, Jia C, Huang S-W, O'Donnell M, Gao X. Nat Commun. 2010; 1:41. [PubMed: 20975706]
20. Mahmoudi M, Amiri H, Shokrgozar MA, Sasanpour P, Rashidian B, Laurent S, Casula MF, Lascialfari A. Chem Commun. 2011; 47:10404.
21. Mahmoudi M, Serpooshan V. ACS Nano. 201210.1021/nn300042m
22. Kassaee MZ, Motamedi E, Majdi M. Chem Eng J. 2011; 170:540.
23. He F, Fan J, Ma D, Zhang L, Leung C, Chan HL. Carbon. 2010; 48:3139.
24. Shen J, Hu Y, Shi M, Li N, Ma H, Ye M. J Phys Chem C. 2010; 114:1498.
25. Amiri H, Mahmoudi M, Lascilfari A. Nanoscale. 2011; 3:1022. [PubMed: 21152576]
26. Mahmoudi M, Simchi A, Imani M, Hafeli UO. J Phys Chem C. 2009; 113:8124.
27. Renyun Z, Magnus H, Gang L, Hakan O. Carbon. 2011; 49:1126.
28. Reena Mary AP, Narayanan TN, Sunny V, Sakthikumar D, Yoshida Y, Joy P, Anantharaman MR. Nanoscale Res Lett. 2010; 5:1706. [PubMed: 21076702]
29. Mahmoudi M, Serpooshan V. J Phys Chem C. 2011; 115:18275.
30. Mahmoudi M, Lynch I, Ejtehadi MR, Monopoli MP, Baldelli F, Laurent S. Chem Rev. 2011; 111:5610. [PubMed: 21688848]
31. Nel AE, Madler L, Velegol D, Xia T, Hoek EMV, Somasundaran P, Klaessig F, Castranova V, Thompson M. Nat Mater. 2009; 8:543. [PubMed: 19525947]
32. Jin M, Jeong H-K, Yu WJ, Bae DJ, Kang BR, Lee Y. J Phys D: Appl Phys. 2009; 42:135109.
33. Li GH, Wu YC, Zhang LD. Chin Phys. 2001; 10:148.
34. Zhou ZH, Xue JM, Chan HSO, Wang J. J Appl Phys. 2001; 90:4169.
35. Chen W, Zhang J. Scr Mater. 2003; 49:321.
36. Thomas S, Sakthikumar D, Yoshida Y, Anantharaman MR. J Nanoparticle Res. 2008; 10:203.
37. Murakami S, Herren M, Rau D, Morita M. Inorg Chim Acta. 2000; 1014:300.
38. Fujii T, Kodaira K, Kawauchi O, Tanaka N. J Phys Chem B. 1997; 101:10631.
39. Gao W, Majumdar M, Alemany LB, Narayanan TN, Ibarra MA, Pradhan B, Ajayan PM. ACS Appl Mater Interfaces. 2011; 3:1821. [PubMed: 21568266]

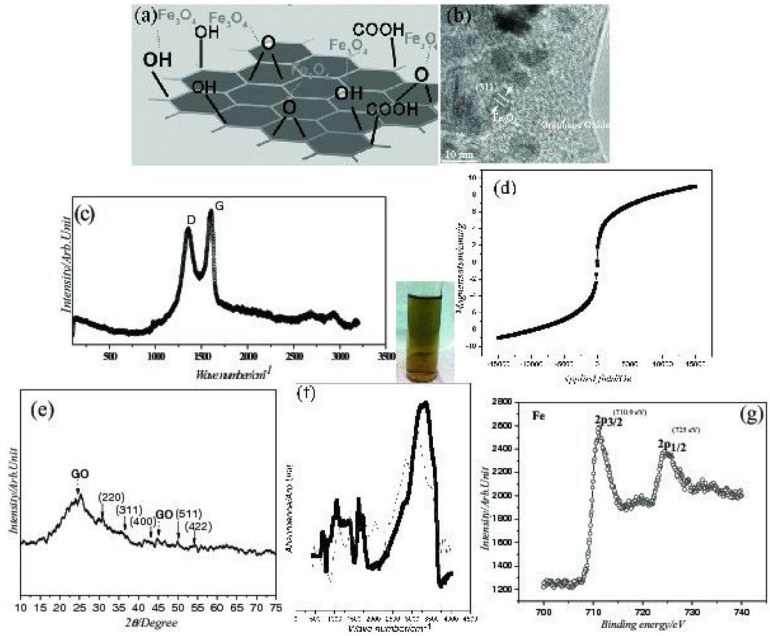

Figure 1.

a) Schematic of the hybrid GO-F. Fe_3O_4 nanoparticles are covalently attached to the graphene plane through oxygen functionalities. b) Transmission electron microscopy (TEM) image of GO-F showing the Fe_3O_4 nanoparticles distributed throughout GO. c) Micro-Raman spectrum. Graphitic order and disorder (G and D) Raman modes are marked. Photograph: GO-F suspension in water. d) Room temperature magnetization curve of GO-F powder. The S-like $M(H)$ loop shows the superparamagnetic nature of the GO-F powder (paramagnetic contribution from the graphite lattice is not subtracted). e) X-ray diffraction (XRD) of GO-F. f) FTIR of GO (dark line) and GO-F (dots) g) Fe 2p X-ray photoelectron spectroscopy (XPS) spectrum of GO-F.

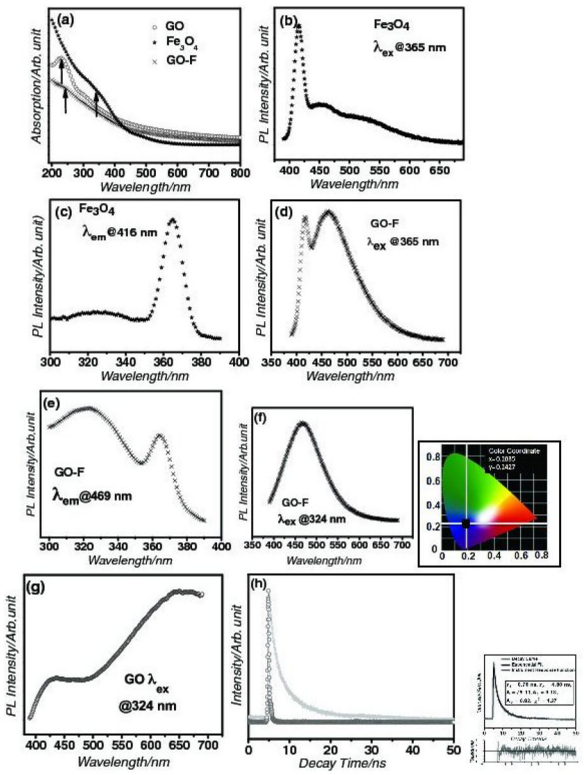

Figure 2.

a) UV-vis absorption spectra of Fe_3O_4, GO, and GO-F fluids. b) Room temperature PL emission spectrum of Fe_3O_4 nanoparticles at 365 nm excitation. c) PL excitation spectrum at 416 nm emission of Fe_3O_4 nanoparticles. d) PL emission spectrum of GO-F nanofluid at 365 nm excitation. e) PL excitation spectrum at 416 nm emission of GO-F nanofluid. Note that an additional interface peak appears after GO forms an interface with Fe_3O_4. f) PL emission spectrum of GO-F nanofluid at 324 nm excitation. g) The color coordinate of the blue emission. h) PL emission spectrum of GO at 324 nm excitation. i) TRPL decay profile of GO-F nanofluid recorded at room temperature while monitoring the emission at 469 nm at an excitation wavelength of 371 nm. j) The lifetime data and the parameter generated by the exponential fitting.

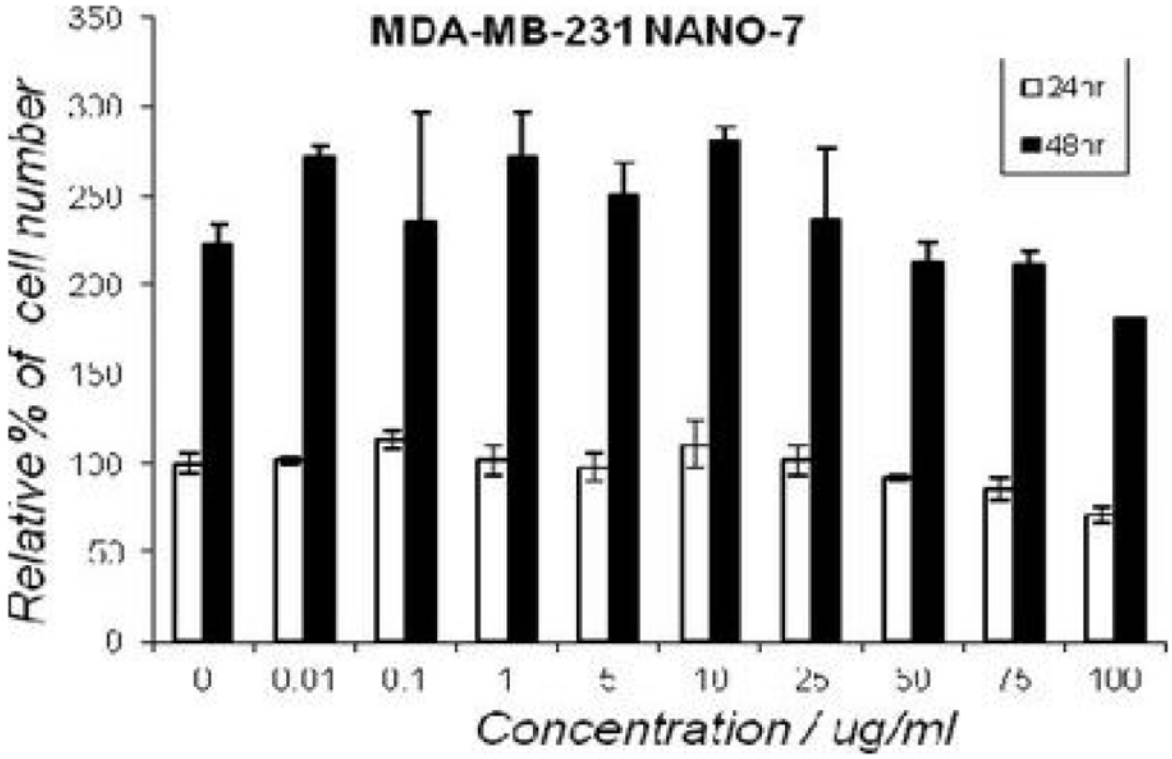

Figure 3.
Cell viability assay with human breast cancer cell lines MDA-MB-231. Cells were treated with different concentrations of GO-F. No significant cytotoxicity was observed with various doses of GO-F treatment.

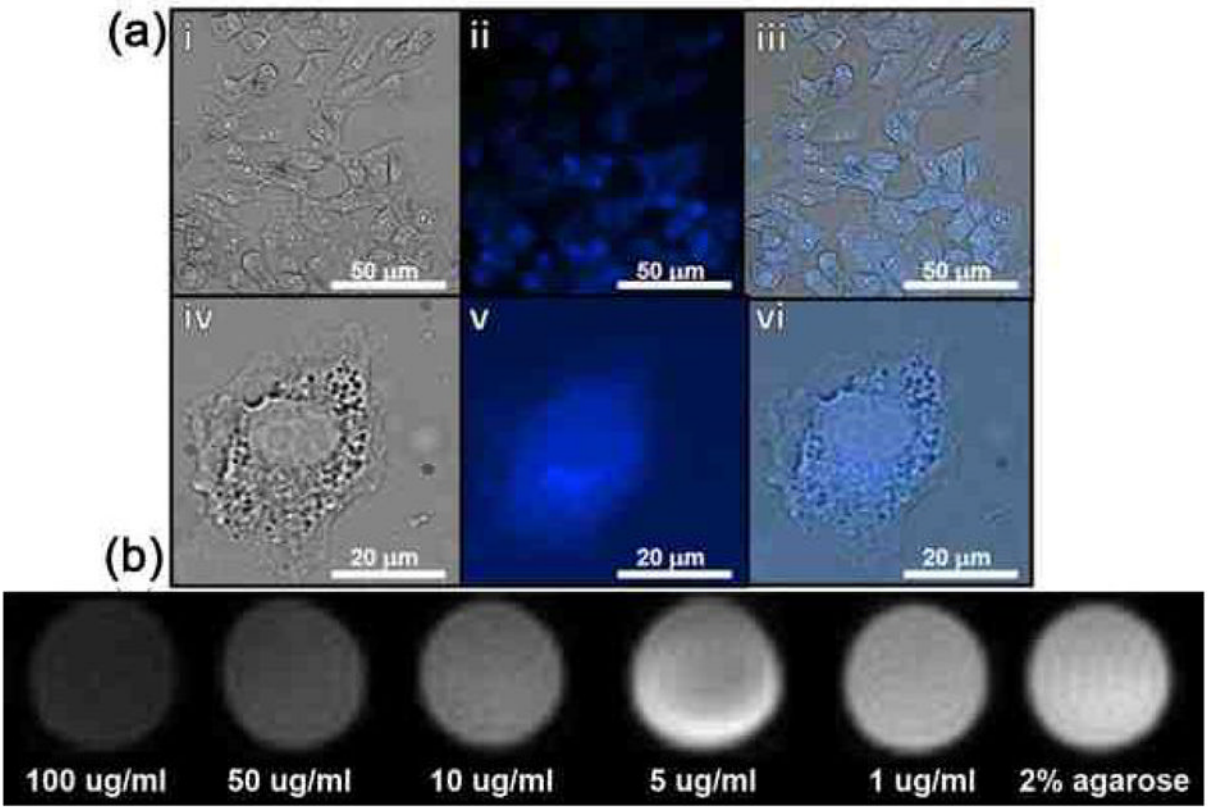

Figure 4.

a) In vitro fluorescence microscopy images of T47D cells treated with GO-F (50 μg mL^{-1}) for 24 h. i–iii) Low magnification images of T47D cells: i) Phase contrast picture, ii) fluorescence images of GO-F, and iii) overlay of images (i) and (ii). iv–vi) High magnification images of an individual T47D cell: iv) phase contrast picture of an individual T47D cell, v) fluorescence image of GO-F, and vi) overlay of images (iv) and (v). The overlay of the phase contrast and fluorescence images clearly demonstrates the localization of GO-F in the cellular cytoplasm, suggesting its suitability for bioimaging. b) T2-weighted MR image showing strong T2 contrast in agarose phantoms. It shows alginate phantoms doped with different concentrations (as shown) of GO-F. The T2-weighted image was acquired in a 7T scanner with multi-slice multi-echo sequence. The T2 relaxivity was 297.06 mM^{-1} s^{-1}.

Published in final edited form as:
Adv Drug Deliv Rev. 2013 December ; 65(15): 2045–2060. doi:10.1016/j.addr.2013.08.001.

Carbon nanotubes in hyperthermia therapy

Ravi Singh[1] and **Suzy V. Torti**[2,*]

[1]Department of Cancer Biology, Wake Forest School of Medicine, Winston Salem NC 27157

[2]Department of Molecular, Microbial and Structural Biology, University of Connecticut Health Center, Farmington CT 06030

Abstract

Thermal tumor ablation therapies are being developed with a variety of nanomaterials, including single-and multiwalled carbon nanotubes. Carbon nanotubes (CNTs) have attracted interest due to their potential for simultaneous imaging and therapy. In this review, we highlight in vivo applications of carbon nanotube-mediated thermal therapy (CNMTT) and examine the rationale for use of this treatment in recurrent tumors or those resistant to conventional cancer therapies. Additionally, we discuss strategies to localize and enhance the cancer selectivity of this treatment and briefly examine issues relating the toxicity and long term fate of CNTs.

Keywords

photothermal therapy; carbon nanotubes; single-walled nanotubes; multiwalled nanotubes; cancer therapy

Introduction

Carbon nanotubes (CNTs) consist of one or more seamless, cylindrical graphitic sheets of sp2 carbon atoms bonded together in an edgeless, hexagonal network [1]. Their combination of electrical, thermal and spectroscopic properties has evoked great interest; biomedical researchers are using CNTs to develop new technologies for the detection, monitoring and therapy of diseases including cancer [2-6]. CNTs can be internalized easily by cells [7-9] and act as delivery vehicles for drugs, nucleic acids, and imaging agents [7, 10-23]. Their unique optical, thermal and cancer selective properties afford the possibility to engineer multiple diagnostic and therapeutic functions into a single particle [2, 24]. This makes CNTs extremely suitable for further biomedical development [25].

Minimally invasive, rapidly administered, and highly selective nanotechnology-based thermal tumor ablation therapies are being developed with a variety of nanomaterials (reviewed in [26]). These include single walled carbon nanotubes (SWCNTs) [27], multiwalled carbon nanotubes (MWCNTs) [28], graphene [29], iron oxide nanoparticles [30], gold nanorods [31] and gold nanoshells [32, 33]. Heat-based cancer therapy requires elevation of malignant tissues to supraphysiologic temperatures [34-39]. Exposure to high temperature for a sufficient amount of time causes physical damage such as protein

*To whom correspondence should be addressed: storti@uchc.edu, Phone: 860-679-6503.

denaturation and membrane lysis and can increase oxidative stress [34, 35, 40, 41]. These effects may be cytotoxic on their own, causing coagulative necrosis or apoptosis[37, 39]. Additionally, hyperthermic treatments that increase temperatures more modestly may enhance the anti-cancer efficacy of ionizing radiation or systemic chemotherapy regimens [40, 42, 43].

Dose limiting toxicities resulting from diffuse heating of non-tumor tissues and the relative invasiveness of thermal ablative instrumentation have limited wider clinical use of thermal ablation for cancer therapy [44]. However, with recent refinements in technology, the role of such therapies should increase in the near future [26, 45, 46], and nanotechnology is playing a key role in these advances. Human clinical trials are ongoing for a gold nanoshell based photothermal cancer therapy (Id: NCT00848042 on ClinicalTrials.gov) and for iron oxide nanoparticle-based magnetic thermotherapy [47, 48]. Although the results of these studies are promising, there remains significant room to improve upon both the generation and localization of heat for thermal therapy.

In this arena, CNTs have emerged as promising, next generation agents for thermotherapy of cancer. Currently, significant efforts are being applied to develop CNT-based, clinical treatments. In this review, we will specifically high-light in vivo applications of CNT-mediated thermal therapy (CNMTT) and examine the rationale for use of this treatment in recurrent tumors or those resistant to conventional cancer therapies. Additionally, we will identify strategies to localize and enhance the cancer selectivity of this treatment, and briefly examine issues relating the toxicity and long term fate of CNTs.

1. CNT-mediated thermal therapy: rationale and current status

Carbon nanotubes offer an exceptional combination of attributes for the development of the next generation of photothermal agents; chief among these is their ability to efficiently convert near infrared radiation (NIR) into heat [49]. Compared to other wavelengths of light, the transmission of NIR through the body is poorly attenuated by biological systems [50, 51]. Penetration of light through tissue is fundamental to photothermal applications of nanomaterials for the treatment of non-superficial cancerous lesions in vivo [28]. Following exposure to NIR, CNTs enter an excited state and release vibrational energy that is transformed into heat, which can induce cell death [27, 52].

CNTs possess an extremely broad electromagnetic absorbance spectrum, covering the full spectras of both the NIR I and II windows [53], which correspond to the “optical transmission window” of biological tissues [50, 51], and the radio frequency and microwave bands as well [54]. Further tuning of the photophysical properties of CNTs can be achieved by tailoring the wall number, diameter, and length of the nanotubes according to the “nano-attenna” effect [52]. Critically, NIR absorption and energy transduction efficiency remains high across a wide frequency range [53], which allows for flexibility in the choice of both material characteristics (diameters from <2 nm - >30 nm; lengths from <100 nm to > 1 um) and excitation wavelengths. This provides great versatility to tailor size, shape, and surface properties to optimize the tissue distribution of CNTs without a significant loss in thermal conversion efficiency. The broad electromagnetic absorbance spectrum of CNTs also offers a significant advantage over plasmonically heated nanomaterials (such as gold nanoshells and nanorods) for which the excitation spectra are highly dependent upon the size and shape of the particles [2]. While direct comparisons are difficult to make, some estimates indicate that CNTs can achieve thermal destruction of tumors at 10-fold-lower doses and 3-fold-lower power than is needed for gold nanorods [53]. However, in contrast to gold nanoparticles, which can be synthesized with great uniformity and have already been tested

in human clinical trials, production of uniform, well-characterized CNTs remains a significant hurdle for clinical translation.

CNTs exhibit both advantages and limitations in thermal therapy when compared to iron oxide nanoparticles. The magnetic field used to excite iron oxide nanoparticles as a means of generating heat offers superior depth of energy penetration as compared to NIR, but the slower rate of heating induced by this technique leads to significant thermal diffusion away from the targeted area (discussed in **section 2.3**), potentially increasing collateral damage to neighboring healthy tissue [55]. A second drawback of this technique is that it also requires the removal of all metallic materials within the magnetic field covering the treatment area including dental fillings, crowns and implants. On the other hand, iron oxide nanoparticles, like gold nanoparticles, share a significant advantage over CNTs because uniform preparations of iron-based nanoparticles can be synthesized and have already been tested in human clinical trials.

In most cases, the clinical model for the use of CNTs as heat transduction agents is based upon laser-induced thermotherapy (LITT) [33, 39], a photothermal ablation technique in which an NIR laser is used to heat a target tissue, such as a tumor, above the thermal ablation temperature threshold of approximately 55°C [33, 56]. A major limitation of LITT has been an inability to consistently achieve thermoablative temperatures throughout the target lesion and to confine treatment exclusively to the tumor [57, 58]. Therefore, to be of clinical benefit, CNTs must greatly improve the deposition of heat following NIR exposure without causing any significant toxicity on their own.

1.1. In vivo anticancer efficacy of CNT-mediated thermal therapy

The efficacy of CNMTT for the treatment of locoregional tumors in vivo has been demonstrated using syngeneic models of cancer in mice [53, 59], rabbits [54], and in human xenografts grown in mice (reviewed in [49]. In most cases, CNTs are injected systemically or directly into the tumor, which is then exposed to an external NIR (typically a YAG or diode laser) or microwave source. As highlighted in table 1, CNMTT has proven effective for the treatment of a wide variety of cancer types both in vitro and in vivo. In this review, we will focus our discussion upon recent developments in CNMTT treatment of human cancer xenografts in animal models.

Initial in vivo studies of CNMTT focused on the use of SWCNTs, and the results were mixed. Moon et al demonstrated that following intratumoral injection of SWCNTs into mice bearing flank xenografts of human mouth carcinoma cells and NIR irradiation (3 W/cm^2; 3 min), the tumors were completely destroyed [60]. Normal tissue adjacent to the treated area was spared; however, the irradiation procedure itself resulted in significant burning of the heated area even in the absence of SWCNTs. Significantly, no indication of tumor recurrence or apparent side effects of treatment were observed during several months of follow-up [60]. Huang et al achieved more modest results following a similar treatment [59]. Using mice bearing syngeneic murine squamous cell tumors, the researchers intratumorally injected SWCNTs and irradiated the tumor with a low power (200 mW/cm^2) NIR laser for 10 minutes. They observed that treatment resulted in a maximum tumor temperature of approximately 55°C, indicating that the thermal ablation threshold was reached. However, while a reduction in tumor growth and a modest survival advantage were documented, this treatment failed to achieve a durable cancer remission. In contrast to Moon et al [60], necrotic normal tissue was present adjacent to the treatment site, indicating significant heat transfer away from the targeted site and into the surrounding non-tumor region. As discussed in more detail in **section 2.3**, recent work by Xie et al [61] modeling the effects of energy deposition rate on the efficacy of CNMTT suggest that the slower rate of energy deposition used by Huang et al [59] as compared to Moon et al [60] may have resulted in

greater heat diffusion leading to lesser treatment efficacy and more collateral damage to surrounding tissue.

Following synthesis, SWCNTs are a mixture of metallic and semiconducting SWCNTs. Differences in the density of state at the Fermi level of metallic SWCNTs (which have a finite value ≠ 0) and semiconducting SWCNTs (which have a value of zero) imply that metallic SWNTs more efficiently absorb and convert NIR into heat, and this was recently confirmed by Murakami et al [62]. Consistent with the concept that CNTs with a more metallic nature possess enhanced NIR thermal conversion efficiency, both Burke et al [28] and Ghosh et al [63] reported that MWCNTs, which are inherently more metallic than unpurified SWCNTs, were 20-100 fold more efficient than bulk SWCNTs at conversion of NIR into heat. As shown in figure 1, in vivo studies demonstrated durable remission and long-term survival (> 6 months post-treatment) after intratumoral injection of MWCNTs into tumors implanted in the flanks of nude mice combined with exposure to NIR (3 W/cm^2; 30 sec) [28]. Significantly, this result was achieved using one-sixth of the energy Moon et al [60]required to achieve a similar result using SWCNTs. Because of this, laser treatment in the absence of MWCNTs resulted in only minimal superficial burning [28]. In the same study, electron microscopy studies revealed that at least a portion of MWCNTs remained intact at the injection site, but no toxicity was detected [28]. Ghosh et al observed similar results for in vivo treatment of tumors using MWCNTs and NIR [63]. Moreover, they confirmed the importance of CNT dispersion on the efficacy of such therapy. By self-assembly, they encased MWCNTs in DNA, which disentangled the tubes. Compared to dispersions of MWCNTs prepared in the absence of DNA, well dispersed DNA encased MWCNTs were more efficient at converting NIR into heat, which led to more effective tumor treatment in mice [63].

As previously noted, CNTs can be heated by externally delivered microwave radiation. Therefore, CNTs may be capable of non-invasively treating tumors in any part of the body, a capability currently not shared by NIR laser-based treatments. In the first study to investigate cancer treatment using an external (non-contacting) microwave source to heat intratumoral SWCNTs, treatment of VX2 hepatocellular carcinoma xenografts in rabbits resulted in complete thermal necrosis of the tumor. No toxicity was seen but there was a 2-5 mm zone of thermal injury to the surrounding liver [54]. To date, studies on microwave or radiofrequency heating of CNTs for cancer therapy are extremely limited and more research will be needed to determine if this promising strategy is clinically viable.

1.2 Selective delivery of CNTs to tumors for CNT-mediated thermal therapy

Fueled by the promise demonstrated by these early studies, researchers are now evaluating strategies to selectively deliver CNTs to tumor sites following systemic administration. One such strategy, known as the enhanced permeation and retention effect (EPR), proposes that increases in tumor accumulation can be achieved by nanoparticles that remain in circulation for long periods due to the nanoparticles' ability to extravasate through the leaky vasculature surrounding the tumor and enter the tumor site [64]. Like many nanoparticles, the blood circulation half-life and tumor accumulation of CNTs can be increased in mice by coating nanoparticles with steric stabilizers such as polyethylene glycol (PEG), which inhibit nanoparticle blood clearance by macrophages and other components of the mononuclear phagocyte system [10, 65-68].

Recently, a significant step toward the development of tumor selective, systemically delivered CNTs for photothermal ablation was achieved by Robinson et al [53]. The researchers coated, short (140 nm) SWCNTs with a PEG-funtionalized phospholipid by self-assembly and then injected the CNTs into mice bearing 4T1 murine breast tumors at a dose of 3.6 mg/kg via the tail vein. Three days later, the inherent NIR photoluminescence of the

SWCNTs was quantified using an optical imaging system to confirm the accumulation of SWCNTs at the tumor site. Following exposure to NIR (0.6 W/cm^2; 5 min), complete tumor ablation was observed on mice previously administered SWCNTs. These mice survived without recurrence for the duration of the six month study and no toxicity was seen [53].

In another study, Liu et al systematically evaluated the relationship between the length and density of PEGylation on the SWCNT surface and the biodistribution, tumor accumulation and photothermal ablation efficacy of PEG-functionalized SWCNTs injected intravenously into mice [69]. They observed long blood circulation half-lives (16-21 hrs) for heavily PEGylated SWCNTs and high tumor uptake. However, this came at the cost of extensive accumulation of SWCNTs in the mouse skin dermis. They found that by controlling the degree of PEGylation to achieve a blood circulation half-life of 12-13 hrs, they were able to balance high tumor uptake of the SWCNTs with low skin retention. Two days after intravenous injection of the SWCNTs into tumor bearing mice, the researchers exposed the tumors to NIR, achieving a surface temperature of over 50°C. In contrast, the temperature rise in tumors treated with NIR in the absence of SWCNT injection was only 1-2°C. Significant reduction in tumor growth was observed in the SWCNTs and NIR treated mice, and three of the seven mice treated exhibited complete regression for the two week study [69]. This study suggests that fine tuning the surface properties of CNTs is critical to enhancing their passive tumor targeting capabilities.

Notably, the intravenously injected nanotubes used by Robinson [53] or Liu [69] were not modified to display a specific targeting ligand, nor is it known if they were they internalized by the cancer cells themselves. Attachment of ligands with an enhanced binding affinity for cancer specific biological moieties is one strategy which may allow for more selective therapy. This can be accomplished by conjugation of peptides, proteins or antibodies to the surface of CNTs, and has been shown to increase the specificity of CNT tumor targeting following intravenous injection in mice [27, 68, 70, 71]. Targeting CNTs to cancer cells in vitro using agents including folic acid [72-74], the breast cancer associated receptor Her2 [75, 76], and anti-GD2, a monoclonal antibody targeting a carbohydrate antigen overexpressed in neuroblastomas [77] has been shown to increase the specificity and efficacy of CNMTT as compared to non-targeted tubes. Additionally, CNTs can effectively display more than one targeting ligand on their surface which is a strategy that can be used to expand both the tropism and specificity of cancer-targeted CNTs. For example, SWCNTs conjugated to antibodies targeting Her2 and insulin-like growth factor 1 receptor (IGF1R) attached to SWCNTs [78] were shown to be effective at targeting CNMTT to cells expressing one or both of the targeted receptors.

The benefits of actively targeting nanoparticles to tumors in vivo remain the subject of much debate [79], and more research is needed to determine if active targeting will offer an additional benefit for delivery of CNTs. The underlying mechanisms by which CNTs are taken up by cells are still under investigation with both energy-dependent internalization mechanisms (e.g. phagocytosis; clatherin or caveolae mediated endocytosis) and passive diffusion through the plasma membrane (e.g. “nanoneedle” effects) apparently playing a role [9]. As noted above, comparative studies between actively targeted and non-targeted CNTs generally indicate that targeted CNTs are taken up to a greater degree than untargeted tubes. Give the many non-specific mechanisms through which CNTs can bind to and enter cells, precisely how targeting increases the binding and/or uptake of actively targeted CNTs remains to be determined. It is conceivable that the PEG coating commonly used to functionalize the CNT surface may reduce the interaction of coated CNTs with cells; introduction of a binding moiety to the PEGylated CNT would then greatly increase the targeting specificity. To date, direct comparisons of the binding and uptake of PEGylated and uncoated CNTs have not been conducted. Comparative studies of nanoparticle binding

kinetics are complicated because the physical properties that influence cellular interactions of nanoparticles also affect their solution dynamics [80]. Nanoparticles diffuse, settle and agglomerate in cell culture media as a function of systemic and particle properties (e.g. media density and viscosity, particle size, shape and density). Therefore the delivered dose of nanoparticles in cell culture is a function not only of cell binding and uptake pathways, but of the rate of transport in solution as well. To date, most studies using targeted CNTs fail to account for changes in solution dynamics induced by structural alterations in the CNTs caused by the addition of targeting ligands, and further research will be needed to thoroughly understand how such alterations influence binding specificity. Nevertheless, there is strong evidence that internalization of CNTs prior to exposure to NIR can improve the treatment efficacy of CNMTT [75]. For example, Zhou et al demonstrated SWCNTs coated with a phospholipid-PEG conjugate selectively accumulate intracellularly at the mitochondrial membrane [81]. Their proximity to mitochodria allowed for selective destruction of these organelles following NIR exposure, inducing mitochondrial depolarization, cytochrome *c* release, and caspase 3 activation. Treatment of murine breast cancer tumors in vivo with these modified SWCNTs reduced tumor growth and induced complete tumor regression in some mice [82].

1.3 Efficacy of CNMTT for treatment of resistant or recurrent cancers

Thermal ablation therapies based upon CNTs are being tested for the treatment of cancers that are highly resistant to current therapies, including stem-cell like cancer sub-populations [83, 84]. In many types of tumors, cancer stem cells (CSCs) have been putatively identified as self-renewing, therapy-resistant populations [85].

In glioblastomas and other brain tumors, the CD133 receptor appears to be a CSC marker associated with malignancy, tumor recurrence, and poor survival. [86-88]. CD133+ subpopulations in glioblastoma are enriched following radiotherapy, are radio and chemotherapy resistant, and may be responsible for tumor recurrence following treatment [86, 89, 90]. Treatment strategies based on targeting this subpopulation may prevent the development of resistance to therapy. To test this hypothesis, Wang et al conjugated a monoclonal antibody directed against CD133 to MWCNTs [83]. They observed specific internalization of these targeted MWCNTs in primary clinical isolates of glioblastoma that expressed CD133, but not in cells which did not. To determine the in vivo efficacy of this treatment, CD133 expressing glioblastoma cells were pre-treated with targeted MWCNTs before inoculation into mice. The cells took up the MWCNTs, and xenograft growth was abolished after NIR exposure. This key study demonstrated the potential for CNTs to treat glioblastomas and other currently untreatable cancers.

Another recent report describes a novel application of the CNMTT technique to target invasive CSCs in systemic blood circulation [91]. In this study, Galanzha, et al. used the photoacoustic (PA) and photothermal (PT) properties of CNTs for the detection and elimination of circulating CSCs, which are thought to be the primary drivers of metastatic tumor spread [91]. The development of technology to purge these cells from the vasculature of cancer patients could reduce the incidence of metastatic disease. To accomplish this, the researchers constructed NIR-absorbing, gold plated SWCNTs and conjugated them to anti-human CD44 antibodies. These particles selectively labeled circulating human breast CSCs (which overexpress CD44 [92]) in the blood stream. Rare $CD44^+$ circulating cancer stem cells binding nanoparticles were identified in the vasculature of nude mice which bore human breast cancer xenografts by detection of photoacoustic waves generated by excitation of the nanoparticle-labeled cancer cells using a low powered laser [91]. Furthermore, these cells could be ablated following more extended irradiance with NIR [91].

Importantly, CNTs may be superior to other heat delivery modalities in ablating cancer stem cells. Burke and co-authors compared the response of breast cancer stem cells (BCSCs) to both conventional hyperthermia and CNMTT to determine the relative therapeutic efficacy of each approach for the treatment of these cancer cells [84]. Key results of this study are shown in figure 2. Notably, BCSCs exhibited high basal expression levels of heat shock protein 90 (HSP 90) which contributed to their ability to tolerate conventional hyperthermia treatments (modeled by water bath heating) that were lethal to non-stem breast cancer cells [84]. BCSCs were found to be resistant to hyperthermia across a range of temperatures, and heat treatments did not reduce the long-term proliferative capacity of these cells. A significant enrichment of BCSCs was detected in the surviving fraction of a mixed population of stem and non-stem breast cancer cells treated with conventional hyperthermia. In contrast, the researchers were able to overcome the resistance to hyperthermia observed in BCSCs through the use of CNMTT. Furthermore, BCSCs that survived CNMTT did not retain long-term proliferative capabilities. The researchers generated precise temperature increases in mixed or isolated populations of BCSCs and non-stem breast cancer cells by exposing the cells to MWCNTs followed by NIR irradiation, which resulted in cell death that was proportional to laser exposure time. In vivo treatment by CNMTT induced complete regression of BCSC-driven tumors in mice for the duration of the 30 day study. In contrast, control groups exhibited >80% mortality at identical time points. Based on these findings, CNMTT may represent a rapid, minimally invasive approach for the simultaneous elimination of both the bulk breast tumor and the BCSC components of tumors and represents a significant therapeutic advance for the treatment of refractory, stem cell-driven cancers [84].

Flow cytometric characterization of the cells following treatment indicated that CNMTT, but not conventional hyperthermia, led to rapid membrane permeabilization and necrotic death in treated cancer cells [84]. The high surface temperature of NIR-stimulated MWCNTs [93] may irreversibly permeabilize cell membranes [94, 95], leading to the rapid cytolysis observed in CNMTT-treated cells. Therapies that preferentially cause necrotic death may be therapeutically advantageous by bypassing resistance mechanisms to apoptotic cell death because they do not provide selective pressure toward the emergence of treatment resistant cancer cell clones [96, 97]. The significance of this for CNMTT is exemplified by the fact that elevated HSP90 in BCSCs conferred at least partial protection to classical hyperthermic cell death, but did not protect BCSCs from nanotube-mediated hyperthermic death [84]. Fisher et al also indicated that CNMTT leads to a necrotic rather than apoptotic cell death mechanism [98]. Nevertheless, necrosis has not been universally observed following treatment with NIR and MWCNTs [99], and to date, extensive research has not been conducted to determine factors that may influence the mechanism(s) of cell death induced by CNMTT.

1.4. Enhancement of conventional cancer therapy by CNMTT

Hyperthermia synergistically enhances tumor cell cytotoxicity when combined with chemotherapy or radiotherapy, in part by increasing the permeability of tumor vasculature, which can enhance the delivery of drugs into tumors [41]. Thus, in addition to ablation of cancer cells, the thermal effects generated by CNMTT may enhance the efficacy of other therapies. Such strategies may enable the development of therapeutic agents with increased cancer selectivity, reduce the dose necessary for efficacy, decrease the toxicity of such treatments, and thus increase their therapeutic index.

For example, NIR irradiation of MWCNTs to sublethally heat cancer cells increased the uptake of co-delivered chemotherapeutic drugs and enhanced cancer cell death both in vitro and in vivo in a murine ascites tumor model [100]. Excitation of CNTs by exposure to an appropriately tuned radio frequency field has been shown to permeabilize cell membranes to

allow cell uptake of normally impermeable drugs or gene expression vectors both in in vitro and in vivo in brain tissue [101]. Similarly, treatment of cancer cells or tumor bearing mice using SWNTs chemically conjugated with platinum-based chemotherapeutics [102] or loaded with doxorubicin by hydrophobic interactions [103] and combined with NIR mediated photothermal heating were significantly more effective than either therapy alone. Dual mode carbon nanomaterials have been developed to allow excitation by a single wavelength of light to initiate both photothermal and photodynamic events, allowing for simultaneous generation of therapeutic heat and reactive oxygen species [62, 104].

Conjugation of antigens to the surface of CNTs may enhance immune responses by increasing the uptake of such antigens by dendritic cells and macrophages [105]. Recently, the combination of an immunologically modified nanotube and CNMTT was shown to generate a sustained anti-tumor immune response in mice following treatment [106]. Glycated chitosan (GC), an immunoadjuvant, was used as a surfactant to disperse SWCNTs. BALB/c mice bearing syngeneic EMT6 flank tumors were injected intratumorally with GC coated SWCNTs (SWCNT-GC) then exposed to a 980 nm laser (0.75 W/cm2 for 10 min). All mice treated with the combination of laser and SWNT-GC survived for at least 100 days following treatment. In contrast, only 43.75% of mice treated with laser and SWNTs without GC, 25% of mice treated with laser and GC without SWCNTs, and 12.5% of mice in the laser only group survived. Importantly, mice that were successfully treated by the combination of laser irradiation and SWNT-GC did not develop tumors following rechallenge with EMT6 cells100 days after the initial tumor inoculation. This study shows the combination of laser irradiation and immunologically modified nanotubes can induce systemic antitumor response through a local intervention, with few adverse side effects [106].

1.5. Beyond cancer therapy: novel applications of photothermal properties of CNTs

Although most studies have focused on anti-tumor applications of CNMTT, additional applications have also been proposed. Kosuge et al. recently investigated the use of SWNT-mediated photothermal ablation of inflammatory macrophages in a mouse model of athlerosclerosis [107]. Following the creation of macrophage-rich atherosclerotic lesions in the carotid arteries, mice were injected with fluorescently tagged SWNTs, which accumulated in the macrophages. Excision of the arteries and ex-vivo illumination with NIR induced heating and apoptosis selectively in SWNT-containing macrophages, providing a proof of principle demonstration that the photothermal properties of CNTs may be useful in treatment of vascular inflammation. Another group used laser excitation of carbon nanohorns to induce expression of genes driven by a heat shock protein- responsive promoter in living mice [108]. The use of NIR-activated SWNTS for ‘remote control’ of gene expression in living animals may represent both a powerful experimental tool and a new therapeutic venue. Similarly, a recent report indicates that CNTs also may be useful for the development of implantable bioelectronic devices operated by laser irradiation from outside the body [109]. In this study, a unique CNT-based photothermal-electrical (PTE) converter is described. This device is able to convert the thermal energy generated by NIR irradiated with NIR light and convert it to electrical power. Devices powered by this system could be implanted beneath the skin and activated by laser irradiation, providing a new opportunity for biomechanical development or possibly for a remotely activated drug delivery system.

2. Clinical translation of CNMTT: accomplishments and challenges

As described above, proof of principle studies in animals have established that CNMTT can address several limitations of contemporary clinical thermal ablation methodologies: (1) the procedure is minimally-invasive, potentially expanding the type and location of tumors that

can be treated; (2) because each nanoparticle generates heat in response to stimulation electromagnetic radiation, a uniform temperature distribution can be generated throughout the tumor mass; and (3) the heated region is defined by both the location of the CNTs and the position of the irradiation source, confining treatment to the intended lesion and diminishing off-target toxicities. However, as described in the following sections, significant hurdles still must be addressed before CMNTT will be a clinically viable modality.

2.1 Intratumoral dissemination of CNTs

Delivery of CNTs and other engineered nanoparticles across large (> 1cm) tumors represents a major, under-investigated need for biomedical use of nanomaterials [110-116]. As highlighted in figure 3, multiple inter-related properties influence particle distribution; these are dependent not only on the characteristics of the particular type of CNT, but also upon the environment in which the particle is to be used and the strategy by which it will be delivered. As more information on the use of CNTs in animal models becomes available, it is clear that like other nanoparticles, even minor structural or chemical changes to the particle surface significantly alter the biodistribution of CNTs [117].

The in vivo intratumoral distribution of CNTs largely is related to the physicochemical properties of the tubes, which include length, diameter, degree of agglomeration, surface chemistry, and flexibility [25]. The interactions of these properties with the pathophysiology and anatomy of the target site will dictate the biological interactions of the CNTs [118]. Furthermore, it is important to realize that small molecules and proteins frequently adsorb onto the surface of nanoparticles, creating an interface at which all further interactions occur. The environment obviously influences the composition of this interface, and creates an additional factor that is rarely taken into account when evaluating the efficacy and distribution of CNT preparations.

Current delivery strategies, which are limited to either intravenous injection or direct intratumoral injection do not address the issue of limited macromolecular diffusion of CNTs once they enter the tumor microenvironment. Recent work suggests that this may be an issue of considerable complexity [119]. Using intravital microscopy, the authors demonstrated that SWNTs and spherical particles with similar surface coating, area, and charge nevertheless exhibit different abilities to extravasate into tumors. Rather remarkably, the relative penetrance of these particles was dependent on tumor type: spherical particles preferentially extravasated into LS174T colon tumors, whereas SWNTs accumulated preferentially into U87MG gliobastoma tumors; neither particle extravasated into SKOV-3 ovarian adenocarcinoma tumors. The mechanistic basis for this difference remains to be determined, but these results suggest that biological characteristics of the tumor itself will be an important determinant in the optimization of therapeutic nanoparticles.

Among the options for enhancing intratumoral dissemination, a dense PEG coating is known to improve penetration of large nanoparticles in tissue [120], but the role of PEG coating on CNT diffusion in tumors has not yet been assessed. Furthermore, pressure-driven infusion techniques such as convection enhanced delivery (CED), which rely on a pressure gradient rather than diffusion to distribute macromolecules, may be of benefit. CED of nanomaterials is an area of current research [121] but has not yet been tested for the delivery of CNTs. Positive indications for use of CED for CNTs include: (1) CNTs can be synthesized with diameters (<30 nm) far smaller than the estimated pore size in the extracellular matrix (ECM) of many tumors [112, 122, 123]; (2) CNTs tend to align parallel to the direction of fluid flow [124]; and (3) their diffusion can be enhanced by selectively tuning their surfaces to the physical properties of porous media [119, 125-128] like the ECM.

More research is needed to identify specific properties or strategies that will enhance intratumoral transport of CNTs both during and after infusion. It will be particularly important to these studies that CNTs for use in biomedical applications have well-defined preparation chemistries combined with rigorous physicochemical characterization, and, as discussed below, that their in vivo performance can be tracked by non-invasive imaging techniques.

2.2 Monitoring intratumoral distribution of CNTs

For the clinical application of CNMTT for cancer treatment, CNTs must be specifically engineered to be compatible with an imaging modality to spatially define the margins of the target lesion, assess the distribution of injected CNTs within the tumor, and to allow for placement of the electromagnetic radiation source. The versatility of CNTs as a platform technology has seen the development of CNT-based imaging agents for use as magnetic resonance imaging (MRI) contrast enhancers[22, 129-132], positron and single photon emission correlation spectroscopy (PET/SPECT) [19, 70, 133, 134], fluorescence imaging [71, 129, 135] and photoaccoustic and Raman imaging [136]. Carbon nanotubes offer several advantages for targeted molecular imaging techniques, including their ability to deliver large numbers of imaging agents per each targeted molecular recognition, which can improve the sensitivity of imaging, and their ability to simultaneously display several different types of agents to perform multimodality imaging.

A unique feature of SWCNTs is that they possess an intrinsic fluorescence in the second near-infrared window (NIR II, 1.1-1.4 μm) upon excitation by laser emission in the traditional near-infrared region (NIR I, 0.75-0.9 μm) [137]. Compared to the NIR I window, the longer wavelength emission in NIR II offers great promise for the development of SWCNT imaging agents due to minimal autofluorescence and tissue scattering, which allows for deeper anatomical penetration and greater spatial resolution than is currently available for traditional NIR imaging agents [137]. Studies by Welsher et al indicate the SWCNT-based fluorophores can be imaged deep inside mice following excitation with a modest laser power [135]. Similarly, injection of SWCNTs into the blood allows for quantifications of blood velocity and mapping of small vessels which an accuracy that is far beyond the capabilities of ultrasonography [137]. Initial studies show that intravenously injected SWNTs could be used as as photoluminescent agents for in vivo tumor imaging in the 1.0-1.4 μm emission region and as NIR absorbers and heaters at 808 nm for photothermal cancer therapy [53]. Additional clinical applications of these tubes potentially could include contrast enhancement for delineation of tumors/metastasis, or for mapping intratumoral vasculature.

Several additional studies have examined dual modality CNTs for both imaging and photothermal applications. In one study, Ding et al constructed MWCNTs containing increasing amounts of ferrocene, an iron-based catalyst used in the production of CNTs [22]. These iron-containing MWCNTs were studied for their potential use as dual modality agents for both MR contrast enhancement and photothermal energy transduction. The researchers demonstrated that iron-containing MWCNTs were effective MR contrast agents. In vivo MR imaging provided a clear indication of intratumoral distribution of the CNTs, allowing for image guided intervention. Following multiple rounds of NIR exposure, the contrast enhancing and heating properties of the MWCNTs did not change, even after reaching thermal ablative temperatures [22]. When injected into tumor bearing mice, the iron-containing MWCNTs could be detected at the injection site before and during heating, and until the end of the study one week later [22]. An additional advantage conferred by this imaging strategy was the ability to monitor temperature in real time using MR thermometry (see section **2.3**). Conceptually, this demonstrates that multiple or fractionated laser

treatments could be targeted to the tumor without the need for additional injections, and the distribution of the MWCNTs could be monitored over time.

In addition to MR imaging, photoacoustic molecular imaging using CNTs has shown some early promise [138]. Photoaccoustic imaging relies upon detection of the shock wave that is generated following heating of the CNTs by an external NIR source. Recent studies by Zhou and colleagues indicate that CNTs targeted to αvβ3 integrin could be designed to possess both high photoaccoustic contrast and and efficient targeting of αvβ3 integrin positive U87 human glioblastoma tumors in mice, suggesting that photoacoustic molecular imaging with targeted SWNTs has the potential for use as a tumor diagnostic method [138]. In another study, Zarov and colleagues developed golden carbon nanotubes (GNTs) consisting of SWCNTs encased in gold layers [139]. The gold coating not only enhanced the photothermal transduction efficiency of the tubes, it introduced a high plasmon resonance at 850-900 nm, indicating the the GNTs could be used for both non-invasive photoaccoustic (PA) imaging and photothermal cancer therapy [140]. Moreover, cancer diagnosis and therapy applications using these tubes could be performed with the same laser in real time using a unique in vivo flow cytometry based imaging system [139]. Using anti-CD44 labeled GNTs, the researchers were able to detect single CD44+ circulating breast cancer stem cells in the blood stream of tumor bearing mice following NIR irradiation. They postulate that these cells could be eliminated by increasing the laser power [139].

From these studies, it is clear that CNTs can be developed for both cancer imaging and effective photothermal therapy and are compatible with current imaging technologies. Future developments of such agents would have a dramatic effect on non-invasive cancer diagnosis, targeted therapies, selection of patient specific treatments, and monitoring of cancer progression or recurrence.

2.3 Optimizing heat localization and treatment efficacy of CNMTT

Heat delivery for photothermal applications is dependent upon the total laser energy incident upon the target and the efficiency of the target at converting that energy into heat. Temperature elevation by CNMTT is limited by the maximum laser output, penetration of the light, the CNT concentration in the tumor target, and heat dissipation away from the tumor target. Heat dissipation away from the tumor target is a complex process that is dependent upon environmental factors including proximity to heat absorbers (i.e. blood vessels and neighboring normal tissue), solvent, and the substrate (tissue type) into which the CNTs are dispersed. This process is dynamic, making it essential to develop strategies to reproducibly control the spatial and temporal distribution of heat used to ablate tumors [141].

To reduce off-target damage due to thermal diffusion, the total energy deposited into the tissue should be minimized such that only the amount of heat needed for treatment is delivered to the targeted area. To accomplish this, it is necessary to monitor in real-time spatio-temporal changes in temperature resulting from CNMTT using infrared cameras [59, 141] or magnetic resonance imaging (MRI)-based methods[28, 61]. Infrared cameras are useful for optimizing both CNT concentration and NIR irradiation parameters in model tissue and in tumor bearing mice, but cannot accurately map temperature deep within tissue. However, a more clinically relevant method of non-invasive temperature mapping is a MRI-based thermometry method known as proton resonance frequency (PRF) MR temperature mapping (reviewed in [142]). This technique allows for superposition of both temperature information and anatomical images at any depth, and is currently used clinically to monitor the efficacy of thermal ablation techniques. By relating the treatment temperature to actual thermal tissue damage, PRF MR temperature mapping can be useful in predicting the treatment outcome [61].

Extensive work by Torti and colleagues has demonstrated the compatibility of PRF MR temperature mapping with CNMTT [22, 28, 61]. For example, Burke et al used PRF MR temperature maps to measure the temperature increase in kidney tumor xenografts following CNMTT [28]. Use of MRI contrast enhancing CNTs allows for monitoring of nanomaterial distribution [22] in the tumor and can aid in placement of the NIR source [143]. Ding et al showed that iron-containing MWCNTs act as dual mode MRI T2 contrast agents and photothermal mediators [22]. However, a potential limitation of iron-containing MWCNTs is their propensity to attenuate MR signals, which can interfere with temperature mapping by PRF MR thermometry [22].

Though dependent upon tumor type and location, generation of sufficiently high temperatures to ablate large (>3 cm) tumors while minimizing damage to healthy tissue surrounding the tumor due to heat delocalization is the major limitation to all current approaches to thermal ablation therapy [144]. Experimental use of nanosecond pulsed lasers has been successfully applied to localize heat on the cancer cell level in the presence or absence of CNTs [144-147]. However, use of continuous irradiation for tenths of seconds or longer (rather than nanosecond pulses) to heat a large number of nanoparticles dispersed throughout a tumor produces an overall temperature rise several orders of magnitude larger than the localized (nanoscale) temperature rise near each particle [141, 148]. Recently, Xie et al used a combination of experimental data in tissue phantoms and diffusive heat modeling to determine the thermal distribution CNT-bearing tumors during and following NIR irradiation and used clinically relevant damage predicting algorithms to quantify the likely efficacy of CNMTT following treatment with different laser pulse strengths and durations (summarized in figure 4). Fitting of the data to diffusive heat models indicates that it may be possible to achieve thermally ablative temperatures within in sharply defined regions (<1 mm margins) in as little as 2 seconds using clinically available continuous NIR lasers in combination with modest CNT concentrations [61]. In this short time scale, heat deposition is more rapid than thermal diffusion and convective cooling, which will simplify treatment planning and reduce heat diffusion to surrounding normal tissue as compared to current clinical thermal ablation techniques which require tissue to be heated for up to several minutes to achieve ablative temperatures.

More extended NIR treatment exposure may be necessary for treating bulky tumors because the generated heat can effectively spread over centimeter size regions [61, 141]. Moreover, modeling and experimental data in breast cancer tissue phantoms have shown that the presence of CNTs can extend the effective treatment volume for a fixed NIR energy input [149, 150]. Burke et al made similar observations in vivo using the induction of heat shock proteins (HSPs) 27, 70, and 90 as endogenous cellular markers of thermal stress for indirect measurement of heat generation in full-depth tissue sections taken from tumors of mice after NIR exposure [28]. In tumors treated with NIR plus MWCNTs, HSPs were seen at deeper tissue levels than in mice treated only with NIR, confirming that CNTs combined with NIR can be used to extend the effective volume of thermal therapy.

There remain several areas, summarized in figure 5, for further study. The temperature distribution following CNMTT is determined by the rate of energy input and efficiency of NIR conversion to heat, which is influenced by concentration [28], aggregation [63], length [52] and wall number of the CNTs [63]. Therefore, careful matching of both CNT type and distribution with NIR irradiation parameters can more effectively treat targeted cell populations. It is not clear how intratumoral distribution of CNTs will affect the efficacy of CNMTT. A homogeneous distribution of CNTs throughout the tumor mass may allow generation of a more predictable and uniform temperature in the targeted area following laser irradiation. However, the effective tissue penetration depth of NIR may be far smaller than the tumor volume to be treated, and thus a more modest distribution of CNTs may be

needed. Additionally, a better understanding of the contribution of heat dissipation caused by the presence of blood and body fluids will be required to determine both the optimal concentration of CNTs and NIR irradiation parameters required for clinical applications. Finally, a greater understanding of how different cancer cell populations respond to CNMTT -- including heat resistant stem-like cells and tumor cells that have received prior treatment -- may greatly assist in the development of new therapeutic strategies for non-resectable tumors that are resistant to current therapeutic modalities.

2.4. CNT toxicity and long-term fate

Progress towards the clinical use of CNTs has been limited in part due to the lack of a comprehensive understanding of the basic determinants of CNT toxicity and clearance from the human body. Fear of exposure to CNTs has been exacerbated because CNTs can act as ‘nano-needles’, easily piercing cell membranes [8, 9], traversing to the nucleus [23] and potentially inducing genotoxicity [151]. One preliminary study on the toxicity of CNTs indicated that when they are injected into the abdominal cavity or lungs of mice, they can induce inflammatory responses and granuloma formation similar to those associated with asbestos exposure [152, 153]; a more recent study further demonstrated mesothelial cell injury and formation of mesotheliomas following peritoneal injection of pristine CNTs [154]. In contrast, a two year study on the potential carcinogenic nature of CNTs injected into the peritoneal cavity of rats found no evidence of CNTs causing cancer [155]. In light of these conflicting results, the future outlook for biomedical application of CNTs continues to be met with scepticism. Fears over CNT exposure increased due to the perception that they were not degraded in the body, though now it is known that some types of CNTs can be degraded in biological systems by oxidative enzymes [156, 157]. The persistence of these concerns indicates that for biomedical use of CNTs to progress, the toxicity, and therefore the potential risk–benefit balance for these materials, must be resolved.

Use of CNTs in cancer therapy requires bypassing the body's natural defenses, generating concern that toxicities not previously observed might be induced. However, many strategies have evolved to reduce the toxic effects of CNTs by altering lengths, diameters, or chemically modifying their surfaces [158]. Biomedical use of CNTs requires modification of the highly hydrophobic surface of the tubes to render them hydrophilic [159], but not all chemical treatments alleviate the toxicity risks associated with CNTs. It is essential to identify which characteristics CNTs should possess to be “safe-for-use”. It is becoming clear that modifications that render carbon nanotubes short (<1000 nm), flexible and permit stable suspension in biological fluids are necessary to ameliorate the risks identified for exposure to pristine (unmodified) CNTs [160].

For example, work by Donaldson and colleagues established that the inflammation and fibrosis induced by CNTs introduced into the pleural cavity of mice could be reduced by shortening the length of CNTs [161]. Shorter tubes (<1000 nm) were not retained in the pleural cavity and eventually were excreted. In another related study, Ali-Boucetta et al described two different chemical modifications to CNT surfaces and asked if either could reduce the inflammatory toxicity of the CNTs following intraperitoneal injection of the tubes [160]. They found that CNTs functionalized using the 1,3-dipolar cycloaddition of azomethine ylides first described by Prato and colleagues [23] to introduce pyrrolidine rings bearing an ammonium-terminated tri(ethylene glycol) chain to the side wall of CNTs do not induce inflammation. In contrast, CNTs functionalized using the method of Billups et al [162] to introduce an octyl chain on the side walls induce an inflammatory response comparable to that observed for long, pristine CNTs [163]. Functionalization of CNTs using the 1,3-dipolar cycloaddition method shortened and debundled the tubes following aqueous dispersion while CNTs functionalized by the Billups method remained aggregated in aqueous suspension [160]. The authors suggest that not all chemical treatments will alleviate

the toxicity risks associated with CNTs; only chemical reactions to CNT surfaces that lead to CNT shortening and aid in disentangling/debundling of CNTs following aqueous dispersion will reduce the risks [160].

In addition to length and dispersibility in aqueous solvents, a third critical factor which determines the potential of CNTs to cause cell injury appears to be CNT diameter. In a recent study, pristine MWCNTs of differing thickness were suspended in saline solution containing albumin, and their uptake by mesothelial cells was compared to that of asbestos fibers [154]. Mesothelial cells were shown to take up MWCNTs and asbestos by two distinct mechanisms: MWCNTs directly pierced mesothelial plasma and nuclear membranes, whereas asbestos fibers were internalized by endocytosis. Consistent with the observation that the force needed to penetrate cell membranes is proportional to CNT diameter [164], thick MWCNTs (150 nm diameter) were less likely to pierce mesothelial cells than thin MWCNTs (50 nm diameter) [154] . In contrast, asbestos fibers, even those thicker than 150 nm, were easily internalized by the cells because they do not necessarily enter mesothelial cells in the same way as CNTs. This work suggests that not only should CNT toxicology be evaluated differently than asbestos toxicology, but also that control of the diameter of MWCNTs could reduce the potential for mesothelial injury and other hazards caused by CNTs.

The potential risks due to inflammatory responses caused by chronic exposure to CNTs in different tissue are compounded by the possibility of acute risks associated with blood-borne delivery of CNTs [165-168]. Despite the fact that no long-term, or chronic toxicity has been exhibited by mice injected with CNTs that have been chemically functionalized to improve aqueous dispersion [6, 67, 133, 169-171], concerns have persisted regarding the potential thrombogenic nature of CNTs. In this regard, several groups have shown that CNTs have a high propensity to activate elements of the coagulation cascade in vitro [166, 167, 172]. However, in an extensive study comparing the role played by chemical functionalization of CNTs on blood toxicity in vitro to indicators of thrombosis following intravenous injection into mice (platelet counts; D-dimer levels; murine Von Willebrand factor; histology), Burke et al found that in vitro analysis of CNT induced coagulation was a poor predictor of actual in vivo outcomes [173]. Specifically, the researchers found that pristine MWCNTs appeared to be less thrombogenic than chemically functionalized MWCNT (acid oxidized; acid oxidized then amidated) in vitro as indicated by activation of the coagulation cascade, coagulation time, and platelet activation, which is consistent with other recent reports [174]. However, following intravenous injection in mice, pristine MWCNTs were found to rapidly deplete platelets, and induce elevated D-dimer and Von Willebrand factor levels, indicating severe thrombosis, disseminated intravascular coagulation, and endothelial cell injury [173]. At a dose of 250 μg, pristine MWCNT were acutely lethal, inducing blockage of the pulmonary vasculature. In contrast, the sole measurable effect of an equivalent dose of the two types of functionalized MWCNTs was a transient depletion of platelets [173]. Although more detailed studies must be undertaken before the toxicity profile of CNTs is fully understood, these results support the hypothesis that CNTs can be designed to be suitable for systemic delivery.

Importantly, chemical functionalization of CNTs is also known to greatly influence their blood clearance profile. Following early debates regarding whether the primary clearance route for intravenously administered CNTs was via renal or biliary pathways [133, 175, 176], it is now known that the type and degree of chemical functionalization, degree of agglomeration, and length of the tubes determine the tissue distribution and excretion of CNTs [177-179]. Renal clearance of CNTs in particular has caused much debate as many believe that 5 nm is the maximum diameter that permits for clearance of nanoparticles via the urine [180]. However, several groups have shown that intact CNTs as long as 500 nm

with diameters of up to 25-30 nms can exit the blood stream and be excreted in urine by orienting themselves along their smaller axis to pass through the fenestrated endothelium of the glomerular capillary wall, across the glomerular basement membrane, and through the filtration slits [133, 134, 179, 181] despite these openings being approximately 43 nm in diameter [182]. A more recent study by Kostarelos et al convincingly confirms these previous works, showing: 1) individualization of CNTs resulting from a high degree of chemical functionalization to introduce hydrophilic groups to the CNT surface aids in rapid renal clearance and low tissue retention; 2) shorter CNTs exhibit greater renal clearance than longer CNTs; and 3) in general, increasing hydrophilic chemically functionalization is associated with renal clearance while decreasing functionalization favors clearance by the mononuclear phagocyte system [177].

Combined, the studies described above indicate that it should be possible to engineer CNTs suitable for future use in humans. New strategies to synthesize and modify CNTs in a highly controlled manner continue to evolve and show tremendous potential for designing CNTs with optimal in vivo characteristics. As more research evaluating the relationship between CNT characteristics and in vivo kinetics, excretion, and toxicity emerges, the clinical use of CNTs is becoming more and more feasible.

3. Conclusions

The translation of carbon nanotubes from an interesting nanomaterial to an effective cancer therapeutic agent is an actively evolving field [25]. As discussed in **section 1** of this review, CNTs offer enormous possibilities for the development of the next generation of cancer therapeutic and diagnostic agents. Their desirable features include the following: 1) they efficiently convert incident NIR into heat for use in cancer thermal ablation or imaging; 2) they can be used for additional therapeutic applications including chemotherapeutic drug or gene delivery; 3) their high surface area to volume ratio per particle allows for incorporation of a high density of imaging agents which can improve the sensitivity of imaging; 4) they can simultaneously deliver several different types of agents to perform multimodality imaging and cancer therapy; 5) they easily cross cell membranes and can be engineered to be exhibit a positive biocompatibility profile.

As research in this field has advanced, a number of issues in the use of CNTs for CNMTT, identified in **section 2** in this review, remain to be addressed. Size of the tumor is one consideration. Many cancers do not present until tumors are significantly larger than one or several centimeters in diameter, which is larger than most tumors treated in animal models to date. Delivery of both CNTs and therapeutic heat across these larger tumors represents a major challenge in the pre-clinical development of CNMTT. Most applications to date have relied on NIR, which has a finite range of tissue penetration. Although biological tissues are relatively transparent to NIR, treatment of deep-seated tumors may require either the use of RF or longer wavelength electromagnetic radiation; such strategies are being actively pursued [54, 183]. Alternatively, the development of companion technology, such as fiber optic probes that can deliver NIR to the target site, may enable the utilization of NIR for thermal activation of CNTs in even deep-seated tumors. Additionally, strategies must be developed to monitor both the distribution of the CNTs and the deposition, localization, and efficacy of heat treatment.

Conversely, it is also desirable to treat small micrometastases. Currently, CNMTT relies on conventional clinical imaging to detect and localize tumors prior to treatment, and tumors that are too small to be visualized by such methodology will remain untreated. Use of targeted nanoparticles conjugated to imaging moieties may overcome this limitation by allowing the detection and treatment of such small tumors. Targeted nanotubes may also

permit dose reduction, since each nanotube would have a higher probability of associating with its tumor target. Of particular interest would be the development of CNT-based PET agents, which would allow for extremely high detection sensitivity and depth of penetration. Because the risk of nanoparticle toxicity will go down with decreased exposure, the use of PET as an imaging modality may further push the envelope on clinical development of CNT-based therapeutic and diagnostic agents. A number of potential agents have been tested in mice [19, 70, 133, 134], but their utility in cancer diagnosis has yet to be evaluated.

Most importantly, the long term fate and toxicity of CNTs must be determined. It has become clear that specifics matter: that each change in particle design creates an entirely new particle with novel toxicological, pharmacological and therapeutic properties. This necessitates that both the biomedical and toxicological investigations of these materials take place simultaneously. The debate over toxicity of CNTs continues despite research showing that appropriate design can ameliorate many unwanted effects of CNTs; thus, overcoming the perceived and real potential toxicities of nanotubes may represent the largest hurdle towards their clinical application. Based upon the current evidence, a series of guidelines for future development of CNT-based therapeutics has been proposed by Kostarelos and colleagues [183]. Briefly summarized, these recommendations are: (1) use aqueous preparations of small, hydrophilic, well dispersed CNTs that can easily be internalized by target cells and that macrophages can efficiently take-up and clear after the therapeutic effect is achieved; (2) use colloidal dispersions of CNTs that are stable under physiologic pH and salinity to minimize aggregation in vivo; and (3) use easily excreted or chemically-modified CNTs that are readily degraded in vivo.

The promise of CNTs in photothermal cancer therapy still remains; realization of this potential will depend on production of well-characterized, biocompatible, homogeneous materials and well-designed efficacy and toxicology studies.

Acknowledgments

This work was supported in part by grants RO1CA12842 (SVT) from the National Cancer Institute/National Institutes of Health, W81XWH-10-1-0434 (SVT) from the Department of Defense, and by R00CA154006 (RS) from the National Cancer Institute/ National Institutes of Health. The content is solely the responsibility of the authors and does not necessarily represent the official views of the National Cancer Institute, the National Institutes of Health, or the Department of Defense.

References

1. Ebbesen TW. Carbon nanotubes. Physics Today. 1996; 49:26–32.
2. Sailor MJ, Park JH. Hybrid Nanoparticles for Detection and Treatment of Cancer. Advanced Materials. 2012; 24:3779–3802. [PubMed: 22610698]
3. Fisher C, Rider AE, Han ZJ, Kumar S, Levchenko I, Ostrikov K. Applications and Nanotoxicity of Carbon Nanotubes and Graphene in Biomedicine. Journal of Nanomaterials. 2012 Article ID 315185. 19 pages.
4. Gulati N, Gupte H. Two Faces of Carbon Nanotube: Toxicities and Pharmaceutical Applications. Critical Reviews in Therapeutic Drug Carrier Systems. 2012; 29:65–88. [PubMed: 22356722]
5. Harris DL, Bawa R. The carbon nanotube patent landscape in nanomedicine: an Expert opinion. Expert Opinion on Therapeutic Patents. 2007; 17:1165–1174.
6. Lacerda L, Bianco A, Prato M, Kostarelos K. Carbon nanotubes as nanomedicines: From toxicology to pharmacology. Advanced Drug Delivery Reviews. 2006; 58:1460–1470. [PubMed: 17113677]
7. Lacerda L, Bianco A, Prato M, Kostarelos K. Carbon nanotube cell translocation and delivery of nucleic acids in vitro and in vivo. Journal of Materials Chemistry. 2008; 18:17–22.
8. Lacerda L, Raffa S, Prato M, Bianco A, Kostarelos K. Cell-penetrating CNTs for delivery of therapeutics. Nano Today. 2007; 2:38–43.

9. Lacerda L, Russier J, Pastorin G, Herrero MA, Venturelli E, Dumortier H, Al-Jamal KT, Prato M, Kostarelos K, Bianco A. Translocation mechanisms of chemically functionalised carbon nanotubes across plasma membranes. Biomaterials. 2012; 33:3334–3343. [PubMed: 22289266]
10. Bhirde AA, Patel S, Sousa AA, Patel V, Molinolo AA, Ji YM, Leapman RD, Gutkind JS, Rusling JF. Distribution and clearance of PEG-single-walled carbon nanotube cancer drug delivery vehicles in mice. Nanomedicine. 2010; 5:1535–1546. [PubMed: 21143032]
11. Singh R, Pantarotto D, McCarthy D, Chaloin O, Hoebeke J, Partidos CD, Briand JP, Prato M, Bianco A, Kostarelos K. Binding and condensation of plasmid DNA onto functionalized carbon nanotubes: Toward the construction of nanotube-based gene delivery vectors. Journal of the American Chemical Society. 2005; 127:4388–4396. [PubMed: 15783221]
12. Xue YD, Bao L, Xiao XR, Ding L, Lei JP, Ju HX. Noncovalent functionalization of carbon nanotubes with lectin for label-free dynamic monitoring of cell-surface glycan expression. Analytical Biochemistry. 2011; 410:92–97. [PubMed: 21094122]
13. Ananta JS, Matson ML, Tang AM, Mandal T, Lin S, Wong K, Wong ST, Wilson LJ. Single-Walled Carbon Nanotube Materials as T-2-Weighted MRI Contrast Agents. Journal of Physical Chemistry C. 2009; 113:19369–19372.
14. Bhirde AA, Sousa AA, Patel V, Azari AA, Gutkind JS, Leapman RD, Rusling JF. Imaging the distribution of individual platinum-based anticancer drug molecules attached to single-wall carbon nanotubes. Nanomedicine. 2009; 4:763–772. [PubMed: 19839812]
15. Adeli M, Hakimpoor F, Ashiri M, Kabiri R, Bavadi M. Anticancer drug delivery systems based on noncovalent interactions between carbon nanotubes and linear-dendritic copolymers. Soft Matter. 2011; 7:4062–4070.
16. Ali-Boucetta H, Al-Jamal KT, McCarthy D, Prato M, Bianco A, Kostarelos K. Multiwalled carbon nanotube-doxorubicin supramolecular complexes for cancer therapeutics. Chemical Communications. 2008:459–461. [PubMed: 18188467]
17. Al-Jamal KT, Toma FM, Yilmazer A, Ali-Boucetta H, Nunes A, Herrero MA, Tian BW, Eddaoui A, Al-Jamal WT, Bianco A, Prato M, Kostarelos K. Enhanced cellular internalization and gene silencing with a series of cationic dendron-multiwalled carbon nanotube:siRNA complexes. Faseb Journal. 2010; 24:4354–4365. [PubMed: 20647548]
18. Kostarelos K, Lacerda L, Partidos CD, Prato M, Blanco A. Carbon nanotube-mediated delivery of peptides and genes to cells: translating nanobiotechnology to therapeutics. Journal of Drug Delivery Science and Technology. 2005; 15:41–47.
19. Ruggiero A, Villa CH, Holland JP, Sprinkle SR, May C, Lewis JS, Scheinberg DA, McDevitt MR. Imaging and treating tumor vasculature with targeted radiolabeled carbon nanotubes. International Journal of Nanomedicine. 2010; 5:783–802. [PubMed: 21042424]
20. Sahoo NG, Bao HQ, Pan YZ, Pal M, Kakran M, Cheng HKF, Li L, Tan LP. Functionalized carbon nanomaterials as nanocarriers for loading and delivery of a poorly water-soluble anticancer drug: a comparative study. Chemical Communications. 2011; 47:5235–5237. [PubMed: 21451845]
21. de la Zerda A, Zavaleta C, Keren S, Vaithilingam S, Bodapati S, Liu Z, Levi J, Smith BR, Ma TJ, Oralkan O, Cheng Z, Chen XY, Dai HJ, Khuri-Yakub BT, Gambhir SS. Carbon nanotubes as photoacoustic molecular imaging agents in living mice. Nat Nanotechnol. 2008; 3:557–562. [PubMed: 18772918]
22. Ding XF, Singh R, Burke A, Hatcher H, Olson J, Kraft RA, Schmid M, Carroll D, Bourland JD, Akman S, Torti FM, Torti SV. Development of iron-containing multiwalled carbon nanotubes for MR-guided laser-induced thermotherapy. Nanomedicine. 2011; 6:1341–1352. [PubMed: 21506687]
23. Pantarotto D, Singh R, McCarthy D, Erhardt M, Briand JP, Prato M, Kostarelos K, Bianco A. Functionalized carbon nanotubes for plasmid DNA gene delivery. Angewandte Chemie-International Edition. 2004; 43:5242–5246.
24. Shi DL. Integrated Multifunctional Nanosystems for Medical Diagnosis and Treatment. Advanced Functional Materials. 2009; 19:3356–3373.
25. Kostarelos K, Bianco A, Prato M. Promises, facts and challenges for carbon nanotubes in imaging and therapeutics. Nat Nanotechnol. 2009; 4:627–633. [PubMed: 19809452]

26. Day ES, Morton JG, West JL. Nanoparticles for thermal cancer therapy. J Biomech Eng. 2009; 131:074001. [PubMed: 19640133]
27. Kam NW, O'Connell M, Wisdom JA, Dai H. Carbon nanotubes as multifunctional biological transporters and near-infrared agents for selective cancer cell destruction. P Natl Acad Sci USA. 2005; 102:11600–11605.
28. Burke A, Ding XF, Singh R, Kraft RA, Levi-Polyachenko N, Rylander MN, Szot C, Buchanan C, Whitney J, Fisher J, Hatcher HC, D'Agostino R, Kock ND, Ajayan PM, Carroll DL, Akman S, Torti FM, Torti SV. Long-term survival following a single treatment of kidney tumors with multiwalled carbon nanotubes and near-infrared radiation. P Natl Acad Sci USA. 2009; 106:12897–12902.
29. Yang K, Zhang S, Zhang G, Sun X, Lee ST, Liu Z. Graphene in mice: ultrahigh in vivo tumor uptake and efficient photothermal therapy. Nano lett. 2010; 10:3318–3323. [PubMed: 20684528]
30. Jordan A. Hyperthermia classic commentary: 'Inductive heating of ferrimagnetic particles and magnetic fluids: Physical evaluation of their potential for hyperthermia' by Andreas Jordan et al., International Journal of Hyperthermia, 1993;9:51-68. International Journal of Hyperthermia. 2009; 25:512–516. [PubMed: 19848613]
31. Dickerson EB, Dreaden EC, Huang X, El-Sayed IH, Chu H, Pushpanketh S, McDonald JF, El-Sayed MA. Gold nanorod assisted near-infrared plasmonic photothermal therapy (PPTT) of squamous cell carcinoma in mice. Cancer Letters. 2008; 269:57–66. [PubMed: 18541363]
32. Hirsch LR, Stafford RJ, Bankson JA, Sershen SR, Rivera B, Price RE, Hazle JD, Halas NJ, West JL. Nanoshell-mediated near-infrared thermal therapy of tumors under magnetic resonance guidance. P Natl Acad Sci USA. 2003; 100:13549–13554.
33. O'Neal DP, Hirsch LR, Halas NJ, Payne JD, West JL. Photo-thermal tumor ablation in mice using near infrared-absorbing nanoparticles. Cancer Lett. 2004; 209:171–176. [PubMed: 15159019]
34. Emami B, Song CW. Physiological mechanisms in hyperthermia: a review. International Journal of Radiation Oncology, Biology, Physics. 1984; 10:289–295.
35. Fajardo LF, Egbert B, Marmor J, Hahn GM. Effects of hyperthermia in a malignant tumor. Cancer. 1980; 45:613–623. [PubMed: 7353209]
36. Coss RA, Dewey WC, Bamburg JR. Effects of hyperthermia on dividing Chinese hamster ovary cells and on microtubules in vitro. Cancer Res. 1982; 42:1059–1071. [PubMed: 7199378]
37. Roti JLR. Cellular responses to hyperthermia (40-46C): Cell killing and molecular events. International Journal of Hyperthermia. 2008; 24:3–15. [PubMed: 18214765]
38. Subjeck JR, Sciandra JJ, Chao CF, Johnson RJ. Heat shock proteins and biological response to hyperthermia. The British journal of cancer. 1982; 5:127–131. [PubMed: 6950747]
39. Nikfarjam M, Muralidharan V, Christophi C. Mechanisms of Focal Heat Destruction of Liver Tumors. Journal of Surgical Research. 2005; 127:208–223. [PubMed: 16083756]
40. Dewhirst MW, Prosnitz L, Thrall D, Prescott D, Clegg S, Charles C, MacFall J, Rosner G, Samulski T, Gillette E, LaRue S. Hyperthermic treatment of malignant diseases: current status and a view toward the future. Seminars in oncology. 1997; 24:616–625. [PubMed: 9422258]
41. Falk MH, Issels RD. Hyperthermia in oncology. International Journal of Hyperthermia. 2001; 17:1–18. [PubMed: 11212876]
42. Atkinson RL, Zhang M, Diagaradjane P, Peddibhotla S, Contreras A, Hilsenbeck SG, Woodward WA, Krishnan S, Chang JC, Rosen JM. Thermal enhancement with optically activated gold nanoshells sensitizes breast cancer stem cells to radiation therapy. Science Translational Medicine. 2011; 2:55ra–79.
43. Wust P, Hildebrandt B, Sreenivasa G, Rau B, Gellermann J, Riess H, Felix R, Schlag PM. Hyperthermia in combined treatment of cancer. The Lancet Oncology. 2002; 3:487–497. [PubMed: 12147435]
44. V R, Llovet Josep M, Brú Concepció, Bianchi Lluís, Salmeron Joan Manuel, Boix Loreto, Ganau Sergi, Sala Margarita, Pagès Mario, Ayuso Carmen, Solé Manel, Rodés Joan, Bruix Jordi. The Barcelona Clínic Liver Cancer Group. Increased risk of tumor seeding after percutaneous radiofrequency ablation for single hepatocellular carcinoma. Hepatology. 2001; 33:1124–1129. [PubMed: 11343240]

45. Baronzio G, Gramaglia A, Fiorentini G. Review. Current role and future perspectives of hyperthermia for prostate cancer treatment. In Vivo. 2009; 23:143–146. [PubMed: 19368139]
46. Krishnan S, Diagaradjane P, Cho SH. Nanoparticle-mediated thermal therapy: Evolving strategies for prostate cancer therapy. International Journal of Hyperthermia. 2010; 26:775–789. [PubMed: 20858069]
47. Silva AC, Oliveira TR, Mamani JB, Malheiros SM, Malavolta L, Pavon LF, Sibov TT, Amaro E Jr, Tannus A, Vidoto EL, Martins MJ, Santos RS, Gamarra LF. Application of hyperthermia induced by superparamagnetic iron oxide nanoparticles in glioma treatment. International Journal of Nanomedicine. 2011; 6:591–603. [PubMed: 21674016]
48. Maier-Hauff K, Ulrich F, Nestler D, Niehoff H, Wust P, Thiesen B, Orawa H, Budach V, Jordan A. Efficacy and safety of intratumoral thermotherapy using magnetic iron-oxide nanoparticles combined with external beam radiotherapy on patients with recurrent glioblastoma multiforme. Journal of Neuro-Oncology. 2011; 103:317–324. [PubMed: 20845061]
49. Iancu C, Mocan L. Advances in cancer therapy through the use of carbon nanotube-mediated targeted hyperthermia. International Journal of Nanomedicine. 2011; 6:1675–1684. [PubMed: 21904457]
50. Konig K. Multiphoton microscopy in life sciences. Journal of Microscopy. 2000; 200:83–104. [PubMed: 11106949]
51. Weissleder R. A clearer vision for in vivo imaging. Nature biotechnology. 2001; 19:316–317.
52. Torti SV, Byrne F, Whelan O, Levi N, Ucer B, Schmid M, Torti FM, Akman S, Liu J, Ajayan PM, Nalamasu O, Carroll DL. Thermal ablation therapeutics based on CNx multi-walled nanotubes. International Journal of Nanomedicine. 2007; 2:707–714. [PubMed: 18203437]
53. Robinson JT, Welsher K, Tabakman SM, Sherlock SP, Wang H, Luong R, Dai H. High Performance In Vivo Near-IR (>1 mum) Imaging and Photothermal Cancer Therapy with Carbon Nanotubes. Nano Research. 2010; 3:779–793. [PubMed: 21804931]
54. Gannon CJ, Cherukuri P, Yakobson BI, Cognet L, Kanzius JS, Kittrell C, Weisman RB, Pasquali M, Schmidt HK, Smalley RE, Curley SA. Carbon nanotube-enhanced thermal destruction of cancer cells in a noninvasive radiofrequency field. Cancer. 2007; 110:2654–2665. [PubMed: 17960610]
55. Muller S. Magnetic fluid hyperthermia therapy for malignant brain tumors-an ethical discussion. Nanomedicine-Nanotechnology Biology and Medicine. 2009; 5:387–393.
56. Kangasniemi M, McNichols RJ, Bankson JA, Gowda A, Price RE, Hazle JD. Thermal therapy of canine cerebral tumors using a 980 nm diode laser with MR temperature-sensitive imaging feedback. Lasers in surgery and medicine. 2004; 35:41–50. [PubMed: 15278927]
57. Chen WR, Korbelik M, Bartels KE, Liu H, Sun J, Nordquist RE. Enhancement of laser cancer treatment by a chitosan-derived immunoadjuvant. Photochemistry and Photobiology. 2005; 81:190–195. [PubMed: 15535737]
58. Gnyawali SC, Chen Y, Wu F, Bartels KE, Wicksted JP, Liu H, Sen CK, Chen WR. Temperature measurement on tissue surface during laser irradiation. Medical and Biological Engineering and Computing. 2008; 46:159–168. [PubMed: 17891430]
59. Huang N, Wang H, Zhao J, Lui H, Korbelik M, Zeng H. Single-wall carbon nanotubes assisted photothermal cancer therapy: Animal study with a murine model of squamous cell carcinoma. Lasers in surgery and medicine. 2010; 42:638–648. [PubMed: 20949599]
60. Moon HK, Lee SH, Choi HC. In Vivo Near-Infrared Mediated Tumor Destruction by Photothermal Effect of Carbon Nanotubes. Acs Nano. 2009; 3:3707–3713. [PubMed: 19877694]
61. Xie B, Singh R, Torti FM, Keblinski P, Torti S. Heat localization for targeted tumor treatment with nanoscale near-infrared radiation absorbers. Physics in Medicine and Biology. 2012; 57:5765–5775. [PubMed: 22948207]
62. Murakami T, Nakatsuji H, Inada M, Matoba Y, Umeyama T, Tsujimoto M, Isoda S, Hashida M, Imahori H. Photodynamic and Photothermal Effects of Semiconducting and Metallic-Enriched Single-Walled Carbon Nanotubes. Journal of the American Chemical Society. 2012; 134:17862–17865. [PubMed: 23083004]

63. Ghosh S, Dutta S, Gomes E, Carroll D, D'Agostino R Jr, Olson J, Guthold M, Gmeiner WH. Increased heating efficiency and selective thermal ablation of malignant tissue with DNA-encased multiwalled carbon nanotubes. Acs Nano. 2009; 3:2667–2673. [PubMed: 19655728]
64. Maeda H, Wu J, Sawa T, Matsumura Y, Hori K. Tumor vascular permeability and the EPR effect in macromolecular therapeutics: a review. Journal of Controlled Release. 2000; 65:271–284. [PubMed: 10699287]
65. Liu Z, Tabakman SM, Chen Z, Dai HJ. Preparation of carbon nanotube bioconjugates for biomedical applications. Nature Protocols. 2009; 4:1372–1382.
66. Cato MH, D'Annibale F, Mills DM, Cerignoli F, Dawson MI, Bergamaschi E, Bottini N, Magrini A, Bergamaschi A, Rosato N, Rickert RC, Mustelin T, Bottini M. Cell-type specific and cytoplasmic targeting of PEGylated carbon nanotube-based nanoassemblies. J Nanosci Nanotechno. 2008; 8:2259–2269.
67. Liu Z, Chen K, Davis C, Sherlock S, Cao QZ, Chen XY, Dai HJ. Drug delivery with carbon nanotubes for in vivo cancer treatment. Cancer Res. 2008; 68:6652–6660. [PubMed: 18701489]
68. Liu Z, Cai WB, He LN, Nakayama N, Chen K, Sun XM, Chen XY, Dai HJ. In vivo biodistribution and highly efficient tumour targeting of carbon nanotubes in mice. Nat Nanotechnol. 2007; 2:47–52. [PubMed: 18654207]
69. Liu XW, Tao HQ, Yang K, Zhang SA, Lee ST, Liu ZA. Optimization of surface chemistry on single-walled carbon nanotubes for in vivo photothermal ablation of tumors. Biomaterials. 2011; 32:144–151. [PubMed: 20888630]
70. McDevitt MR, Chattopadhyay D, Kappel BJ, Jaggi JS, Schiffman SR, Antczak C, Njardarson JT, Brentjens R, Scheinberg DA. Tumor targeting with antibody-functionalized, radiolabeled carbon nanotubes. Journal of Nuclear Medicine. 2007; 48:1180–1189. [PubMed: 17607040]
71. Welsher K, Liu Z, Daranciang D, Dai H. Selective probing and imaging of cells with single walled carbon nanotubes as near-infrared fluorescent molecules. Nano lett. 2008; 8:586–590. [PubMed: 18197719]
72. Kamen BA, Smith AK. A review of folate receptor alpha cycling and 5-methyltetrahydrofolate accumulation with an emphasis on cell models in vitro. Adv Drug Deliv Rev. 2004; 56:1085–1097. [PubMed: 15094208]
73. Zhou F, Xing D, Ou Z, Wu B, Resasco DE, Chen WR. Cancer photothermal therapy in the near-infrared region by using single-walled carbon nanotubes. Journal of Biomedical Optics. 2009; 14:021009. [PubMed: 19405722]
74. Kang B, Yu D, Dai Y, Chang S, Chen D, Ding Y. Cancer-Cell Targeting and Photoacoustic Therapy Using Carbon Nanotubes as “Bomb” Agents. Small. 2009; 5:1292–1301. [PubMed: 19274646]
75. Marches R, Mikoryak C, Wang RH, Pantano P, Draper RK, Vitetta ES. The importance of cellular internalization of antibody-targeted carbon nanotubes in the photothermal ablation of breast cancer cells. Nanotechnology. 2011; 22:095101. [PubMed: 21258147]
76. Xiao Y, Gao X, Taratula O, Treado S, Urbas A, Holbrook RD, Cavicchi RE, Avedisian CT, Mitra S, Savla R, Wagner PD, Srivastava S, He H. Anti-HER2 IgY antibody-functionalized single-walled carbon nanotubes for detection and selective destruction of breast cancer cells. BMC Cancer. 2009; 9:351. [PubMed: 19799784]
77. Wang CH, Huang YJ, Chang CW, Hsu WM, Peng CA. In vitro photothermal destruction of neuroblastoma cells using carbon nanotubes conjugated with GD2 monoclonal antibody. Nanotechnology. 2009; 20:315101. [PubMed: 19597244]
78. Ning S, Lu S, Wickstrom E, Panchapakesan B. Integrated molecular targeting of IGF1R and HER2 surface receptors and destruction of breast cancer cells using single wall carbon nanotubes. Nanotechnology. 2007; 18:315101.
79. Mahon E, Salvati A, Bombelli FB, Lynch I, Dawson KA. Designing the nanoparticle-biomolecule interface for “targeting and therapeutic delivery”. Journal of Controlled Release. 2012; 161:164–174. [PubMed: 22516097]
80. Teeguarden JG, Hinderliter PM, Orr G, Thrall BD, Pounds JG. Particokinetics in vitro: Dosimetry considerations for in vitro nanoparticle toxicity assessments. Toxicological Sciences. 2007; 95:300–312. [PubMed: 17098817]

81. Zhou FF, Xing D, Wu BY, Wu SN, Ou ZM, Chen WR. New Insights of Transmembranal Mechanism and Subcellular Localization of Noncovalently Modified Single-Walled Carbon Nanotubes. Nano lett. 2010; 10:1677–1681. [PubMed: 20369892]
82. Zhou FF, Wu SN, Wu BY, Chen WR, Xing D. Mitochondria-Targeting Single-Walled Carbon Nanotubes for Cancer Photothermal Therapy. Small. 2011; 7:2727–2735. [PubMed: 21861293]
83. Wang CH, Chiou SH, Chou CP, Chen YC, Huang YJ, Peng CA. Photothermolysis of glioblastoma stem-like cells targeted by carbon nanotubes conjugated with CD133 monoclonal antibody. Nanomedicine: Nanotechnology, Biology and Medicine. 2011; 7:69–79.
84. Burke AR, Singh RN, Carroll DL, Wood JCS, D'Agostino RB, Ajayan PM, Torti FM, Torti SV. The resistance of breast cancer stem cells to conventional hyperthermia and their sensitivity to nanoparticle-mediated photothermal therapy. Biomaterials. 2012; 33:2961–2970. [PubMed: 22245557]
85. Jordan CT, Guzman ML, Noble M. Cancer stem cells. New England Journal of Medicine. 2006; 355:1253–1261. [PubMed: 16990388]
86. Singh SK, Hawkins C, Clarke ID, Squire JA, Bayani J, Hide T, Henkelman RM, Cusimano MD, Dirks PB. Identification of human brain tumour initiating cells. Nature. 2004; 432:396–401. [PubMed: 15549107]
87. Zeppernick F, Ahmadi R, Campos B, Dictus C, Helmke BM, Becker N, Lichter P, Unterberg A, Radlwimmer B, Herold-Mende CC. Stem Cell Marker CD133 Affects Clinical Outcome in Glioma Patients. Clinical Cancer Research. 2008; 14:123–129. [PubMed: 18172261]
88. Beier D, Wischhusen J, Dietmaier W, Hau P, Proescholdt M, Brawanski A, Bogdahn U, Beier CP. CD133 Expression and Cancer Stem Cells Predict Prognosis in High-grade Oligodendroglial Tumors. Brain Pathology. 2008; 18:370–377. [PubMed: 18371181]
89. Bao S, Wu Q, McLendon RE, Hao Y, Shi Q, Hjelmeland AB, Dewhirst MW, Bigner DD, Rich JN. Glioma stem cells promote radioresistance by preferential activation of the DNA damage response. Nature. 2006; 444:756–760. [PubMed: 17051156]
90. Lee J, Kotliarova S, Kotliarov Y, Li A, Su Q, Donin NM, Pastorino S, Purow BW, Christopher N, Zhang W, Park JK, Fine HA. Tumor stem cells derived from glioblastomas cultured in bFGF and EGF more closely mirror the phenotype and genotype of primary tumors than do serum-cultured cell lines. Cancer Cell. 2006; 9:391–403. [PubMed: 16697959]
91. Galanzha EI, Kim JW, Zharov VP. Nanotechnology-based molecular photoacoustic and photothermal flow cytometry platform for in-vivo detection and killing of circulating cancer stem cells. Journal of biophotonics. 2009; 2:725–735. [PubMed: 19957272]
92. Al-Hajj M, Wicha MS, Benito-Hernandez A, Morrison SJ, Clarke MF. Prospective identification of tumorigenic breast cancer cells. P Natl Acad Sci USA. 2003; 100:3983–3988.
93. Sun X, Xiong Y, Chen P, Lin J, Ji W, Lim JH, Yang SS, Hagan DJ, Van Stryland EW. Investigation of an optical limiting mechanism in multiwalled carbon nanotubes. Applied optics. 2000; 39:1998–2001. [PubMed: 18345099]
94. Chakravarty P, Qian W, El-Sayed MA, Prausnitz MR. Delivery of molecules into cells using carbon nanoparticles activated by femtosecond laser pulses. Nat Nanotechnol. 2010; 5:607–611. [PubMed: 20639882]
95. Urban AS, Fedoruk M, Horton MR, Radler JO, Stefani FD, Feldmann J. Controlled nanometric phase transitions of phospholipid membranes by plasmonic heating of single gold nanoparticles. Nano lett. 2009; 9:2903–2908. [PubMed: 19719109]
96. Pommier Y, Sordet O, Antony S, Hayward RL, Kohn KW. Apoptosis defects and chemotherapy resistance: molecular interaction maps and networks. Oncogene. 2004; 23:2934–2949. [PubMed: 15077155]
97. Gottesman MM. Mechanisms of cancer drug resistance. Annual Review of Medicine. 2002; 53:615–627.
98. Fisher JW, Sarkar S, Buchanan CF, Szot CS, Whitney J, Hatcher HC, Torti SV, Rylander CG, Rylander MN. Photothermal response of human and murine cancer cells to multiwalled carbon nanotubes after laser irradiation. Cancer Res. 2010; 70:9855–9864. [PubMed: 21098701]
99. Kratz F. Albumin, a versatile carrier in oncology. Int J Clin Pharmacol Ther. 2010; 48:453–455. [PubMed: 20557842]

100. Levi-Polyachenko NH, Merkel EJ, Jones BT, Carroll DL, Stewart JHt. Rapid photothermal intracellular drug delivery using multiwalled carbon nanotubes. Molecular Pharmaceutics. 2009; 6:1092–1099. [PubMed: 19545174]
101. Raffa V, Gherardini L, Vittorio O, Bardi G, Ziaei A, Pizzorusso T, Riggio C, Nitodas S, Karachalios T, Al-Jamal KT, Kostarelos K, Costa M, Cuschieri A. Carbon nanotube-mediated wireless cell permeabilization: drug and gene uptake. Nanomedicine (Lond). 2011; 6:1709–1718. [PubMed: 22122583]
102. Feazell RP, Nakayama-Ratchford N, Dai H, Lippard SJ. Soluble single-walled carbon nanotubes as longboat delivery systems for Platinum(IV) anticancer drug design. Journal of the American Chemical Society. 2007; 129:8438–8439. [PubMed: 17569542]
103. Wang L, Shi J, Jia X, Liu R, Wang H, Wang Z, Li L, Zhang J, Zhang C, Zhang Z. NIR-/pH-Responsive Drug Delivery of Functionalized Single-Walled Carbon Nanotubes for Potential Application in Cancer Chemo-Photothermal Therapy. Pharmaceutical Research. 2013 Jun 14. Epub ahead of print.
104. Zhang M, Murakami T, Ajima K, Tsuchida K, Sandanayaka AS, Ito O, Iijima S, Yudasaka M. Fabrication of ZnPc/protein nanohorns for double photodynamic and hyperthermic cancer phototherapy. Proc Natl Acad Sci U S A. 2008; 105:14773–14778. [PubMed: 18815374]
105. Villa CH, Dao T, Ahearn I, Fehrenbacher N, Casey E, Rey DA, Korontsvit T, Zakhaleva V, Batt CA, Philips MR, Scheinberg DA. Single-Walled Carbon Nanotubes Deliver Peptide Antigen into Dendritic Cells and Enhance IgG Responses to Tumor-Associated Antigens. Acs Nano. 2011; 5:5300–5311. [PubMed: 21682329]
106. Zhou FF, Wu S, Song S, Chen WR, Resasco DE, Xing D. Antitumor immunologically modified carbon nanotubes for photothermal therapy. Biomaterials. 2012; 33:3235–3242. [PubMed: 22296829]
107. Kosuge H, Sherlock S, Kitagawa T, Dai HJ, McConnell MV. Carbon Nanotubes Enable Optical Ablation of Vascular Macrophages. Circulation. 2011; 124
108. Miyako E, Deguchi T, Nakajima Y, Yudasaka M, Hagihara Y, Horie M, Shichiri M, Higuchi Y, Yamashita F, Hashida M, Shigeri Y, Yoshida Y, Iijima S. Photothermic regulation of gene expression triggered by laser-induced carbon nanohorns. P Natl Acad Sci USA. 2012; 109:7523–7528.
109. Miyako E, Hosokawa C, Kojima M, Yudasaka M, Funahashi R, Oishi I, Hagihara Y, Shichiri M, Takashima M, Nishio K, Yoshida Y. A Photo-Thermal-Electrical Converter Based On Carbon Nanotubes for Bioelectronic Applications. Angewandte Chemie-International Edition. 2011; 50:12266–12270.
110. Jain RK, Stylianopoulos T. Delivering nanomedicine to solid tumors. Nature Reviews Clinical Oncology. 2010; 7:653–664.
111. Adamson C, Kanu OO, Mehta AI, Di C, Lin N, Mattox AK, Bigner DD. Glioblastoma multiforme: a review of where we have been and where we are going. Expert Opinions in Investigational Drugs. 2009; 18:1061–1083.
112. Jain KK. Use of nanoparticles for drug delivery in glioblastoma multiforme. Expert Review of Neurotherapeutics. 2007; 7:363–372. [PubMed: 17425491]
113. Kanu OO, Mehta A, Di C, Lin N, Bortoff K, Bigner DD, Yan H, Adamson DC. Glioblastoma multiforme: a review of therapeutic targets. Expert Opinion on Therapeutic Targets. 2009; 13:701–718. [PubMed: 19409033]
114. Lima FR, Kahn SA, Soletti RC, Biasoli D, Alves T, da Fonseca AC, Garcia C, Romao L, Brito J, Holanda-Afonso R, Faria J, Borges H, Moura-Neto V. Glioblastoma: Therapeutic challenges, what lies ahead. Biochimica et Biophysica Acta. 2012; 1826:338–349. [PubMed: 22677165]
115. Rozhkova EA. Nanoscale Materials for Tackling Brain Cancer: Recent Progress and Outlook. Advanced Materials. 2011; 23:H136–H150. [PubMed: 21506172]
116. Ferrari M. Frontiers in cancer nanomedicine: directing mass transport through biological barriers. Trends in Biotechnology. 2010; 28:181–188. [PubMed: 20079548]
117. Li SD, Huang L. Pharmacokinetics and biodistribution of nanoparticles. Molecular Pharmaceutics. 2008; 5:496–504. [PubMed: 18611037]

118. Kostarelos K. Rational design and engineering of delivery systems for therapeutics: biomedical exercises in colloid and surface science. Advances in Colloid and Interface Science. 2003; 106:147–168. [PubMed: 14672846]
119. Smith BR, Kempen P, Bouley D, Xu A, Liu Z, Melosh N, Dai HJ, Sinclair R, Gambhir SS. Shape Matters: Intravital Microscopy Reveals Surprising Geometrical Dependence for Nanoparticles in Tumor Models of Extravasation. Nano lett. 2012; 12:3369–3377. [PubMed: 22650417]
120. Nance EA, Woodworth GF, Sailor KA, Shih TY, Xu QG, Swaminathan G, Xiang D, Eberhart C, Hanes J. A Dense Poly (Ethylene Glycol) Coating Improves Penetration of Large Polymeric Nanoparticles Within Brain Tissue. Science Translational Medicine. 2012; 4
121. Biddlestone-Thorpe L, Marchi N, Guo K, Ghosh C, Janigro D, Valerie K, Yang H. Nanomaterial-mediated CNS delivery of diagnostic and therapeutic agents. Advanced Drug Delivery Reviews. 2012; 64:605–613. [PubMed: 22178615]
122. Sykova E, Nicholson C. Diffusion in brain extracellular space. Physiological Reviews. 2008; 88:1277–1340. [PubMed: 18923183]
123. Thorne RG, Nicholson C. In vivo diffusion analysis with quantum dots and dextrans predicts the width of brain extracellular space. P Natl Acad Sci USA. 2006; 103:5567–5572.
124. Fan ZH, Advani SG. Characterization of orientation state of carbon nanotubes in shear flow. Polymer. 2005; 46:5232–5240.
125. Fakhri N, MacKintosh FC, Lounis B, Cognet L, Pasquali M. Brownian Motion of Stiff Filaments in a Crowded Environment. Science. 2010; 330:1804–1807. [PubMed: 21205665]
126. Fatin-Rouge N, Starchev K, Buffle J. Size effects on diffusion processes within agarose gels. Biophysical Journal. 2004; 86:2710–2719. [PubMed: 15111390]
127. Pluen A, Netti PA, Jain RK, Berk DA. Diffusion of macromolecules in agarose gels: Comparison of linear and globular configurations. Biophysical Journal. 1999; 77:542–552. [PubMed: 10388779]
128. Stylianopoulos T, Poh MZ, Insin N, Bawendi MG, Fukumura D, Munn LL, Jain RK. Diffusion of Particles in the Extracellular Matrix: The Effect of Repulsive Electrostatic Interactions. Biophysical Journal. 2010; 99:1342–1349. [PubMed: 20816045]
129. Chen BD, Zhang H, Zhai CX, Du N, Sun C, Xue JW, Yang DR, Huang H, Zhang B, Xie QP, Wu YL. Carbon nanotube-based magnetic-fluorescent nanohybrids as highly efficient contrast agents for multimodal cellular imaging. Journal of Materials Chemistry. 2010; 20:9895–9902.
130. Hartman KB, Laus S, Bolskar RD, Muthupillai R, Helm L, Toth E, Merbach AE, Wilson LJ. Gadonanotubes as ultrasensitive pH-smart probes for magnetic resonance imaging. Nano lett. 2008; 8:415–419. [PubMed: 18215084]
131. Richard C, Doan BT, Beloeil JC, Bessodes M, Toth E, Scherman D. Noncovalent functionalization of carbon nanotubes with amphiphilic Gd3+ chelates: Toward powerful T-1 and T-2 MRI contrast agents. Nano lett. 2008; 8:232–236. [PubMed: 18088153]
132. Yin M, Wang ML, Miao F, Ji YX, Tian Z, Shen HB, Jia NQ. Water-dispersible multiwalled carbon nanotube/iron oxide hybrids as contrast agents for cellular magnetic resonance imaging. Carbon. 2012; 50:2162–2170.
133. Singh R, Pantarotto D, Lacerda L, Pastorin G, Klumpp C, Prato M, Bianco A, Kostarelos K. Tissue biodistribution and blood clearance rates of intravenously administered carbon nanotube radiotracers. P Natl Acad Sci USA. 2006; 103:3357–3362.
134. Lacerda L, Soundararajan A, Singh R, Pastorin G, Al-Jamal KT, Turton J, Frederik P, Herrero MA, Bao SLA, Emfietzoglou D, Mather S, Phillips WT, Prato M, Bianco A, Goins B, Kostarelos K. Dynamic Imaging of functionalized multi-walled carbon nanotube systemic circulation and urinary excretion. Advanced Materials. 2008; 20:225–230.
135. Welsher K, Sherlock SP, Dai HJ. Deep-tissue anatomical imaging of mice using carbon nanotube fluorophores in the second near-infrared window. P Natl Acad Sci USA. 2011; 108:8943–8948.
136. Biris AS, Galanzha EI, Li ZR, Mahmood M, Xu Y, Zharov VP. In vivo Raman flow cytometry for real-time detection of carbon nanotube kinetics in lymph, blood, and tissues. Journal of Biomedical Optics. 2009; 14

137. Hong GS, Lee JC, Robinson JT, Raaz U, Xie LM, Huang NF, Cooke JP, Dai HJ. Multifunctional in vivo vascular imaging using near-infrared II fluorescence. Nature Medicine. 2012; 18:1841–1846.

138. Xiang L, Yuan Y, Xing D, Ou Z, Yang S, Zhou F. Photoacoustic molecular imaging with antibody-functionalized single-walled carbon nanotubes for early diagnosis of tumor. Journal of Biomedical Optics. 2009; 14:021008–021007. [PubMed: 19405721]

139. Kim JW, Galanzha EI, Shashkov EV, Moon HM, Zharov VP. Golden carbon nanotubes as multimodal photoacoustic and photothermal high-contrast molecular agents. Nat Nanotechnol. 2009; 4:688–694. [PubMed: 19809462]

140. de la Zerda A, Kim JW, Galanzha EI, Gambhir SS, Zharov VP. Advanced contrast nanoagents for photoacoustic molecular imaging, cytometry, blood test and photothermal theranostics. Contrast Media & Molecular Imaging. 2011; 6:346–369. [PubMed: 22025336]

141. Picou L, McMann C, Elzer PH, Enright FM, Biris AS, Boldor D. Spatio-temporal thermal kinetics of in situ MWCNT heating in biological tissues under NIR laser irradiation. Nanotechnology. 2010; 21:435101. [PubMed: 20876978]

142. Rieke V, Pauly KB. MR thermometry. Journal of Magnetic Resonance Imaging. 2008; 27:376–390. [PubMed: 18219673]

143. Salvador-Morales C, Gao WW, Ghatalia P, Murshed F, Aizu W, Langer R, Farokhzad OC. Multifunctional nanoparticles for prostate cancer therapy. Expert Review of Anticancer Therapy. 2009; 9:211–221. [PubMed: 19192959]

144. Biris AS, Boldor D, Palmer J, Monroe WT, Mahmood M, Dervishi E, Xu Y, Li Z, Galanzha EI, Zharov VP. Nanophotothermolysis of multiple scattered cancer cells with carbon nanotubes guided by time-resolved infrared thermal imaging. Journal of Biomedical Optics. 2009; 14:021007. [PubMed: 19405720]

145. Anderson RR, Parrish JA. Selective photothermolysis: precise microsurgery by selective absorption of pulsed radiation. Science. 1983; 220:524–527. [PubMed: 6836297]

146. Vitetta ES, Marches R, Mikoryak C, Wang RH, Pantano P, Draper RK. The importance of cellular internalization of antibody-targeted carbon nanotubes in the photothermal ablation of breast cancer cells. Nanotechnology. 2011; 22:095101. [PubMed: 21258147]

147. Zharov VP, Galitovskaya EN, Johnson C, Kelly T. Synergistic enhancement of selective nanophotothermolysis with gold nanoclusters: Potential for cancer therapy. Lasers in Surgery and Medicine. 2005; 37:219–226. [PubMed: 16175635]

148. Keblinski P, Cahill DG, Bodapati A, Sullivan CR, Taton TA. Limits of localized heating by electromagnetically excited nanoparticles. J Appl Phys. 2006; 100:054305.

149. Sarkar S, Zimmermann K, Leng WN, Vikesland P, Zhang JF, Dorn H, Diller T, Rylander C, Rylander MN. Measurement of the Thermal Conductivity of Carbon Nanotube-Tissue Phantom Composites with the Hot Wire Probe Method. Annals of Biomedical Engineering. 2011; 39:1745–1758. [PubMed: 21360225]

150. Sarkar S, Rylander MN. Treatment Planning Model for Nanotube-Mediated Laser Cancer Therapy. Lasers in Surgery and Medicine. 2009; 41:5.

151. Sargent LM, Reynolds SH, Castranova V. Potential pulmonary effects of engineered carbon nanotubes: in vitro genotoxic effects. Nanotoxicology. 2010; 4:396–408. [PubMed: 20925447]

152. Huizar I, Malur A, Midgette YA, Kukoly C, Chen PY, Ke PC, Podila R, Rao AM, Wingard CJ, Dobbs L, Barna BP, Kavuru MS, Thomassen MJ. Novel Murine Model of Chronic Granulomatous Lung Inflammation Elicited by Carbon Nanotubes. American Journal of Respiratory Cell and Molecular Biology. 2011; 45:858–866. [PubMed: 21398620]

153. Kolosnjaj-Tabi J, Hartman KB, Boudjemaa S, Ananta JS, Morgant G, Szwarc H, Wilson LJ, Moussa F. In Vivo Behavior of Large Doses of Ultrashort and Full-Length Single-Walled Carbon Nanotubes after Oral and Intraperitoneal Administration to Swiss Mice. Acs Nano. 2010; 4:1481–1492. [PubMed: 20175510]

154. Nagai H, Toyokuni S. Differences and similarities between carbon nanotubes and asbestos fibers during mesothelial carcinogenesis: Shedding light on fiber entry mechanism. Cancer Science. 2012; 103:1378–1390. [PubMed: 22568550]

155. Muller J, Delos M, Panin N, Rabolli V, Huaux F, Lison D. Absence of Carcinogenic Response to Multiwall Carbon Nanotubes in a 2-Year Bioassay in the Peritoneal Cavity of the Rat. Toxicological Sciences. 2009; 110:442–448. [PubMed: 19429663]

156. Osmond-McLeod MJ, Poland CA, Murphy F, Waddington L, Morris H, Hawkins SC, Clark S, Aitken R, McCall MJ, Donaldson K. Durability and inflammogenic impact of carbon nanotubes compared with asbestos fibres. Particle and Fibre Toxicology. 2011; 8

157. Nunes A, Bussy C, Gherardini L, Meneghetti M, Herrero MA, Bianco A, Prato M, Pizzorusso T, Al-Jamal KT, Kostarelos K. In vivo degradation of functionalized carbon nanotubes after stereotactic administration in the brain cortex. Nanomedicine. 2012; 7:1485–1494. [PubMed: 22712575]

158. Bianco A, Kostarelos K, Prato M. Making carbon nanotubes biocompatible and biodegradable. Chemical Communications. 2011; 47:10182–10188. [PubMed: 21776531]

159. Schipper ML, Nakayama-Ratchford N, Davis CR, Kam NW, Chu P, Liu Z, Sun X, Dai H, Gambhir SS. A pilot toxicology study of single-walled carbon nanotubes in a small sample of mice. Nat Nanotechnol. 2008; 3:216–221. [PubMed: 18654506]

160. Ali-Boucetta H, Nunes A, Sainz R, Herrero MA, Tian B, Prato M, Bianco A, Kostarelos K. Asbestos-like Pathogenicity of Long Carbon Nanotubes Alleviated by Chemical Functionalization. Angewandte Chemie International Edition. 2013; 52:2274–2278.

161. Murphy FA, Poland CA, Duffin R, Al-Jamal KT, Ali-Boucetta H, Nunes A, Byrne F, Prina-Mello A, Volkov Y, Li SP, Mather SJ, Bianco A, Prato M, MacNee W, Wallace WA, Kostarelos K, Donaldson K. Length-Dependent Retention of Carbon Nanotubes in the Pleural Space of Mice Initiates Sustained Inflammation and Progressive Fibrosis on the Parietal Pleura. American Journal of Pathology. 2011; 178:2587–2600. [PubMed: 21641383]

162. Liang F, Sadana AK, Peera A, Chattopadhyay J, Gu ZN, Hauge RH, Billups WE. A convenient route to functionalized carbon nanotubes. Nano lett. 2004; 4:1257–1260.

163. Takagi A, Hirose A, Nishimura T, Fukumori N, Ogata A, Ohashi N, Kitajima S, Kanno J. Induction of mesothelioma in p53+/- mouse by intraperitoneal application of multi-wall carbon nanotube. Journal of Toxicological Sciences. 2008; 33:105–116. [PubMed: 18303189]

164. Vakarelski IU, Brown SC, Higashitani K, Moudgil BM. Penetration of living cell membranes with fortified carbon nanotube tips. Langmuir. 2007; 23:10893–10896. [PubMed: 17894512]

165. Mayer A, Vadon M, Rinner B, Novak A, Wintersteiger R, Fröhlich E. The role of nanoparticle size in hemocompatibility. Toxicology. 2009; 258:139–147. [PubMed: 19428933]

166. Radomski A, Jurasz P, Alonso-Escolano D, Drews M, Morandi M, Malinski T, Radomski MW. Nanoparticle-induced platelet aggregation and vascular thrombosis. British Journal of Pharmacology. 2005; 146:882–893. [PubMed: 16158070]

167. Semberova J, De Paoli Lacerda SH, Simakova O, Holada K, Gelderman MP, Simak J. Carbon nanotubes activate blood platelets by inducing extracellular Ca2+ influx sensitive to calcium entry inhibitors. Nano lett. 2009; 9:3312–3317. [PubMed: 19736974]

168. Dobrovolskaia MA, Aggarwal P, Hall JB, McNeil SE. Preclinical studies to understand nanoparticle interaction with the immune system and its potential effects on nanoparticle biodistribution. Molecular Pharmaceutics. 2008; 5:487–495. [PubMed: 18510338]

169. Deng XY, Wu F, Liu Z, Luo M, Li L, Ni QS, Jiao Z, Wu MH, Liu YF. The splenic toxicity of water soluble multi-walled carbon nanotubes in mice. Carbon. 2009; 47:1421–1428.

170. Qu GB, Bai YH, Zhang Y, Jia Q, Zhang WD, Yan B. The effect of multiwalled carbon nanotube agglomeration on their accumulation in and damage to organs in mice. Carbon. 2009; 47:2060–2069.

171. Yang ST, Wang X, Jia G, Gu YQ, Wang TC, Nie HY, Ge CC, Wang HF, Liu YF. Long-term accumulation and low toxicity of single-walled carbon nanotubes in intravenously exposed mice. Toxicology Letters. 2008; 181:182–189. [PubMed: 18760340]

172. Lacerda SH, Semberova J, Holada K, Simakova O, Hudson SD, Simak J. Carbon nanotubes activate store-operated calcium entry in human blood platelets. Acs Nano. 2011; 5:5808–5813. [PubMed: 21639133]

173. Burke AR, Singh RN, Carroll DL, Owen JD, Kock ND, D'Agostino R Jr, Torti FM, Torti SV. Determinants of the thrombogenic potential of multiwalled carbon nanotubes. Biomaterials. 2011; 32:5970–5978. [PubMed: 21663954]

174. Meng J, Cheng XL, Liu J, Zhang WQ, Li XJ, Kong H, Xu HY. Effects of Long and Short Carboxylated or Aminated Multiwalled Carbon Nanotubes on Blood Coagulation. Plos One. 2012; 7

175. Cherukuri P, Gannon CJ, Leeuw TK, Schmidt HK, Smalley RE, Curley SA, Weisman RB. Mammalian pharmacokinetics of carbon nanotubes using intrinsic near-infrared fluorescence. P Natl Acad Sci USA. 2006; 103:18882–18886.

176. Liu Z, Davis C, Cai WB, He L, Chen XY, Dai HJ. Circulation and long-term fate of functionalized biocompatible single-walled carbon nanotubes in mice probed by Raman spectroscopy. P Natl Acad Sci USA. 2008; 105:1410–1415.

177. Al-Jamal KT, Nunes A, Methven L, Ali-Boucetta H, Li SP, Toma FM, Herrero MA, Al-Jamal WT, ten Eikelder HMM, Foster J, Mather S, Prato M, Bianco A, Kostarelos K. Degree of Chemical Functionalization of Carbon Nanotubes Determines Tissue Distribution and Excretion Profile. Angewandte Chemie-International Edition. 2012; 51:6389–6393.

178. Lacerda L, Ali-Boucettal H, Herrero MA, Pastorin G, Bianco A, Prato M, Kostarelos K. Tissue histology and physiology following intravenous administration of different types of functionalized multiwalled carbon nanotubes. Nanomedicine. 2008; 3:149–161. [PubMed: 18373422]

179. Lacerda L, Herrero MA, Venner K, Bianco A, Prato M, Kostarelos K. Carbon-nanotube shape and individualization critical for renal excretion. Small. 2008; 4:1130–1132. [PubMed: 18666166]

180. Longmire M, Choyke PL, Kobayashi H. Clearance properties of nano-sized particles and molecules as imaging agents: considerations and caveats. Nanomedicine. 2008; 3:703–717. [PubMed: 18817471]

181. Ruggiero A, Villa CH, Bander E, Rey DA, Bergkvist M, Batt CA, Manova-Todorova K, Deen WM, Scheinberg DA, McDevitt MR. Paradoxical glomerular filtration of carbon nanotubes. P Natl Acad Sci USA. 2010; 107:12369–12374.

182. Deen WM, Lazzara MJ, Myers BD. Structural determinants of glomerular permeability. American Journal of Physiology-Renal Physiology. 2001; 281:F579–F596. [PubMed: 11553505]

183. Bussy C, Ali-Boucetta H, Kostarelos K. Safety Considerations for Graphene: Lessons Learnt from Carbon Nanotubes. Accounts of Chemical Research. 2013; 46:692–701. [PubMed: 23163827]

184. Markovic ZM, Harhaji-Trajkovic LM, Todorovic-Markovic BM, Kepic DP, Arsikin KM, Jovanovic SP, Pantovic AC, Dramicanin MD, Trajkovic VS. In vitro comparison of the photothermal anticancer activity of graphene nanoparticles and carbon nanotubes. Biomaterials. 2011; 32:1121–1129. [PubMed: 21071083]

185. Panchapakesan B, Lu S, Sivakumar K, Taker K, Cesarone G, Wickstrom E. Single-wall carbon nanotube nanobomb agents for killing breast cancer cells. NanoBioTechnology. 2005; 1:133–139.

186. Burlaka A, Lukin S, Prylutska S, Remeniak O, Prylutskyy Y, Shuba M, Maksimenko S, Ritter U, Scharff P. Hyperthermic effect of multi-walled carbon nanotubes stimulated with near infrared irradiation for anticancer therapy: in vitro studies. 2010; 32:48–50.

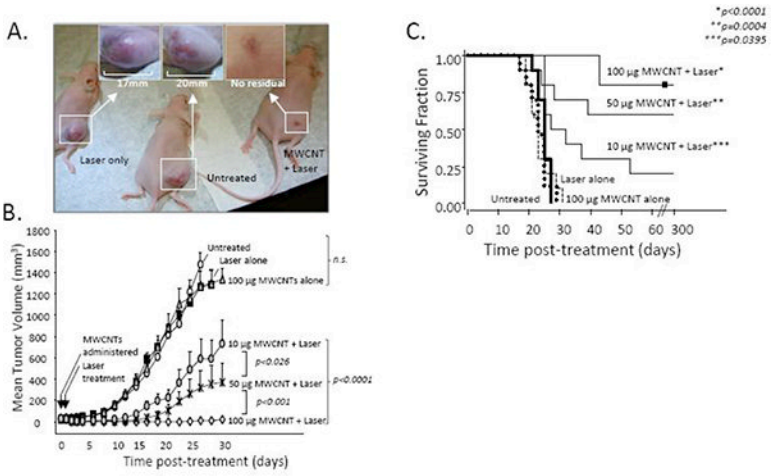

Figure 1.

Treatment of tumor bearing mice by CNMTT reduces tumor growth and increases long term survival. Nu/nu mice were implanted s.c. with RENCA tumors and divided into groups of 10. Mice were either left untreated, treated with MWCNT alone, treated with laser alone, or treated with the combination of MWCNT and laser (3 W/cm^2; 30 s). (A) Photographs at day 21 post-treatment of representative mice from groups treated with laser only, untreated controls, or mice treated with 100 μg of MWCNT plus laser. (B) Mice treated with the combination of MWCNTs and laser were injected with a range of MWCNT doses. Tumor sizes were measured every 2 days. Means and standard errors are shown. Control groups (untreated, treated with MWCNTs alone, or treated with laser alone) were statistically identical. There is a dose-dependent attenuation in tumor growth after 30 s of NIR laser treatment of MWCNT-loaded tumors ($P < 0.0001$). (C) MWCNT-based photothermal therapy increases long-term survival of tumor-bearing mice. Survival of mice treated as described in (C) was assessed for 10 months after treatment. Kaplan–Meier curves demonstrate a significant increase in survival in mice treated with all doses of MWCNTs plus laser ($P < 0.0001$ vs all controls). Survival curves for control groups were statistically identical ($P > 0.775$). Adapted and reproduced with permission from *Burke et al. PNAS 106 (2009) 12897-12902.*

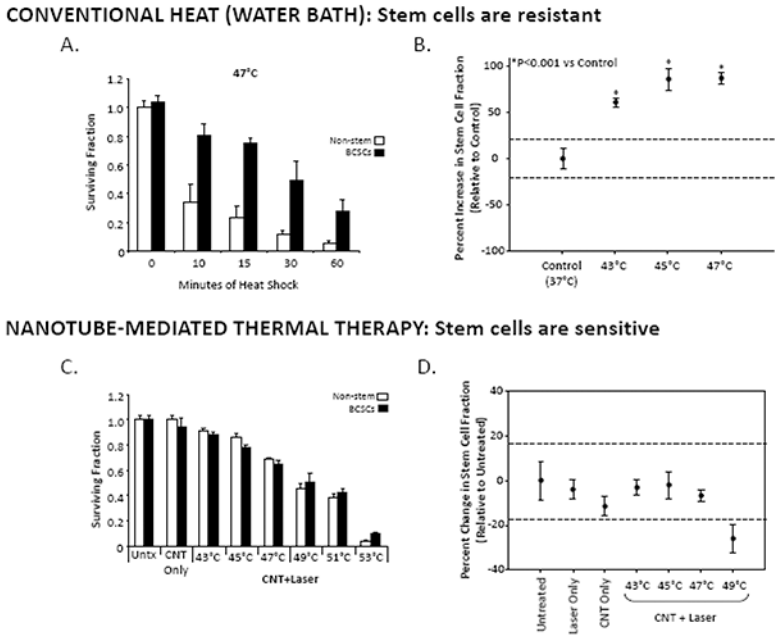

Figure 2.

Breast cancer stem cells are resistant to conventional hyperthermic cell death but sensitive to CNMTT. (A) Relative viability of cancer cells 24 h after water bath heat treatment as a model of conventional hyperthermia. Stem cell-like breast cancer cells (BCSCs) or bulk breast cancer (non-stem) cells were heated in a water bath at 47 °C for 0-60 min. MTT absorbance values were normalized to the untreated condition ("0" minutes heat shock). The results clearly show that BSCC subpopulations are more resistant to heat than breast cancer cells as a whole. (B) Sub-lethal hyperthermia enriches for the BCSC phenotype in bulk breast cancer cells. Changes in the $CD44^{high}/CD24^{low}$ stem cell fraction of surviving bulk breast cancer cells 24 h after water bath heat shock at 43°C, 45°C or 47°C were determined by flow cytometry. Shown are mean percent changes in the $CD44^{high}/CD24^{low}$ cell fraction normalized to the Untreated condition (which is set as 1.0, i.e. "0 percent change"). Dashed lines indicate the 95% C.I. for the Untreated condition. All heat treatments led to significant increases in the stem cell fraction ($p < 0.0001$) relative to Untreated. (C) In contrast, of BCSC and non-stem breast cancer cells are equally sensitive to CNMTT. Cancer cells were heat treated to specific temperatures by the combination of MWCNTs and NIR laser irradiation and the relative viability of BCSC and non-stem breast cancer cells was determined by MTT 24 h later and normalized to the "Untreated" conditions. "CNT Only" describes samples that were mixed with MWCNTs but were not laser treated. "CNT+ Laser" describes samples that were heat shocked to the indicated final temperatures by the combination of 50 mg/mL MWCNTs and 3W laser radiation. In contrast to the water bath heating results, no significant difference between the sensitivity of stem-like and non-stem breast cancer cells was observed, and (D) no enrichment of the stem cell phenotype (quantified as in (B)) in viable cells 24 h after CNMTT was detected. Adapted and reproduced with permission from *Burke et al. Biomaterials 33 (2012) 2961-2970*.

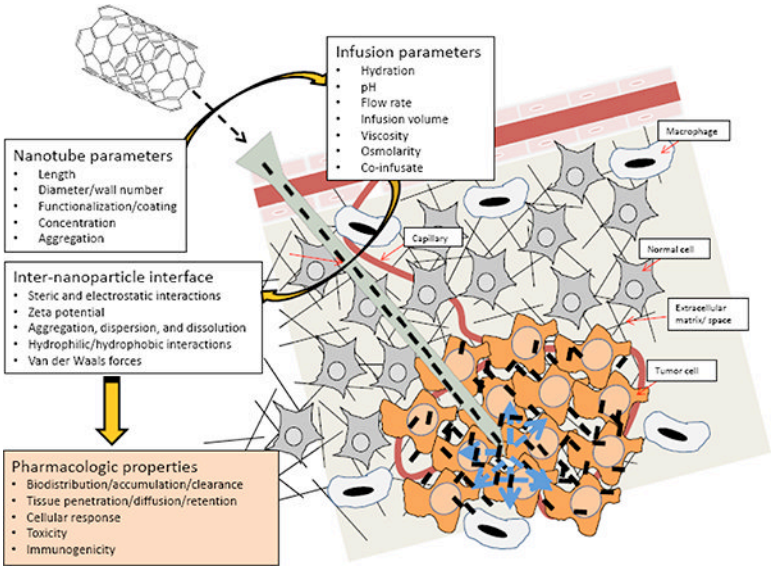

Figure 3.

Effective delivery of CNTs to the tumor is a central challenge for using CNTs to treat cancer. . In spite of the dynamic growth of innovative nanoplatforms, the path from bench to bedside is still challenging. Barriers within the tumor microenvironment, including vascular heterogeneity, extracellar matrix pore size, high interstitial pressure, and immune cell infiltration, limit the uniform penetration of nanotherapeutics, lead to inefficient delivery and reduce the potential efficacy of many treatments. Currently, there is an insufficient understanding of how CNTs interact with the tumor microenvironment. As shown here, there is a patchwork of inter-related properties that are dependent not just on the characteristics of the nanoparticle, but also upon the environment in which the particle is to be used and the strategy by which it will be delivered. These properties influence the pharmacologic behavior of the CNTs in vitro and in vivo. Failure to appropriately characterize CNTs has led to a bottleneck in their clinical translation due to inadequately designed studies at the pre-clinical level that could bridge cell- culture-to-rodent-to-human studies. Identification of CNT physicochemical and surface characteristics under specific infusion parameters and consideration of how the pathophysiology and anatomy of the target site influence the pharmacologic properties of CNTs will be necessary for the development of pharmaceutical grade material for clinical use.

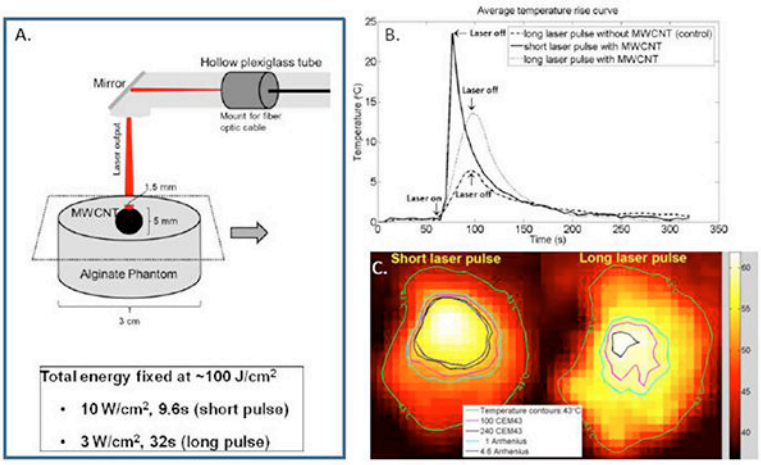

Figure 4.

MR thermography combined with damage modeling algorithms can be used to optimize the delivery of therapeutic heat to tumor targets. (A) Schematic of experimental design. The entire set-up was placed within the magnet of a 7T MRI. A YAG laser tuned to 1064 nm served as the laser source and the phantom was exposed to a total fixed radiant energy of approximately 100 J/cm^2 using either a high power, short duration pulse (10 W/cm^2; 9.6 s; refered to as the “short pulse”) or a low power, longer duration pulse (3 W/cm^2; 32 s; referred to as the “long pulse”). (B) Time evolution of the average temperature measured by MR thermometry achieved in the MWCNT inclusion: Temperature increased approximately linearly with time in response to both long and short pulse irradiation with a rate of average temperature increase of 1.89 and 0.38 °C s^{-1} and for the short and long pulse heating, respectively. Notably, the ratio of these heating rates is about 5 and is significantly greater than the ratio of heating powers (3.3), suggesting more heat diffuses away from the heated region during long pulse heating. (C) Temperature maps calculated by PRF MR thermometry of a coronal slice across the MWCNT inclusion and surrounding nanotube-free phantom generated at the time the laser was turned off. A temperature contour for which the peak temperature reached 43 °C (green curve) is shown. The images clearly show that heat is more localized following the short pulse treatment. Thermal damage contours calculated for 100 or 200 cumulative equivalent minutes at 43°C (100CEM43 (pink curve) and the 240CEM43 thresholds (blue curve)) and contours calculated using the Arrhenius damage integral are shown. Thermal necrosis is predicted to begin when the Arrhenius integral equals 1 (light blue curve), which is roughly equivalent to 100CEM43. Ninety-nine percent of cells are predicted to die when the Arrhenius integral equals 4.6 (dark blue curve), which is roughly equivalent to 240CEM43. Note that 99% cell death as calculated by the Arrhenius damage integral was not achieved using long laser pulse heating. Thus, for a fixed radiant exposure, short pulse heating of CNTs leads to a higher maximum temperature, a more rapid rate of temperature increase, more localized heating, and greater therapeutic efficacy. Adapted and reproduced with permission from *Xie et al. Phys. Med. Biol. 57 (2012) 5765-75*.

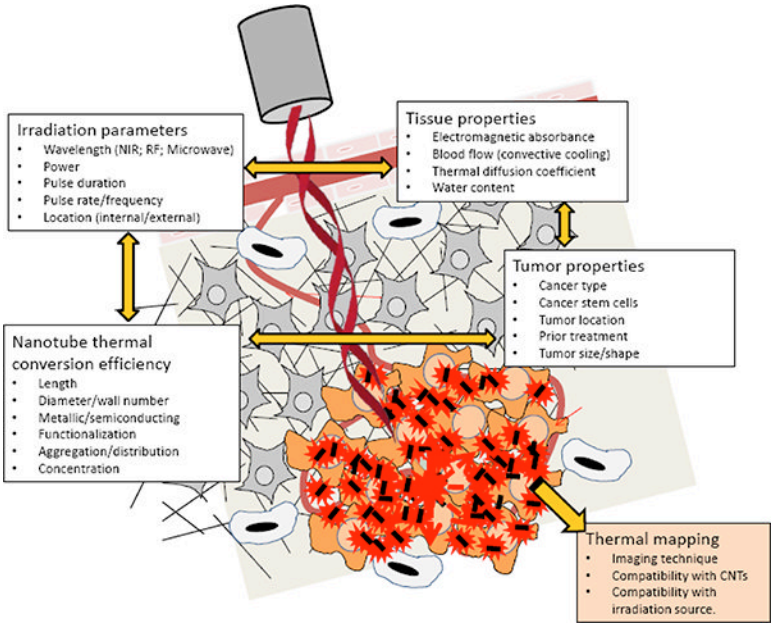

Figure 5.

Summary of important parameters which must be assessed for successful clinical translation of CNMTT. To maximize treatment efficacy and minimize collateral damage due to heat spread, laser irradiation parameters (irradiance, duration, duty cycle) must be carefully matched to the NIR absorptive characteristics and distribution of the CNTs as well as the thermal properties of the targeted and surrounding tissue. These parameters are highly interrelated and must be balanced with the underlying biology and biophysics of the tumor target. An understanding of both the NIR absorptive and thermal dispersive qualities of the tumor target is needed. Specific issues related to the sensitivity of the tumor and surrounding tissue to thermal ablation must be identified. Treatment should be compatible with a non-invasive thermal mapping modality (such as proton resonance frequency shift magnetic resonance (MR) thermography) to monitor temperature localization.

Table 1
Preclinical assessment of CNMTT in cancer models

Cancer Type	Experimental model	Material (effective dose)	Laser (wavelength; radiant exposure)	Reference
Brain (human)	in vitro; adherent primary glioblastoma cells	SWCNT (2.5 μg/well of 24 well plate)	808 nm; 600 J/cm^2	[83]
	in vitro; non-adherent U251 glioblastoma cells	SWCNT (10 μg/ml)	808 nm; 600 J/cm^2	[184]
	in vitro; non-adherent MDA-MB-231 cells	gold coated SWCNTs (estimated 0.5-1×10^4 SWCNTs per cell)	850 nm; 0.5 J/cm^2	[91]
	in vivo murine flank tumor; primary glioblastoma cells	MWCNT (10 μg - ex vivo)	808 nm; 600 J/cm^2	[83]
Breast (human)	in vitro; transformed human mammary epithelial cells	MWCNT (50 μg/mL)	1064 nm; 90 J/cm^2	[84]
	in vitro; adherent BT-474 cells	SWCNT (5-10 μg/ml)	808 nm; 5130 J/cm^2	[75]
	in vitro; adherent SK-BR-3 cells	SWCNT (4 μg/ml)	808 nm; 900 J/cm^2	[76]
	in vitro; non-adherent BT474 cells	SWCNT (100 μg/ml)	800 nm;12 J/cm^2	[185]
	in vitro; non-adherent MCF-7 cells	SWCNT (not reported)	808 nm; 144 J/cm^2	[78]
	in vivo murine flank tumor; MDA-MB-231 cells	MWCNT (100 μg IT)	1064 nm; 90 J/cm^2	[22]
	in vivo murine flank tumor; transformed human mammary epithelial cells	MWCNT (100 μg IT)	1064 nm; 90 J/cm^2	[84]
Breast (murine)	in vitro; adherent EMT6 cells	SWCNT (3.5 μg/ml)	980 nm; 120 J/cm^2	[82]
	in vitro; adherent EMT6 cells	SWCNT (50 μg/ml)	980 nm; 60-150 J/cm^2	[106]
	in vivo murine flank tumor; 4T1 cells	SWCNT (70 μg IV)	808 nm; 180 J/cm^2	[53]
	in vivo murine flank tumor; 4T1 cells	SWCNT (100 μg IV)	808 nm; 300 J/cm^2	[69]
	in vivo murine flank tumor; EMT6 cells	SWCNT (20-25 μg IT)	980 nm; 300 J/cm^2	[73]
	in vivo murine flank tumor; EMT6 cells	SWCNT (1 mg IT)	980 nm; 450 J/cm^2	[82]
Cervical (human)	in vitro; adherent Hela cells	MWCNT (10 μg/ml)	1064 nm; 128 J/cm^2	[144]
	in vitro; non-adherent HeLa cells	SWCNT (25 μg/ml)	808 nm; 168 J/cm^2	[27]
Erlich ascites (murine)	in vitro; non-adherent Erlich ascitic carcinoma cells	MWCNT (100 μg/ml)	780-1400 nm; 315 J/cm2	[186]
Kidney (human)	in vitro; adherent CRL 1932 cells	Nitrogen-doped MWCNT (approx. 83 μg/ml)	1064 nm; 720 J/cm^2	[52]
Kidney (murine)	in vitro; non-adherent RENCA cells	MWCNT (100 μg/ml)	1064 nm; 135 J/cm^2	[28]
	in vitro; non-adherent RENCA cells	MWCNT (100 μg/ml)	1064 nm; 4590J/cm^2	[98]
	in vivo murine flank tumor; RENCA cells	MWCNT (100 μg IT)	1064 nm; 90 J/cm^2	[28]
Liver (human)	in vitro; adherent HepG2 or CRL 4020 cells	MWCNT (1-50 μg/ml)	808 nm; 7680 J/cm^2	[49]

Cancer Type	Experimental model	Material (effective dose)	Laser (wavelength; radiant exposure)	Reference
	in vitro; adherent SK-BR-3 cells	SWCNT (20 μg/ml)	1064 nm; 4 J/cm^2	[74]
Lymph (human)	in vitro; non-adherent Daudi Burkitt's lymphoma cells	SWCNT (90 μg/ml)	808 nm; 2100 J/cm^2	[94]
Mouth (human)	in vivo murine flank tumor; KB epidermoid mouth carcinoma cells	SWCNT (12 μg IT)	808 nm; 684 J/cm^2	[60]
Neuroend ocrine (human)	in vitro; adherent stNB-V1 neuroblastoma cells	MWCNT (5-10 μg/ml)	808 nm; 3000 J/cm^2	[77]
Prostate (human)	in vitro; non-adherent PC-3 cells	MWCNT (100 μg/ml)	1064 nm; 4590J/cm^2	[98]
	in vivo murine flank tumor; PC-3 cells	MWCNT (50 μg IT)	1064 nm; 175 J/cm^2	[63]
Skin (murine)	in vivo murine flank tumor; SCCVII squamous carcinoma cells	SWCNT (60-100 μg IT)	785 nm; 120 J/cm^2	[59]

IT = intratumoral injection; IV = intravenous injection